AD_____

Award Number: W81XWH-11-1-0602

TITLE: In Vivo Imaging of Branched Chain Amino Acid Metabolism in Prostate Cancer

PRINCIPAL INVESTIGATOR: Daniel Spielman

CONTRACTING ORGANIZATION: Stanford University

Stanford, CA 94305

REPORT DATE: October 2014

TYPE OF REPORT: Final

PREPARED FOR: U.S. Army Medical Research and Materiel Command
Fort Detrick, Maryland 21702-5012

REPORT DOCUMENTATION PAGE

Form Approved
OMB No. 0704-0188

1. REPORT DATE	2. REPORT TYPE	3. DATES COVERED
October 2014	Final	15 Jul 2011 - 14 Jul 2014

4. TITLE AND SUBTITLE
In Vivo Imaging of Branched Chain Amino Acid Metabolism in Prostate Cancer

5a. CONTRACT NUMBER

5b. GRANT NUMBER
W81XWH-11-1-0602

5c. PROGRAM ELEMENT NUMBER

6. AUTHOR(S)
Daniel Spielman

E-Mail: spielman@stanford.edu

5d. PROJECT NUMBER

5e. TASK NUMBER

5f. WORK UNIT NUMBER

7. PERFORMING ORGANIZATION NAME(S) AND ADDRESS(ES)

Stanford University
Stanford, CA 94305

8. PERFORMING ORGANIZATION REPORT

9. SPONSORING / MONITORING AGENCY NAME(S) AND ADDRESS(ES)

U.S. Army Medical Research and Materiel Command
Fort Detrick, Maryland 21702-5012

10. SPONSOR/MONITOR'S ACRONYM(S)

11. SPONSOR/MONITOR'S REPORT NUMBER(S)

12. DISTRIBUTION / AVAILABILITY STATEMENT
Approved for Public Release; Distribution Unlimited

13. SUPPLEMENTARY NOTES

14. ABSTRACT

The primary objective of this research effort was the development of noninvasive imaging method to assess branched-chain amino acid metabolism (known to be modified in prostate cancer [PC]) to distinguish malignant from healthy tissue. The approach is to use MRSI of hyperpolarized ^{13}C-ketoisocaproic acid (KIC) to interrogate its conversion to leucine as catalyzed by branched-chain aminotransferase (BCAT). We first determined that while BCAT activity is altered in prostate cancer relative to healthy tissue, insufficient enzymatic levels significantly limits the use of this biomarker for hyperpolarized ^{13}C MR spectroscopic imaging of prostate cancer *in vivo.* Under a revised statement of work, we investigated hyperpolarized ^{13}C MRS markers of prostate cancer metabolism in terms of Krebs's cycle activity (13C-diethylsuccinate) and oxidative stress (13C-cysteine and -cysteine analogs). Hyperpolarized [1,4-^{13}C]-diethylsuccinate was found not to be a useful in vivo imaging biomarker of Krebs's cycle activity. However, [1-^{13}C] mercaptopyruvate was determined to be a viable substrate for the in vitro assessment of oxidative stress, with in vivo studies needed to confirm and extend these findings.

15. SUBJECT TERMS
Hyperpolarized ^{13}C-MRS, metabolism, imaging, KIC, leucine, branched-chain amino acid metabolism, BCAT

16. SECURITY CLASSIFICATION OF:			17. LIMITATION OF ABSTRACT	18. NUMBER OF PAGES	19a. NAME OF RESPONSIBLE PERSON
					USAMRMC
a. REPORT	b. ABSTRACT	c. THIS PAGE			19b. TELEPHONE NUMBER *(include area code)*
U	U	U	UU	40	

Table of Contents

Page

1. Introduction……..…….…….. 4

2. Keywords…… 4

3. Overall Project Summary…… 4

4. Key Research Accomplishments…….…….…….. 17

5. Conclusion…… 17

6. Publications, Abstracts, and Presentations…… 17

7. Inventions, Patents, and Licenses…… 18

8. Reportable Outcomes…… 18

9. Other Achievements……..……. 18

10. References…… 18

11. Appendix……..…… 20

In Vivo Imaging of Branched-Chain Amino Acid Metabolism in Prostate Cancer

1. Introduction

The primary objective of this research effort is the development a novel, non-invasive imaging technique that distinguishes malignant from healthy prostate tissue based upon their distinctive metabolic profiles. Our initial approach was to use MRSI of hyperpolarized ^{13}C-ketoisocaproic acid (KIC) to interrogate its conversion to leucine (Leu) as catalyzed by branched-chain aminotransferase (BCAT). Our primary finding, summarized under **Body: Hyperpolarized ^{13}C-KIC**, was that, despite the fact that BCAT activity is altered in prostate cancer relative to healthy tissue, insufficient enzymatic levels significantly limits the applicability of this biomarker to hyperpolarized ^{13}C MR spectroscopic imaging. As a result of our prostate cancer BCAT findings and in consultation with Army Contracting Officer Representative, Dr. Melissa Cunningham, we revised our Statement of Work with the inclusion of a new Aim focused on investigating new hyperpolarized ^{13}C-labeled substrates for the assessment of prostate cancer (see Appendix 1: Revised Statement of Work). Specifically, as part of these cell-culture and xenograph experiments we have identified several new PC metabolic pathways that may be assessable using hyperpolarized ^{13}C-MRS, and the new Aim is listed below.

Revised Aim: To assess the potential for novel hyperpolarized 13C-labeled substrates for in vivo magnetic resonance spectroscopic imaging of prostate cancer metabolism.

Under this aim, we investigated hyperpolarized 13C MRS markers of TCA cycle efficiency (diethylsuccinate) and oxidative stress (cysteine and cysteine analogs). Results for each of these potential hyperpolarized ^{13}C substrates are given below in the project summary.

2. Key Words

Hyperpolarized, 13C magnetic resonance spectroscopy, ketoisocaprioic acid, diethylsuccinate, cysteine, N-acetylcysteine, mercaptopyruvate, oxidative stress.

3. Overall Project Summary

3.A Hyperpolarized ^{13}C-KIC

Introduction

The recent advent of hyperpolarized ^{13}C MRS[10], which achieves dramatically enhanced signal-to-noise ratios using dynamic nuclear polarization (DNP), provides unprecedented opportunities for real-time imaging of *in vivo* metabolic pathways critical to the identification and evaluation of cancer.[11] As first reported by Karlsson et al., [1-^{13}C]-2-ketoisocaproate ([1-^{13}C]-KIC) is a promising substrate for *in vivo* hyperpolarized ^{13}C MRS studies.[14] [1-^{13}C]-KIC is metabolized to [1-^{13}C]-leucine ([1-^{13}C]-Leu) by branched-chain aminotransferases (BCAT). In humans, BCAT has two major isoforms, BCAT1 (cytosol) and BCAT2 (mitochondria), and the enzyme also catalyzes the transamination of other BCAAs including isoleucine and valine.[15] BCAT, first identified as an overexpressed gene product in a mouse teratocarcinoma cell line,[16] is a target of the proto-oncogene *c-myc* and a putative marker for metastasis.[14,17] Following the bolus injection of hyperpolarized [1-^{13}C]-KIC, the metabolic production of [1-^{13}C]-Leu has been recently shown to correlate with BCAT levels in murine lymphoma (EL4), a tumor with high BCAT activity.[14]

Although as yet unstudied using hyperpolarized ^{13}C MRS techniques, recent reports have demonstrated the critical role of BCAAs in the proliferation of tumorgenic prostate tissue.[18] In particular, a variety of cancerous tissues are characterized by altered BCAA availability and elevated rates of BCAA oxidation.[19] BCAA metabolism is primarily altered in malignant tissue in order to meet the demands of *de novo* protein synthesis.[20] BCAAs can alternatively be utilized for energy production through a catabolic pathway mediated initiated by BCAT. Several other lines of evidence support the potential importance of BCAT metabolism in prostate cancer. In a recent clinical PET study, anti-1-amino-3-^{18}F-fluorocyclobutane-1-carboxylic acid (anti-^{18}F-FACBC), a synthetic leucine analog, was demonstrated to be a promising radiotracer for imaging prostate cancer with significant uptake in both

primary and metastatic disease.[21] In this report, BCAT activity is investigated in various models of prostate cancer and the ability of hyperpolarized [1-^{13}C]-KIC to probe BCAA metabolism is explored.

Materials and Methods

Imaging Agent: The [1-^{13}C]-KIC free acid was prepared in a 96% yield (>99% purity) from the commercially available sodium salt, [1-^{13}C]-ketoisocaproic acid (Cambridge Isotopes, Andover, MA).[14]

Dynamic Nuclear Polarization of [1-^{13}C]-KIC: The samples to be polarized consisted of 20 μL of a mixture of 8 M [1-^{13}C]-KIC and 11 mM Ox063 trityl radical. Dotarem (1 μL of a 1:50 dilution, Guerbet, France) was added just prior to polarization. The samples were polarized via DNP using a HyperSense system (Oxford Instruments Molecular Biotools, Oxford, UK), for 1–1.5 h each, to achieve liquid-state polarization at dissolution of 15%. The polarized sample was initially dissolved in a buffered solution (80 mM NaOH mixed with 40 mM TRIS buffer, 50 mM NaCl and 0.1 g/L EDTA-Na_2) followed by further dilution with a solution (40 mM TRIS buffer, 50 mM NaCl and 0.1 g/L EDTA-Na_2) leading to a 4 mM solution of the hyperpolarized substrate with a pH of ~7.5.

Prostate Cancer Cell Lines: Prostate cancer cell lines (PC-3 and DU-145) were purchased from American Type Culture Collection (ATCC, Manassas, VA). LNCaP and LAPC-4 were generously donated by the Canary Center (Stanford University). Each cell line was cultured with Dulbecco's Modified Eagle Medium (DMEM) supplemented with 10% Fetal Bovine Serum (FBS) and 1% penicillin/streptomycin and grown to >80% confluence prior to *in vitro* studies.

Spectrophotometric BCAT assays: Homogenates were prepared from both healthy and malignant patient prostate tissues, and BCAT enzyme activity levels were determined spectrophotometrically via a previously reported protocol.[22] Human prostate tissue samples were donated by the Urology Department at Stanford University. A series of enzymatic assays were also performed with TRAMP mice, which were purchased from the Charles River Laboratories (Wilmington, MA). For cellular experiments, BCAT enzyme activities in the human prostate cancer cell lines (PC-3, DU-145, LNCaP and LAPC-4) were employed. Protein concentrations for each sample were determined via the Bradford assay.

Tumor induction: Human prostate cancer cell (PC-3) xenografts were induced on either flank of nu/nu nude mice Charles River Laboratories (Wilmington, MA) through the subcutaneous injection of 2-5 million cells in a PBS/matrigel (50:50) medium. PC-3-based xenografts showed relatively slow tumor progression *in vivo* and a growth rate of ~5 mm^3/day was observed.

MR experiments: *In vitro* MRS studies (n = 3 for each cell line) were conducted on the human prostate cancer cell lines utilizing a clinical 3T GE Signa MRI scanner (GE Healthcare, Waukesha, WI, USA). Immediately before dissolution, approximately 1x10^8 PC-3 or DU-145 cells were trypsinized and resuspended in 2 ml culture media. This was followed by an injection of 2 ml of 4 mM hyperpolarized [1-^{13}C]-KIC solution, which had been polarized using a HyperSense dynamic nuclear polarizer (Oxford Instruments Molecular Biotools, Oxford, UK). All MR measurements were performed using a custom-built carbon-13 surface coil ($\varnothing_{inner}$ = 28 mm), operating at 32.16 MHz, was used for both radiofrequency excitation and signal reception. Dynamic free induction decay spectroscopic sequence (spectral width, 5,000 Hz; spectral points, 2048) with hard RF pulse excitations (pulse width, 40μs; nominal flip angle, 10^o) was used to acquire spectra with 3 s of temporal resolution (total T_{acq} = 4:00 min).

The acquired data sets were apodized by a 10-Hz Gaussian filter and zero-filled by a factor of 4 in spectral dimension. After a fast Fourier transform (using MATLAB (Mathworks Inc., Natick, MA, USA), the metabolite peaks were integrated in absorption mode after zero-order phase correction to quantify time-curves of the metabolites. For the display of spectra, both a zero- and a first-order phase correction were performed and the baseline was subtracted by fitting a spline to the signal-free regions of the smoothed spectrum. [1-^{13}C]-Leu-to-[1-^{13}C]-KIC ratios were calculated by summing first 30 time-points (90 s) of each metabolite's time-curve and taking ratios of the metabolite signal intensities.

Results

In vitro assessment of BCAT Activity in human prostate tissue: Healthy prostate tissue was found to display modest levels of BCAT activity (2.96 ± 0.10 U/gram of protein) (Figure 1a). However, prostate cancer homogenates proved to have a significant decrease in enzyme activity as 1.68 ± 0.48 U/gram of protein was detected (P = 0.0045). Although BCAT activity is not at high levels in either state, this unique metabolic profile displayed by the malignant tissue could still be exploitable as a biomarker.

In vitro assessment of BCAT Activity in models of human prostate cancer: In *ex vivo* experiments, homogenates of TRAMP prostate tissues were found to possess an enzyme activity of 0.84 ± 0.17 U/gram of protein (Figure 1b); therefore, TRAMP mice display a decreased level of BCAT activity relative to human disease. In addition, a variety of human prostate cancer cell lines were examined in order to determine whether they would serve as appropriate models for spectroscopic studies. BCAT enzymatic assays were conducted with four cell lines: PC-3, DU-145, LNCaP and LAPC-4 (Figure 1c).[23] In these experiments, the human prostate cancer cell line, PC-3, displayed the highest level of BCAT activity (1.05 ± 0.39 U/gram of protein) followed by the DU-145 cell line (0.97 ± 0.16 U/gram of protein). Both were found to have increased enzyme activity in comparison to the TRAMP mouse model. Low levels of BCAT activity were detected *in vitro* from both the LNCaP and LAPC-4 cell lines.

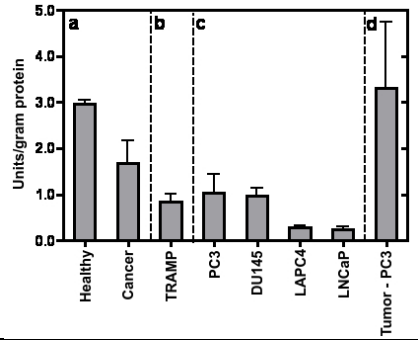

Figure 1. BCAT activity detected from the various prostate sources: (a) human, (b) TRAMP mouse model, (c) human prostate cancer cell lines and (d) PC-3 xenografts. Human prostate cancer displayed significantly lower levels of BCAT activity than normal tissue. Comparison of *in vitro* and *ex vivo* results obtained from PC-3 cell line after preparation of prostate cancer xenografts in immunocompromised nu/nu mice showed elevated enzyme activity levels after tumor induction.

Hyperpolarized ^{13}C MRS of human prostate cancer cell lines: Figure 2 displays averaged (a) spectra and (b) time-courses obtained after administration of hyperpolarized [1-^{13}C]-KIC to PC-3 cells in culture media (substrate concentration = 2 mM). In these experiments, [1-^{13}C]-KIC was observed at 172.6 ppm, and [1-^{13}C]-Leu was detected at 176.8 ppm. [1-^{13}C]-KIC•H_2O and [2-^{13}C]-KIC (natural abundance) were also present in the spectra but are not related to metabolism. The metabolic product, [1-^{13}C]-Leu, was immediately formed upon exposure of the prostate cancer cells to hyperpolarized [1-^{13}C]-KIC. The maximum product signal was detected after 15-20 s. Higher concentrations (up to 5 mM) of [1-^{13}C]-KIC did not result in increased product formation, which may suggest saturation of the BCAT active site at 2 mM. In addition, incubation (10 min) of cells with unlabelled leucine (1 mM) prior to analysis did not substantially affect [1-^{13}C]-Leu signal. Experiments were also performed with DU-145 cells and analogous metabolic products and time-courses were found (results not shown).

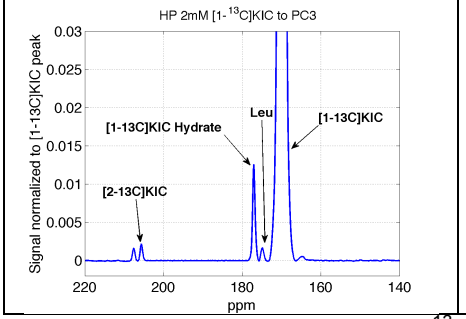

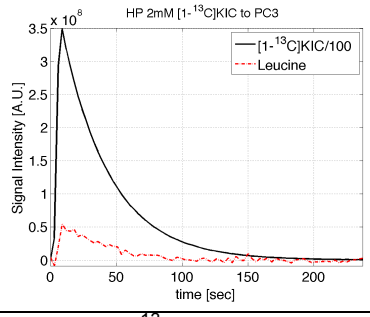

Figure 2. (a) Representative time-averaged spectra obtained from PC-3 prostate cancer cell line after incubation with of 2 mM [1-^{13}C]-KIC. (b) Representative time course demonstrate rapid uptake of hyperpolarized substrate and production of metabolic product, [1-^{13}C]-Leu.

Figure 3 summarizes the [1-^{13}C]-Leu-to-[1-^{13}C]-KIC ratios obtained for PC-3 and DU-145 cell lines from hyperpolarized ^{13}C MRS analysis. The metabolic product was observed over the first 100 s of the experiment, and PC-3 cells displayed a conversion ratio of 1.73 ± 0.38 a.u (mean ± ste, n = 3). [1-^{13}C]-Leu production and the area under the curve for this metabolic product were higher in DU-145 cells, and a 2.20 ± 0.47 ratio (mean ± ste, n = 3) was found. These results are consistent with our *in vitro* BCAT activity assays of these prostate cancer cell lines (Figure 1c). In addition, the [1-^{13}C]-Leu-to-[1-^{13}C]-KIC ratio provides a metric for evaluation of BCAT activity via hyperpolarized ^{13}C MRS.

Evaluation of BCAT activity in animal models of prostate cancer ex vivo: PC-3 xenografts were grown in immunocompromised nu/nu mice, and after euthanization, the tumors were examined *ex vivo* for BCAT activity. These results are summarized in Figure 1d. PC-3 xenografts displayed a 3.31 ± 1.43 U/gram of protein level of BCAT activity, which represents a >2.5-fold increase in enzyme activity in respect to the *in vitro* results. Similar elevated levels in tissues relative to the corresponding cell lines have been observed in tumor models of murine lymphoma and rat mammary adenocarcinoma.[14] In addition, as part of this initial study of hyperpolarized [1-^{13}C]-KIC for analysis of BCAA metabolism in prostate cancer, preliminary *in vivo* studies were conducted with PC-3 xenografts as well as TRAMP mice (n = 2). However, despite the levels of BCAT activity found *ex vivo* for these tumor models, [1-^{13}C]-Leu production has yet to be observed *in vivo*.

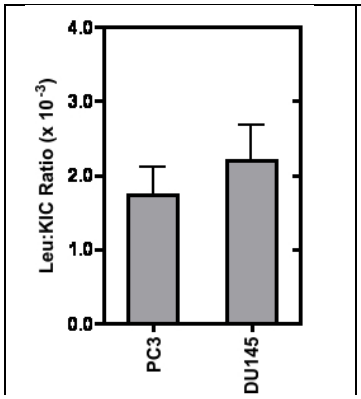

Figure 3. Metabolite ratio observed from *in vitro* hyperpolarized ^{13}C MR experiments with PC-3 and DU-145 prostate cancer cell lines. [1-^{13}C]-Leu-to-[1-^{13}C]-KIC ratio reflects the BCAT activity displayed in the respective cell lines.

Discussion

In this report, we investigated BCAT activity in several models of prostate cancer via both traditional and spectroscopic methods. While the work of Karlsson et al. demonstrated the initial observation of metabolite formation from hyperpolarized [1-^{13}C]-KIC,[14] this study sought to validate [1-^{13}C]-KIC as a practical method for characterizing malignant prostate tissues. Through initial examination of BCAT activity *in vitro* via conventional spectrophotometric methods, we demonstrated that alterations in BCAA metabolism could assist in the evaluation of various prostate cancer models. In particular, healthy human prostate tissue was found to have an elevated BCAT levels relative to malignant tissue. Normal prostate tissue primarily relies upon fatty acid metabolism and glycolysis for energy production because the tricarboxylic acid (TCA) cycle is inhibited due to the high concentration of zinc. However, in prostate cancer, the TCA cycle is restored and can also contribute to meeting the energy requirements of the cell;[24] therefore, the observed changes in BCAT enzyme activity are in principle consistent with BCAAs being utilized for protein synthesis rather than for energy production.

Animal and cellular models are vital tools for exploring the onset and progression of human disease. In addition, a sufficient model, which maintains comparable rates of BCAT activity as human prostate cancer, was necessary for spectroscopic evaluation with hyperpolarized [1-^{13}C]-KIC. However, there remain a limited number of reports concerning alterations in BCAA demand and metabolism in models of prostate cancer. Through the initial spectrophotometric examination of the TRAMP mouse and prostate cancer cell lines, PC-3 and DU-145 cell lines were discovered to have similar BCAT activity levels as detected in human disease. These models were then employed in the development of ^{13}C MRS techniques for analyzing BCAA metabolism with hyperpolarized [1-^{13}C]-KIC in prostate cancer. To this end, we demonstrated that hyperpolarized [1-^{13}C]-KIC could be employed *in vitro* for models of prostate cancer. In both the PC-3 and DU-145 cell lines, BCAT activity was successfully examined through measuring [1-^{13}C]-Leu production after administration of the molecular probe. In the validation of this technique, we correlated our spectroscopically determined BCAT activities (reflected in [1-^{13}C]-Leu-to-[1-^{13}C]-KIC ratio) with those detected via standard spectrophotometric methods. The agreement of these results further validates the probe as measuring BCAT activity and supports [1-^{13}C]-KIC as a tool assessing of BCAT activity in models of prostate cancer. Importantly, this [1-^{13}C]-Leu-to-[1-^{13}C]-KIC ratio provides direct insight into the state of BCAA metabolism and, specifically, the propensity for BCAA oxidation, a pathway that can be utilized to drive energy production in proliferating cells.

Conclusion

Based upon our analysis, BCAA metabolism is altered in human prostate cancer relative to healthy tissue. However, only low levels of BCAT activity were found in all animal and cellular models examined. Despite these modest activities, we have successfully demonstrated that BCAT activity can be determined with hyperpolarized ^{13}C MRS *in vitro* using [1-^{13}C]-KIC, and the ratio of metabolite product to substrate ([1-^{13}C]-Leu-to-[1-^{13}C]-KIC) could be used as metric for monitoring changes in

metabolic state. These spectroscopic results were further correlated with traditional *in vitro* assays. **However, despite the fact that BCAT activity is altered in prostate cancer relative to healthy tissue, insufficient enzymatic levels significantly limit the potential use of this biomarker for hyperpolarized ^{13}C MR spectroscopic imaging *in vivo*.**

3.B Hyperpolarized ^{13}C-DES

Introduction

The tricarboxylic acid cycle (TCA) performs an essential role in the regulation of energy and metabolism, and deficiencies in this pathway are commonly correlated with various diseases. However, the development of non-invasive techniques for the assessment of the cycle *in vivo* has remained challenging. In this work, the applicability of a novel imaging agent, [1,4-^{13}C]-diethylsuccinate, for hyperpolarized ^{13}C metabolic imaging of the TCA cycle was explored. *In vivo* spectroscopic studies were conducted in conjunction with *in vitro* analyses to determine the metabolic fate of the imaging agent. Contrary to previous reports (Zacharias, N. M. et. al. *J. Am. Chem. Soc.* **2012**, *134*, 934-943)(3225), [^{13}C]-labeled diethylsuccinate was primarily metabolized to succinate-derived products not originating from TCA cycle metabolism. These results illustrate potential issues of utilizing dialkyl ester analogs of TCA cycle intermediates as molecular probes for hyperpolarized ^{13}C metabolic imaging.

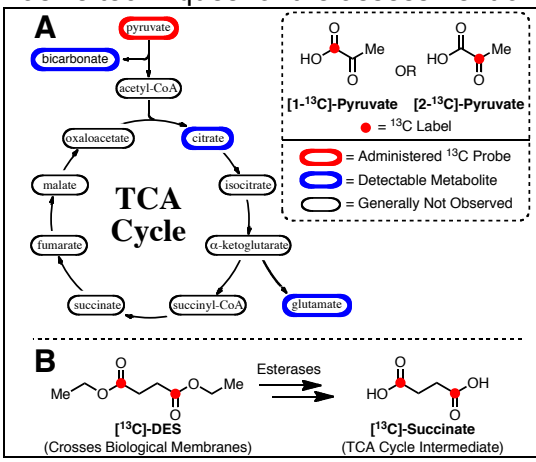

Figure 4. (A) Overview of compounds related to the TCA cycle that are generally detected when employing hyperpolarized [1-^{13}C]- or [2-^{13}C]-pyruvate. (B) Strategy for probing TCA cycle metabolism. DNP substrate, [^{13}C]-DES, enters intracellular environment and is converted into TCA cycle intermediate.

Experimental Details

General: All reagents were purchased from Aldrich Chemical Co. unless otherwise noted and used without further purification.

Synthesis of [1,4-^{13}C]-Diethylsuccinate: [^{13}C]-DES was prepared by the following procedure: In an oven-dried 100 mL round-bottom flask equipped with magnetic stir bar, 425 mg (3.54 mmol) of [1,4-^{13}C]-succinic acid (99% 1,4-^{13}C, CLM-1084, Cambridge Isotopes, Andover, MA) was added. After the addition of anhydrous ethanol (35 mL), 1.8 mL (1.54 g, 14.2 mmol) of trimethylsilyl chloride was added dropwise via syringe over the course of two minutes. The reaction was allowed to stir at room temperature. After 5 h, the reaction was quenched with 10 mL of saturated sodium bicarbonate solution. Additional bicarbonate was removed via filtration, and ethanol was removed under vacuum. The desired product was extracted from the aqueous solution with 4 x 8 mL of dichloromethane. Organic layers were combined, dried over anhydrous sodium sulfate, and filtered; the solvent was removed by evaporation and 480 mg (77% yield) of pure product was isolated as a colorless oil. ^{1}H NMR ($CDCl_3$, 500 MHz) δ 4.15 (q, *J* = 7 Hz, 4H), 2.60 (s, 4H), 1.12 (t, *J* = 7 Hz, 6H) ppm; ^{13}C NMR ($CDCl_3$, 125 MHz) δ 172.4, 60.8, 29.1, 14.1 ppm.

Synthesis of [1,4-^{13}C]-Monoethylsuccinate: In order to reference [^{13}C]-MES, a sample containing [^{13}C]-succinate, [^{13}C]-MES, and [^{13}C]-DES was prepared by the following procedure: In an oven-dried 100 mL round-bottom flask equipped with magnetic stir bar, 100 mg (0.83 mmol) of [1,4-^{13}C]-succinic acid was added. After the addition of anhydrous ethanol (5 mL), 0.106 mL (90.5 mg, 0.83 mmol) of trimethylsilyl chloride was added dropwise via syringe over the course of one minute. The reaction was allowed to stir at room temperature. After 30 min, the reaction was quenched with 2 mL of saturated sodium bicarbonate solution. Additional bicarbonate was removed via filtration, and ethanol was removed under vacuum. The desired product was extracted from the aqueous solution with 4 x 4 mL of dichloromethane. Organic layers were combined, dried over anhydrous sodium sulfate, and filtered; the solvent was removed by evaporation to yield a sample with 2:3:6 ratio of [^{13}C]-succinate:[^{13}C]-DES:[^{13}C]-MES as determined by ^{1}H-NMR (D_2O).

Dynamic Nuclear Polarization of [1,4-^{13}C]-Diethylsuccinate: The samples to be polarized consisted of 40 μL of a mixture of [^{13}C]-DES (6 M, neat) and 20-mM α,γ-Bisdiphenylene-β-phenylallyl

(BDPA) radical. The samples were polarized via dynamic nuclear polarization using a HyperSense system (Oxford Instruments Molecular Biotools, Oxford, UK). The polarized samples were dissolved in a solution of 40-mM TRIS buffer, 50-mM NaCl and 0.1 g/L EDTA-Na_2, leading to an 80-mM solution of the hyperpolarized substrate with a pH of approximately 7.5.

In Vivo Experiments: Healthy male Wistar rats (393 ± 48 g body weight, n = 3) were injected with 2.6-3.2 mL of the hyperpolarized solution (target dose = 1 mmol/kg body weight) through a tail vein catheter at a rate of approximately 0.25 mL/s. The time from dissolution to start of injection was approximately 20 s.

The rats were anesthetized initially with 2.5% isoflurane in oxygen (1.5 L/min) for tail vein catheterization. Respiration, rectal temperature, heart rate and oxygen saturation were monitored throughout the experiments with temperature regulated using a warm water blanket placed underneath the animals. Each animal received two injections of the hyperpolarized substrate, approximately 1.5 - 2 h apart. All animal procedures were approved by the SRI Institutional Animal Care and Use Committee.

All experiments were performed on a clinical 3T Signa MR scanner (GE Healthcare, Waukesha, WI), using a custom-built ^{13}C transmit/receive surface coil (dia = 28 mm) placed over the heart with rat supine. A quadrature volume rat ^{1}H coil (diameter = 70 mm) was used for anatomical localization and to confirm the position of the ^{13}C coil with respect to the heart. Single-shot fast spin-echo (FSE) ^{1}H MR images in the axial, sagittal and coronal planes with nominal in-plane resolution of 0.47 mm and 2-mm slice thickness were acquired as anatomical references for prescribing the ^{13}C MRS experiments. A non-selective pulse-and-acquire sequence with an excitation flip angle of 6°, spectral width of 5 kHz and 2048 points was used to acquire ^{13}C spectra from the heart every 3 s over a 4-min period starting at the same time as the [^{13}C]-DES injection.

In Vitro Experiments: *In vitro* experiments were performed in order to facilitate the identification of the metabolites observed from [^{13}C]-DES *in vivo* experiments. These experiments include exposure of [^{13}C]-DES to:

(1) Pig Liver Esterase. [^{13}C]-DES (10 mM) was incubated at 37 °C with pig liver esterase (7.5 Units/mL) in RPMI media supplemented with 10% fetal bovine serum and 5% penicillin-streptomycin. Pig liver esterase has been previously shown to selectively cleave a single ester of DES (3926). After 5 min, the solution was then analyzed via ^{13}C-NMR on an 11.7 T instrument to determine the product distribution.

(2) Rat blood. Blood draws were performed from healthy male Wistar rats via tail vein catheter. The freshly drawn blood (1 mL) was immediately dosed with [^{13}C]-DES (100 mM) and the solution was incubated at 37 °C. At various times points (1, 5, 20 and 60 min), a 0.25 mL aliquot of the solution was removed, and the sample was quenched with methanol (0.25 mL). Each sample was then analyzed via ^{13}C-NMR on an 11.7 T instrument to determine the metabolic fate of [^{13}C]-DES.

(3) Homogenates of Rat Heart. Rat hearts were obtained from male Wistar rats and samples were maintained at -80 °C. Samples were thawed, homogenized in buffer (210 mM mannitol, 70 mM sucrose, 5 mM MOPS and 1 mM EDTA in D_2O), and centrifuged at 3000*g* to obtain desired homogenates. These homogenates were dosed with [^{13}C]-DES (10 mM) and incubated at 37 °C for 5 min. These samples were analyzed at various time points (5, 20, 60 and 300 min) via ^{13}C-NMR on an 11.7 T instrument to determine the product distribution.

Results and Discussion

[^{13}C]-DES was successfully formulated for dynamic nuclear polarization through the addition of 20 mM BDPA to 6 M [^{13}C]-DES (neat). The solid-state polarization build-up time constant was 1517 ± 91 s (n = 8) with a liquid-state polarization level of 5.5% (Figure 5). The T_1 (^{13}C-labeled carbonyls) was found to be 37.9 s in solution at 3 T. No observable toxicity (pulse or respiration) was detected upon i.v. administration of a TRIS-buffered solution containing up to 80 mM [^{13}C]-DES. In addition, no detectable ester hydrolysis of [^{13}C]-DES to yield [1,4-^{13}C]-monethylsuccinate ([^{13}C]-MES) or [1,4-^{13}C]-succinate was observed when [^{13}C]-DES was exposed to the dissolution conditions (40-mM TRIS buffer, 50-mM NaCl and 0.1 g/L EDTA-Na_2, pH = 7.5) for a period of up to 20 min. Furthermore, no hydrolysis was observed during the dissolution process, which requires superheating the frozen sample (see supporting information).

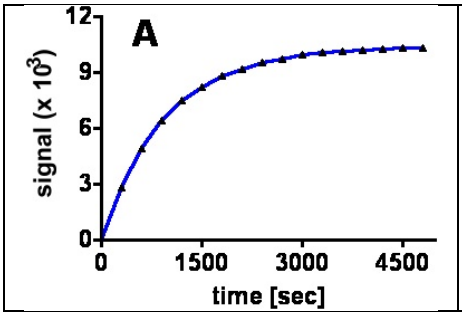

Figure 5. (A) Polarization buildup curves (3.35 T, 1.4 K) of [^{13}C]-DES doped with 20 mM BDPA taken at P(+) = 94.116 GHz. (B) Liquid-state T_1 decay (3 T, 298 K) of [^{13}C]-DES samples with 20 mM BDPA (T_1 = 38 s).

Figure 6 displays a representative (A) spectrum and (B) time-resolved stackplot obtained from a rat heart after i.v. administration of hyperpolarized [^{13}C]-DES. In these experiments, a bolus injection of 80 mM [^{13}C]-DES was performed, and the substrate was observed at 176.4 ppm along with three other distinct signals at 182.5, 177.6, and 172.7 ppm. Lower substrate concentration (40 mM) did not significantly affect metabolites observed or the relative quantities detected. Importantly, our spectra closely resembled the previously observed product distribution found in the report by Zacharias et al. on PHIP-mediated hyperpolarization of [1-^{13}C, 2,3-d_2]-diethylsuccinate (32). The PHIP study of DES did, however, consistently detect a minor signal at 175.2 ppm, which is not observed in our experiments and was indicated to be fumarate. The previous work assigned the three major signals at 182.5, 177.6, and 172.7 ppm to succinate, malate and aspartate, respectively. Despite the overall similarity of the spectra, we found several inconsistencies with the previous report's assignments: (1) the chemical shifts found in the metabolite reference data did not agree with the assigned spectra (32) and (2) a single resonance was attributed to asymmetric compounds (i.e. malate and aspartate) that should display two resolvable signals due to scrambling of the ^{13}C label between the C1 and C4 positions (4027). Given these issues, we sought to reexamine the fate of [^{13}C]-DES *in vivo* and conduct a thorough study to determine the metabolite distribution.

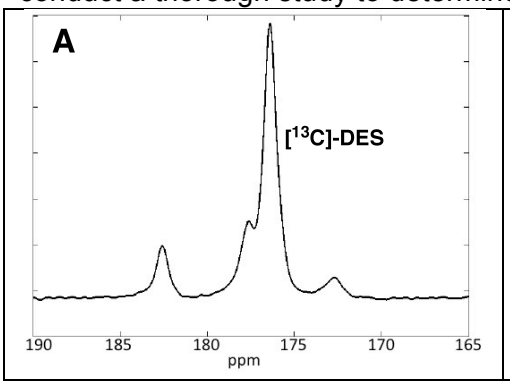

Figure 6. (A) Representative time-averaged spectra from 6 - 45 s obtained from heart beginning at the administration of 80 mM [^{13}C]-DES. (B) Representative stackplot of spectra obtained from heart at 3 s intervals beginning at the administration of 80 mM [^{13}C]-DES.

In order to evaluate whether the metabolites observed *in vivo* correspond to products of esterase cleavage (i.e.[^{13}C]-MES and/or [1,4-^{13}C]-succinate), a reference standard was prepared with a mixture of these products. A sample containing a 2:3:6 ratio of succinate:DES:MES was prepared through treating [1,4-^{13}C]-succinate with 1.0 equivalent of trimethylsilyl chloride in ethanol at room temperature (Figure 7). The ratio of metabolites was determined through analysis of the ^{1}H-NMR of the sample. This standard was then used to reference the MES and succinate carbonyl shifts via ^{13}C-NMR on an 11.7 T NMR instrument. Both [1,4-^{13}C]-succinate (183.7 ppm) and [^{13}C]-DES (176.4 ppm) yield a single resonance as they are symmetric molecules. It was discovered that peaks 182.5 and 177.6 ppm correspond to [^{13}C]-MES and do not originate from metabolism via the TCA cycle (Figure 3B). Based upon the difference in chemical shifts, [1,4-^{13}C]-succinate should be resolvable *in vivo* from the signal corresponding to [4-^{13}C]-MES, so we conclude that [1,4-^{13}C]-succinate is not forming in detectable quantities during the time frame of the *in vivo* experiment.

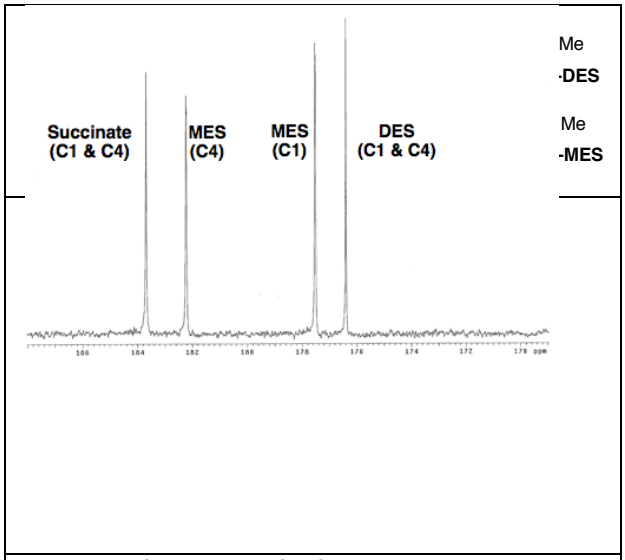

Figure 7. Synthesis of reference sample containing succinate, DES and MES. ^{13}C-NMR spectrum displays the relative chemical shift of these compounds.

DES was developed as agent for hyperpolarized ^{13}C metabolic imaging because it was hypothesized to cross biological membranes more readily than the parent compound. However, given that esterases are known to be present in the blood (4128), we sought to examine whether cleavage of [^{13}C]-DES to [^{13}C]-MES could occur extracellularly prior to entry into the cytosol or mitochondria. In order to initially confirm that [^{13}C]-DES was a substrate for esterases, the substrate was incubated with pig liver esterase. As anticipated, [^{13}C]-MES was cleanly formed and two signals (182.5 and 177.6 ppm) were observed. Next, [^{13}C]-DES was added to a freshly drawn rat blood sample, and [^{13}C]-MES was again rapidly formed in the first 5 min (Figure 8). No signal corresponding to the unknown compound (172.7 ppm) was detected under these conditions.

In order to determine the identity of this unknown metabolite, we sought to generate, isolate and characterize the species via *in vitro* methods. [^{13}C]-DES was incubated with homogenates of rat heart tissue. In all trials, conversion to [^{13}C]-MES was observed. However, only trace levels of the unknown metabolite at 172.7 ppm were detected, and unfortunately, the product could not be successfully characterized via this process. Furthermore, prostate cancer cells (PC-3) were dosed with [^{13}C]-DES (10 mM), but no metabolic product corresponding to the signal at 172.7 ppm was observed (see supporting information).

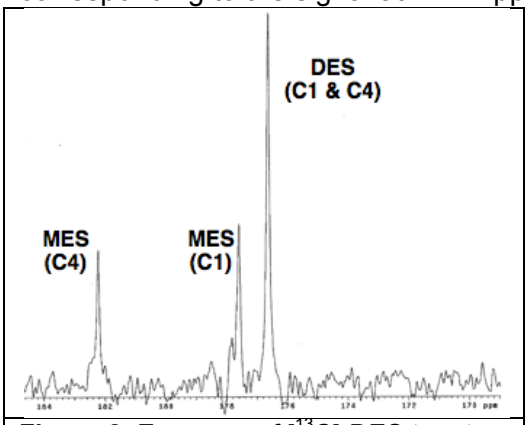

Figure 8. Exposure of [^{13}C]-DES to rat blood. Representative spectrum (20 min) shown to display the conversion to [^{13}C]-MES via endogenous esterases.

In order to assign the unknown signal, a series of succinate-derived compounds were referenced and compared with previously published TCA cycle metabolites (Table 1). As described above, the signal at 172.7 ppm did not coincide with any intermediate of the TCA cycle. The chemical shifts of aspartate and glutamate, which are products typically formed from TCA cycle intermediates, were also not consistent with the unknown metabolite. However, based upon this analysis, the unknown species in the *in vivo* spectra was assigned to [1,4-^{13}C]-succinic anhydride. This assignment was also in agreement with the fact that only a single resonance is observed, which would be expected from a symmetrical molecule like [1,4-^{13}C]-succinic anhydride. In addition, [1,4-^{13}C]-succinic anhydride maintains the carbon skeleton of [^{13}C]-DES without performing any C-C bond cleavage steps, which in the TCA cycle would be associated with the loss and subsequent observation of [^{13}C]-CO_2 at 125 ppm, which is in fast exchange with [^{13}C]-bicarbonate at 161 ppm. Neither resonance was observed in the *in vivo* experiment.

Succinate would be expected to have a relatively slow rate of dehydration under normal physiological conditions (4229-4330); therefore, it is unlikely that [1,4-^{13}C]-succinate converts to [1,4-^{13}C]-succinic anhydride. However, monoesters of succinate have been shown to be unstable due to the close proximity of the neighboring carboxyl group (44). Although the precise mechanism of the formation of [1,4-^{13}C]-succinic anhydride remains unclear, this process could potentially be enzyme- or esterase-mediated from [^{13}C]-MES. Upon formation, [1,4-^{13}C]-succinic anhydride should slowly hydrolyze to furnish [1,4-^{13}C]-succinate, which may then be metabolized by the TCA cycle but is not observed at detectable levels in our experiments.

Conclusion

Although the diester analog, [^{13}C]-DES, of [^{13}C]-succinate is more adept at crossing cellular membranes, the substrate is not successfully metabolized by the TCA cycle. [^{13}C]-DES is initially metabolized to [^{13}C]-MES via endogenous esterases, which may occur in the blood rather than the intracellular environment. Further metabolism of the substrate leads to formation of [1,4-^{13}C]-succinic anhydride. Contrary to previous reports of PHIP hyperpolarized [^{13}C]-labeled DES, TCA cycle-derived metabolites (succinate, malate and aspartate) were not observed.

3.C Hyperpolarized ^{13}C- Cysteine

Introduction

Oxidative stress (OS) is a state of imbalance that arises from overproduction of reactive radical species, such as reactive oxygen species (ROS), within normal cells. ROS are products of normal metabolisms and they can be beneficial or harmful to cells and tissues based on their biological concentrations. At physiological low levels, ROS function as messengers in intracellular signaling and regulation, whereas excess ROS induce oxidative modification of biological macromolecules that affects many protein functions. As cells lose their ability to maintain physiological level of ROS, they become susceptible to mutation and death. Indeed, OS has been implicated in various diseases such as atherosclerosis, diabetes, neurodegeneration and cancer. In plasma, there is redox interaction between the oxidized species cystine (CySS) and the reduced molecule cysteine (Cys), which forms the basis for a standard in vitro assay for the degree of OS in the blood. This measure of oxidative stress is currently determined by liquid chromatography of plasma to provide the ratio [Cys]/[CySS], which will be relatively high in a state of low OS, and lower in high OS conditions. There is currently no noninvasive technique available to measure in vivo OS levels in organs other than the blood.

The aim of this line of research is the development of an in vivo, non-invasive technique for imaging and quantifying OS. If achieved, give promise for substantially advancing the scientific study of OS and improving the general health of the population as oxidative stress plays a critical role in cancer (e.g. prostate) as well as other pathologies. For example, the reducing environment of many cancers might be revealed via a relatively high local [Cys]/[CySS] ratio, and the ability to image OS would allow the assessment of the effectiveness of techniques designed for OS mitigation.

Methods

For this work, we focused on hyperpolarize ^{13}C-MRS to achieves dramatically enhanced signals to measure real-time metabolic rates. We first performed several experiments to investigate the optimal conditions to polarize ^{13}C-Cysteine samples. Single-labeled ^{13}C1-Cysteine (A, Fig 9) were dissolved in 1:1 (v/v) water/glycerol (6M) or 2:3 (v/v) water/DMA solution (2M), mixed with trityl radical OX063 (15 mM) and a 1:50 Dotarem solution (0.1 v/v), and polarized at ~94 GHz in a field of 3 T. We were also interested in identifying the specific carbon position of the Cysteine that exhibited the highest possible polarization. Therefore, we investigated the polarization level of each individual carbon using a triple-labeled Cysteine (^{13}C3-^{2}H3-^{15}N-Cysteine) (B, Fig 9) by co-polarizing the cysteine sample with unlabeled pyruvic acid (neat, 1M). The increased solubility of ^{13}C3-Cysteine in pyruvic acid was aimed to improve its polarization level, while the deuterium exchange was designed to increase the T1 relaxation time. In addition, we were interested in developing other hyperpolarized redox-sensitive MRS probes that utilized sulfur-based chemistry to image and quantify oxidative stress in vivo. Specifically, we focused on two other MRS probes, N-acetyl cysteine (NAC) (C, Fig 9) and Mercaptopyruvate (MCP) (D, Fig 9). NAC is a common antioxidant that has been widely used as a prescription drug and dietary supplement. Due to its close similarity with cysteine, NAC is likely to undergo oxidation to form disulfide product, while its acetyl group is important for improved solubility and cellular uptake. MCP exists as a downstream product of cysteine metabolism in the cell and is implicated in mitochondrial redox homeostasis. Given its structural similarity to pyruvate, we envision MCP to be highly polarizable and possess long T1 relaxation time, possibly comparable to the standard pyruvic acid measurement. Furthermore, MCP is responsible for generating H_2S in cells, which has been identified as an important signaling molecule in many pathophysiological processes such as neurodegeneration, inflammation and cardiovascular diseases. More importantly, MCP can be converted to pyruvate in vivo by the enzyme mercaptosulfur transferase (MST), enabling the interrogation of both redox state and cellular metabolism. Therefore, we hypothesized that any changes in the ratio of MCP to its oxidized form, MCP-s-s-MCP, is indicative of an oxidative stress measurement (e.g. H_2S production) and monitoring the fate of the resulting downstream products (i.e.

pyruvate) reflects cellular metabolism (**Fig 10**). Efforts are currently underway to synthesize ^{13}C-labeled NAC and MCP as they are not commercially available.

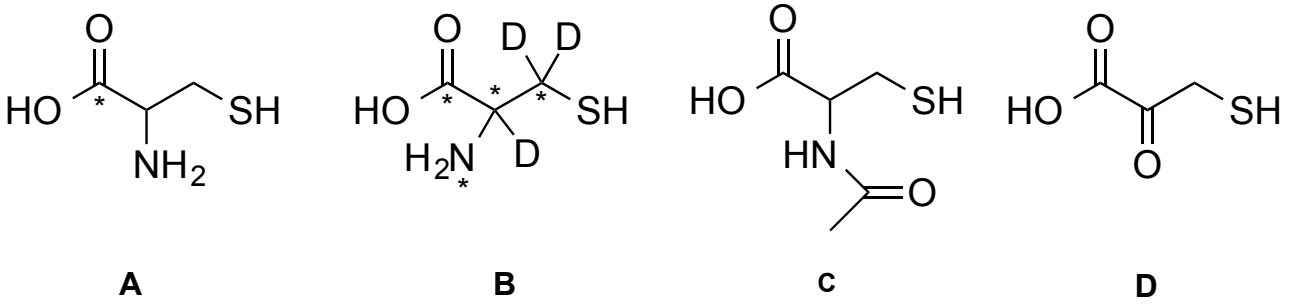

Figure 9. Structure of Hyperpolarized Redox-sensitive MRS Probe. A) Single-Labeled Cysteine (^{13}C1-Cysteine); B) Triple-Labeled Cysteine (^{13}C3-^{2}H3-^{15}N-Cysteine); C) N-acetyl Cysteine; D) Mercaptopyruvic Acid.

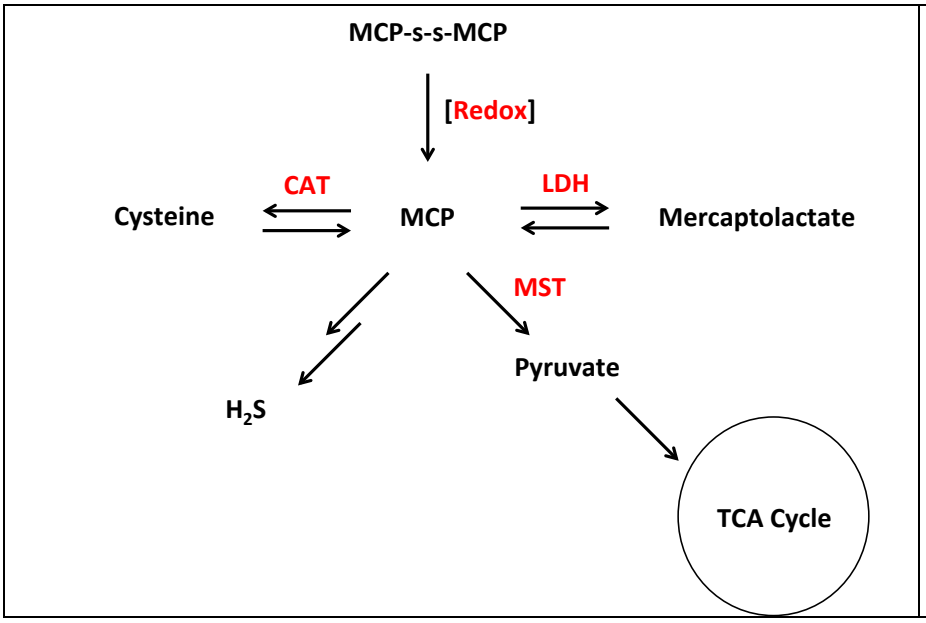

Figure 10. Mercaptopyruvate disulfide (MCP-s-s-MCP) undergoes cellular reduction to mercaptopyruvate (MCP). MCP is converted to cysteine or mercaptolactate, metabolized to pyruvate and hydrogen sulfide (H_2S). CAT = cysteine amino transferase; LDH = lactate dehydrogenase; MST = mercaptosulfur transferase.

We next evaluated the feasibility of using [Cys]/[CySS] ratio as a biomarker for therapy monitoring *in vitro.* To achieve this goal, we examined the chemical shift differences between the reduced (Cys) and oxidized (CySS) species by high-resolution ^{13}C nuclear magnetic resonance (NMR). These experiments were performed independent of polarization level (i.e. natural ^{13}C abundance) to identify whether Cys-CySS is chemically distinguishable and thus viable candidates for redox measurement. We postulated that the resolution between these two species must be large enough *in vitro* (11.7 T) to be identifiable *in vivo.* To generate oxidized CySS, we reacted cysteine hydrochloride with 1 equimolar H_2O_2 (30% solution) and 0.01 equimolar NaI in water (pH ~ 7.4) for 24 hr. The mixture was purified using size exclusion column (LH-20, GE Healthcare) and the desired CySS was collected as a lyophilized product. Candidate **C** and **D** were also examined as described above from which the oxidized species were generated and compared to their reduced form for their chemical shift difference.

Results

Polarization of ^{13}C1- cysteine in water/glycerol or water/DMA mixture gave comparable low liquid-state polarization level (~ 2-3%) with T_1 relaxation time of 22 sec (Fig 11). Given the low C1 polarization level, we measured hyperpolarization at different carbon position using triple-labeled cysteine to identify whether different carbon ^{13}C-labeling gave more desirable polarization. Our results

indicated that ^{13}C1 exhibited the highest level of polarization and the longest T_1 relaxation time among the different cysteine carbons (Fig 12).

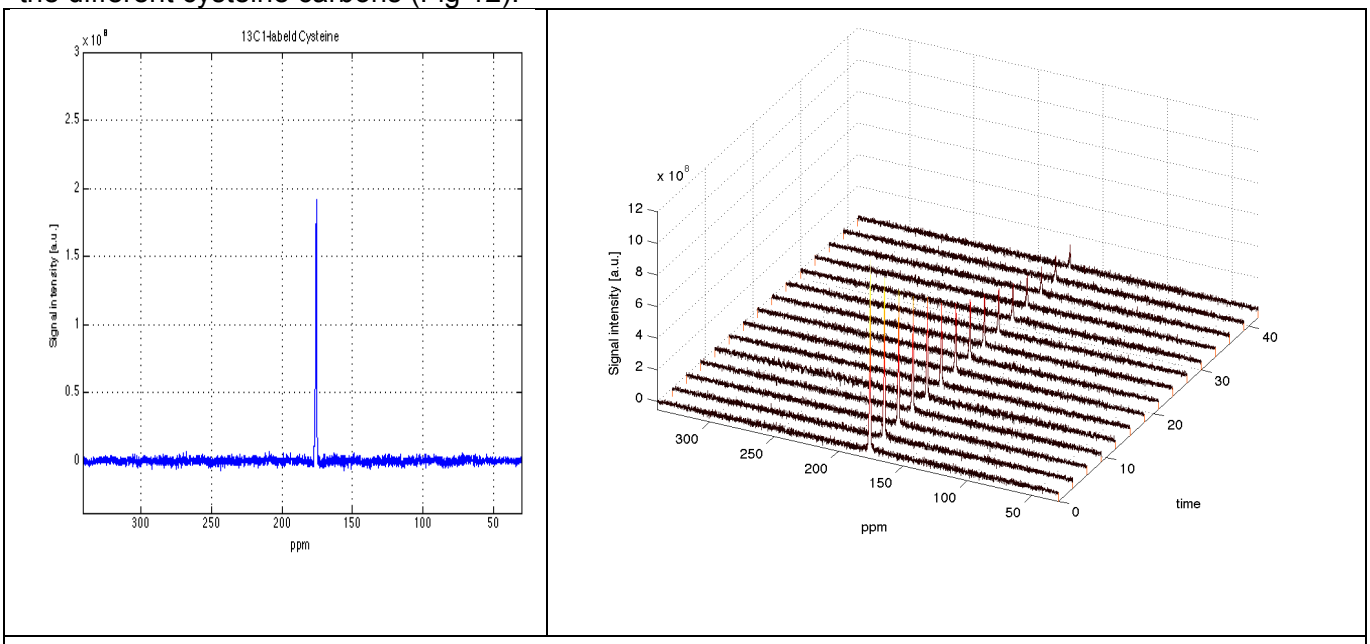

Figure 11. Polarization signal and T_1 relaxation of ^{13}C1-Cysteine

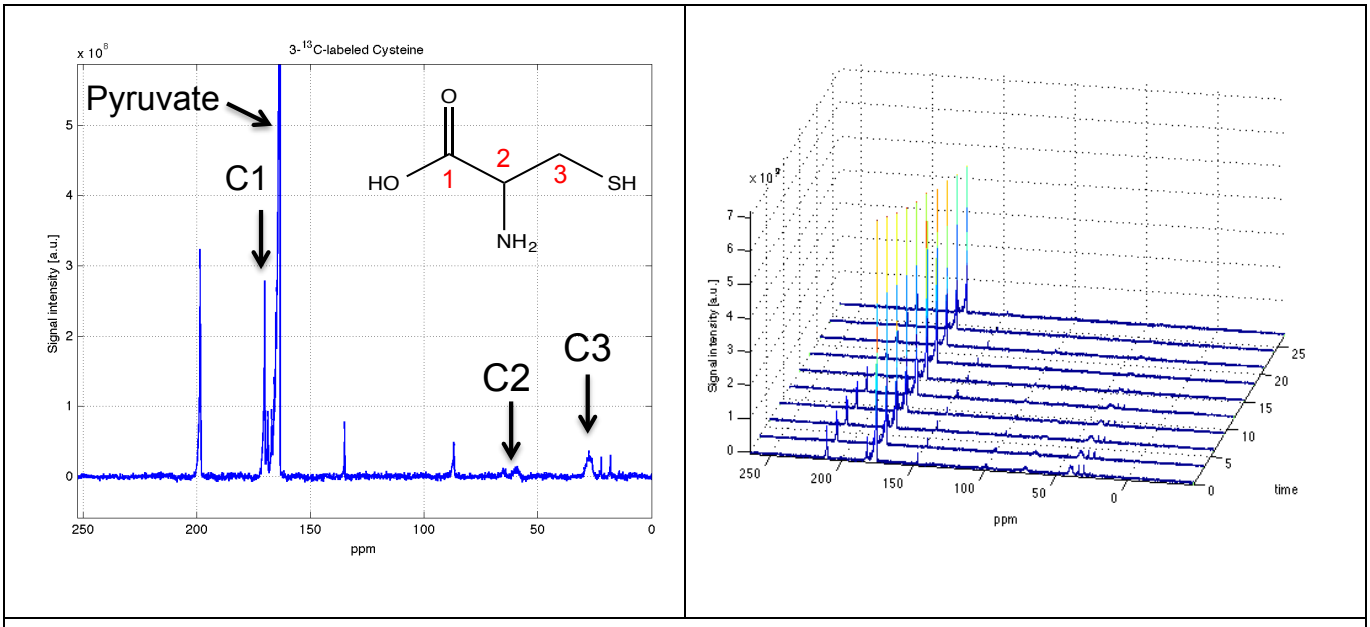

Figure 12. Polarization signal and T_1 relaxation of ^{13}C3-^{2}H3-^{15}N-Cysteine

Based on the low polarization of ^{13}C1-Cysteine, we sought to investigate other potential MRS probes for OS measurement. We examined NAC because of its structural similarity with cysteine, and compared the chemical shift differences between its reduced and oxidized species. Similar to cysteine, we reasoned that the polarization level of NAC would have been greatest at the C1 position while the biggest chemical shift due to any redox changes would have been at the C3 position. As ^{13}C-labeled NAC is not commercially available, we tested our hypothesis with high-res ^{13}C NMR and observed a minimal δ0.4 ppm change at the C1 carbon (Fig 13). Expectedly, the largest chemical shift difference (δ13.7 ppm) was observed at the C3 carbon. Similarly, we investigated the chemical shift difference of cysteine by high-res 13C NMR and found a small δ1.2 ppm change at the C1 position *in vitro* (Fig 14).

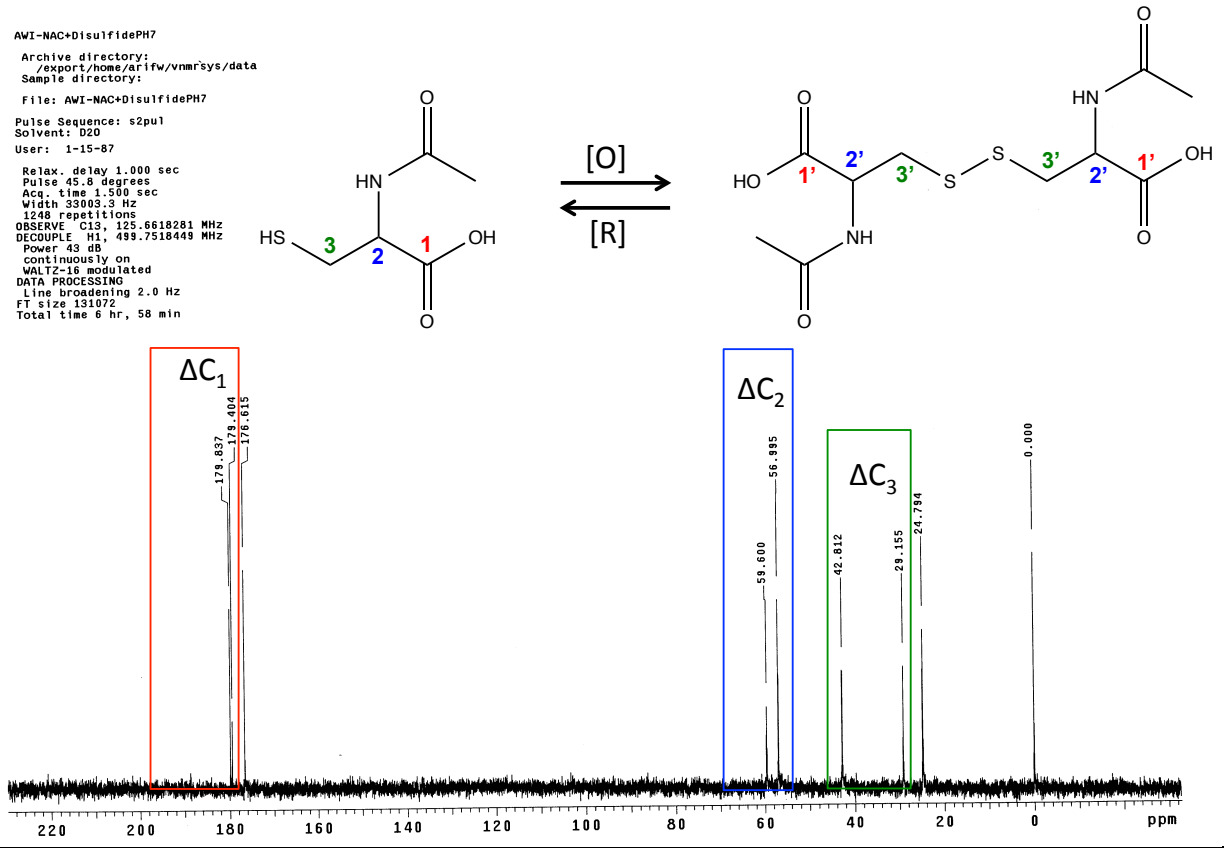

Figure 13. High-resolution (11.7T) NMR of NAC and NAC Disulfide

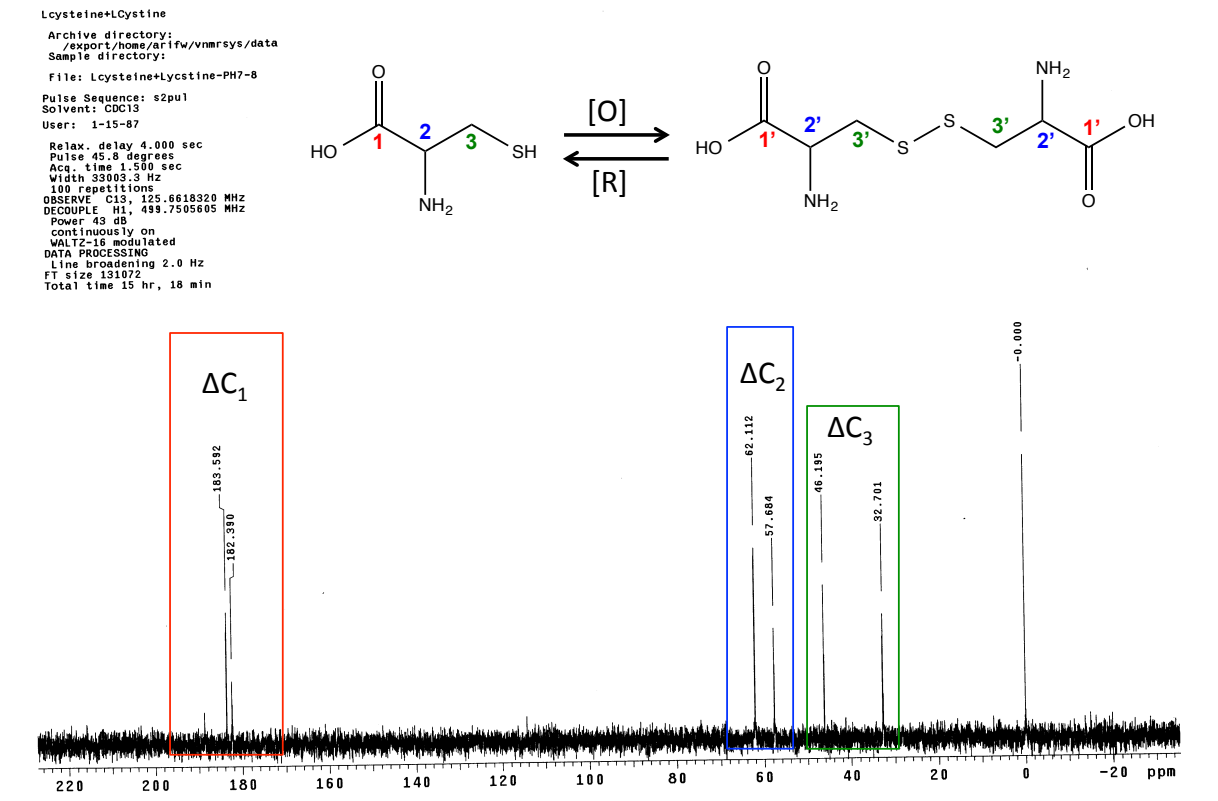

Figure 14. High-resolution (11.7T) NMR of cysteine and cysteine (CySS)

Figures 13 and 14 demonstrate too small of a change in C1 chemical shift with oxidation of both cysteine and NAC to be useful for *in vivo* detection. In addition, ^{13}C labeling at the C1 carbon was limiting even though it gave the highest polarization level among all other carbon positions. As a result, we explored MCP as potential MRS probes for OS measurement. As ^{13}C-labeled MCP is not commercially available, we measured the chemical shift between the oxidized and reduced MCP species with high-res ^{13}C NMR and observed a δ3.3 ppm change at the C1 carbon (Fig 15). While the chemical shift is small, we are confident that it should be detectable *in vivo*. Furthermore, its chemical reactivity (within the typical sec-min T_1 relaxation time frame) is consistent with both cellular redox and metabolism changes, and made MCP viable for measuring OS *in vivo*.

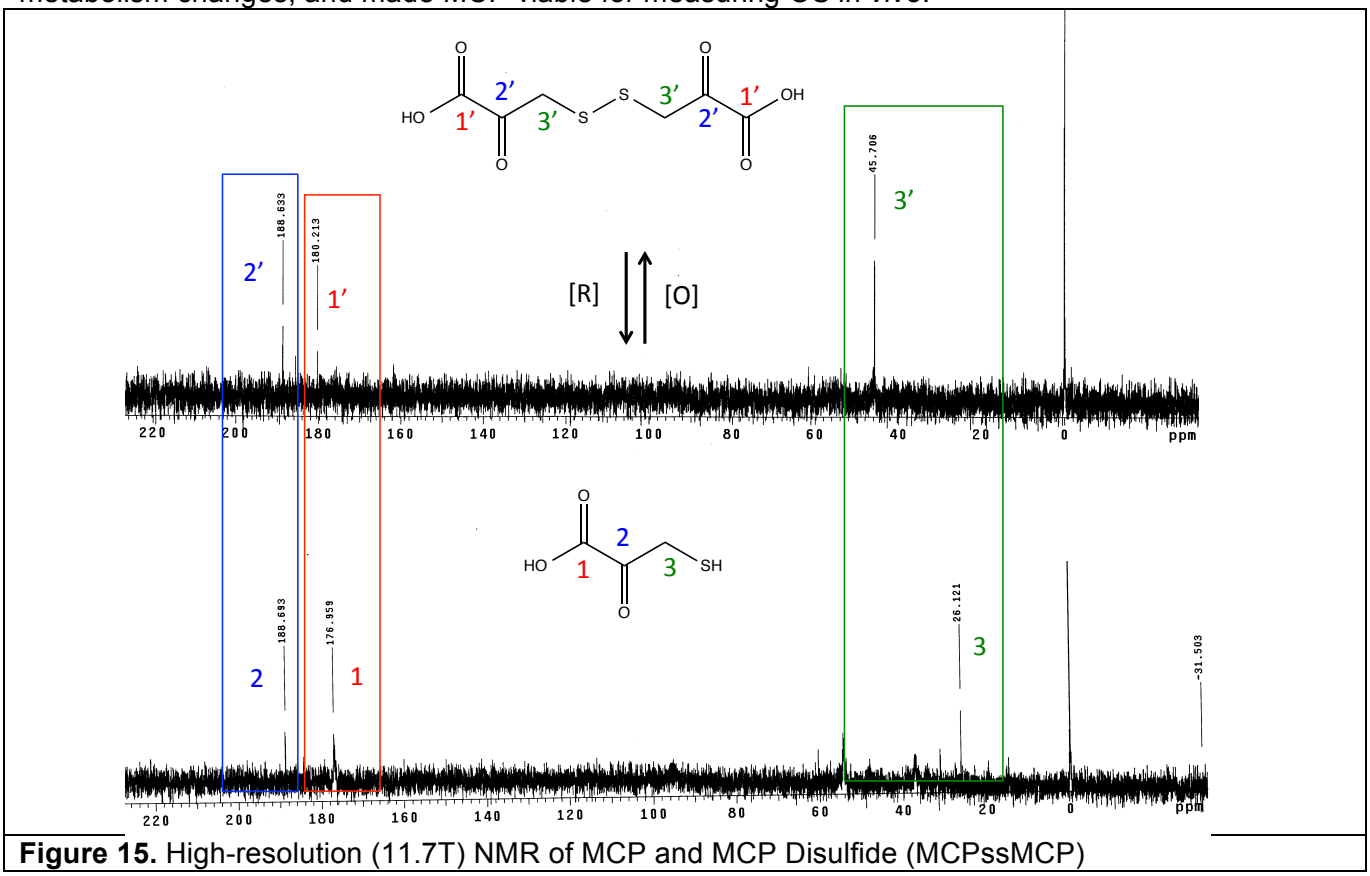

Figure 15. High-resolution (11.7T) NMR of MCP and MCP Disulfide (MCPssMCP)

Conclusions

In this report, we described our efforts in characterizing ^{13}C-Cysteine as a potential MRS probe for OS measurement. Polarization of ^{13}C-Cysteine by dynamic nuclear polarization achieved a low liquid-state polarization level (~ 3%) with a T1 relaxation time of 22 sec. Efforts to improve cysteine hyperpolarization by targeting different carbon positions were not successful as demonstrated by the low polarization level of the triple-labeled ^{13}C3-Cysteine. In addition, we sought to identify whether NAC and/or MCP are viable for OS measurement *in vivo*. Based on high-res NMR experiments, we reported δ0.4 and δ3.3 ppm chemical shift change at the C1 carbon of NAC and MCP respectively. Given the small difference, we anticipate oxidized and reduced NAC to be chemically indistinguishable *in vivo*. In comparison, MCP exhibited a larger chemical shift than cysteine (δ1.2 ppm) at its C1 carbon. **This difference, coupled with the potentially larger polarization level (as shown by its close analog ^{13}C-pyruvic acid), suggests that MCP could be exploited for measuring cellular redox state *in vivo*. However, to date, we have not found a stable enough synthesis process to generate the quantities of MCP needed for in vivo experiments.**

4. Key Research Accomplishments

- Branched-chain amino acid metabolism is altered in human prostate cancer relative to healthy tissue. However, only low levels of BCAT activity were found in all prostate cancer animal and cellular models examined.
- BCAT activity can be determined with hyperpolarized ^{13}C MRS *in vitro* using [1-^{13}C]-KIC, and the ratio of metabolite product to substrate ([1-^{13}C]-Leu-to-[1-^{13}C]-KIC) can be used as metric for monitoring changes in metabolic state.
- Despite the fact that BCAT activity is altered in prostate cancer relative to healthy tissue, insufficient enzymatic levels significantly limits the use of this biomarker for hyperpolarized ^{13}C MR spectroscopic imaging of prostate cancer *in vivo*.
- Contrary to previous reports of PHIP hyperpolarized [^{13}C]-labeled DES, TCA cycle-derived metabolites (succinate, malate and aspartate) are not observed following the bolus injection of hyperpolarized [1,4-^{13}C]-diethylsuccinate.
- Within the time constraints of hyperpolarized 13C MRS, [^{13}C]-DES is initially metabolized to [^{13}C]-MES via endogenous esterases, which may occur in the blood rather than the intracellular environment. Further metabolism of the substrate leads to formation of [1,4-^{13}C]-succinic anhydride.
- Although [1-^{13}C]cysteine is readily polarizable, its exhibits and insufficiently small chemical shift with oxidation to be useful for in vivo hyperpolarized 13C MRS studies. However, [1-^{13}C] mercaptopyruvate does exhibit the necessary properties to be useful as an in vivo biomarker of oxidative stress. Larger quantities of [1-^{13}C] mercaptopyruvate need to be synthesized to verify this finding in vivo.

5. Conclusions

The initial objective of this research was the development of a noninvasive imaging method to assess branched-chain amino acid metabolism (known to be modified in prostate cancer [PC]) to distinguish malignant from healthy tissue. Our approach used magnetic resonance spectroscopy (MRS) and spectroscopic imaging (MRSI) MRSI of hyperpolarized ^{13}C-ketoisocaproic acid (KIC) to interrogate its conversion to leucine as catalyzed by branched-chain aminotransferase (BCAT). We first determined that while BCAT activity is altered in prostate cancer relative to healthy tissue, insufficient enzymatic levels significantly limits the use of this biomarker for hyperpolarized ^{13}C MR spectroscopic imaging of prostate cancer *in vivo.* Under a revised statement of work, we investigated hyperpolarized ^{13}C MRS markers of prostate cancer metabolism in terms of Krebs's cycle activity (13C-diethylsuccinate) and oxidative stress (^{13}C-cysteine and -cysteine analogs). Hyperpolarized [1,4-^{13}C]-diethylsuccinate was found not to be a useful in vivo imaging biomarker of Krebs's cycle activity. However, [1-^{13}C]mercaptopyruvate was determined to be a viable substrate for the in vitro assessment of oxidative stress, with in vivo studies needed to confirm and extend these findings.

6. Publications, Abstracts, and Presentations

Lay Press

Nothing to report.

Peer-Reviewed Scientific Journals

1. Josan S, Hurd R, Billingsley K, Senadheera L, Park JM, Yen YF, Pfefferbaum A, Spielman D, Mayer D. Effects of isoflurane anesthesia on hyperpolarized (13)C metabolic measurements in rat brain. Magn Reson Med. 2013 Oct;70(4):1117-24. doi: 10.1002/mrm.24532. Epub 2012 Oct 19. PubMed PMID: 23086864; PubMed Central PMCID: PMC3674171.
2. Billingsley KL, Josan S, Park JM, Tee SS, Spielman-Sun E, Hurd R, Mayer D, Spielman D. Hyperpolarized [1,4-(13)C]-diethylsuccinate: a potential DNP substrate for in vivo metabolic imaging. NMR Biomed. 2014 Mar;27(3):356-62. doi: 10.1002/nbm.3071. Epub 2014 Jan 13. PubMed PMID: 24421249; PubMed Central PMCID: PMC4005842.
3. Billingsley KL, Park JM, Josan S, Hurd R, Mayer D, Spielman-Sun E, Nishimura DG, Brooks JD, Spielman D. The feasibility of assessing branched-chain amino acid metabolism in cellular models of prostate cancer with hyperpolarized [1-(13)C]-ketoisocaproate. Magn Reson

Imaging. 2014 Sep;32(7):791-5. doi: 10.1016/j.mri.2014.04.015. Epub 2014 Apr 28. PubMed PMID: 24907854; PubMed Central PMCID: PMC4099288.

Invited Articles

Nothing to report.

Abstracts

1. Senadheera L., Mayer D., Josan S. Yen Y Darpolor M., Luong R., Spielman D. M., Xing L., "Hyperpolarized 13C MRSI for Assessing Radiation Response of Prostate Cancer in Transgenic Mice," in the annual meeting of American Association of Physicists in Medicine (AAPM), Vancouver , BC, Canada, 2011
2. Senadheera L., Mayer D., Josan S., Darpolor M., Yen Y., Luong R., Spielman D. M., Xing L., "Hyperpolarized 13C Magnetic Resonance Metabolic Imaging for Assessing Therapeutic Response of Prostate Cancer to Radiotherapy," in Innovative Minds in Prostate Cancer Today (IMPaCT), Orlando, FL, USA, 2011
3. Josan S, Billingsley K, Senadheeera L, Park JM, Yen YF, Hurd R, Pfefferbaum A, Spielman D, Mayer D, Effect of isoflurane anesthesia on hyperpolarized 13C metabolic measurements in rat brain, World Molecular Imaging Conference, Dublin, Ireland, 2012.

Presentations during the last year (*denotes corresponding manuscript).

1. *Billingsley K, Josan S, Park JM, Yen YF, Hurd RE, Mayer D, Nishimura DG, Brooks J, Spielman D, Branched-Chain Amino Acid Metabolism in Prostate Cancer: Hyperpolarized [1-13C]-Ketoisocaproate as a Novel Molecular Probe, Program Number: 3933, 21st ISMRM Annual Scientific Meeting, Salt Lake City, UT, 2013.
2. *Billingsley K, Josan, S, Park JM, Tee SS, Yen YF, Hurd R, Mayer D, Spielman D, Hyperpolarized [1,4-13C]-Diethylsuccinate: A Potential DNP Substrate for in vivo Metabolic Imaging, Program Number: 3935, 21st ISMRM Annual Scientific Meeting, Salt Lake City, UT, 2013.

7. Inventions, Patents, and Licenses

Nothing to report.

8. Reportable Outcomes

- Identification of [1-^{13}C]mercaptopyruvate as a possible hyperpolarized ^{13}C MRS substrate for the in vivo assessment of oxidative stress.

9. Other Achievements

- Training – Dr. Kelvin Billingsley successfully completed his postdoctoral appointment under this award and obtained a new position as an Assistant Professor of Chemistry and Biochemistry, San Francisco State University.
- New grant funding obtained: GE Healthcare BlueSky Research Award: "Imaging and mitigation of oxidative stress".

10. References

1. Ferlay J, Shin HR, Bray F, Forman D, Mathers C, Parkin DM. GLOBOCAN 2008 v1.2, Cancer Incidence and Mortality Worldwide: IARC CancerBase No. 10 [Internet] Lyon, France: International Agency for Research on Cancer, 2010.
2. Singh H, et al. Predictors of prostate cancer after initial negative systematic 12 core biopsy. *J Urol* 2004; **171**: 1850-4.
3. Jemal A, et al. Cancer statistics. *CA Cancer J Clin* 2008; **58**: 71-96.
4. Makarov DV. Biomarkers for Prostate Cancer. *Ann Rev Med* 2009; **60**: 139-151.
5. Pound CR, et al. Natural history of progression after PSA elevation following radical prostatectomy. *JAMA* 1999; **281**: 1591-7.
6. Kirkham AP, Emberton M, Allen C. How good is MRI at detecting and characterising cancer within the prostate? *Eur Urol* 2006; **50**: 1163-74.

7. Kurhanewicz J, Vigneron DB. Advances in MR spectroscopy of the prostate. *Magn Reson Imaging Clin N Am* 2008; **16**: 697-710.
8. Jiang Z, Woda BA. Diagnostic utility of alpha-methylacyl CoA racemase (P504S) on prostate needle biopsy. *Adv Anat Pathol* 2004; **11**: 316-21.
9. Jadvar, H. Molecular imaging of prostate cancer: PET radiotracers. *AJR Am J Roentgenol* 2012; **199**: 278-291.
10. Ardenkjaer-Larsen JH, et al. Increase in signal-to-noise ratio of > 10,000 times in liquid-state NMR. *Proc Natl Acad Sci U S A* 2003; **100**: 10158-63.
11. Day SE, et al. Detecting tumor response to treatment using hyperpolarized 13C magnetic resonance imaging and spectroscopy. *Nat Med* 2007; **13**: 1382-1387.
12. Kurhanewicz J, et al. Current and potential applications of clinical 13C MR spectroscopy. *J Nucl Med* 2008; **49**: 341-4.
13. Nelson, S. Implementation and Applications of Hyperpolarized C-13 MRI in Medicine. in 16th Scientific Meeting of the International Society of Magnetic Resonance in Medicine. 2008. Toronto, Ontario, Canada.
14. Karlsson M, et al. Imaging of branched chain amino acid metabolism in tumors with hyperpolarized (13)C ketoisocaproate. *Int J Cancer* 2010; **127**: 729-736.
15. Brosna JT, et al. Branched-chain amino acids: enzyme and substrate regulation. *J. Nutr*. 2006; **136**: 207S-211S.
16. Niwa O, et al. A cDNA clone overexpressed and amplified in a mouse teratocarcinoma line. *Nucleic Acids Res*, 1990; **18**: 6709.
17. Ben-Yosef T, et al. Involvement of Myc targets in c-myc and N-myc induced human tumors. *Oncogene* 1998; **17**: 165-71.
18. Wang Q, et al. Androgen receptor and nutrient signaling pathways coordinate the demand for increased amino acid transport during prostate cancer progression. *Cancer Research* 2011; **71**: 7525-7536.
19. Baracos VE, et al. Investigations of branched-chain amino acids and their metabolites in animal models of cancer. *J Nutr* 2006; **136**: 237S-242S.
20. Blomstrand, E. Branched-chain amino acids: metabolism, physiological, function, and application. *J Nutr* 2006; **136**: 269S-273S.
21. Schuster DM, et al. Initial experience with the radiotracer anti-1-amino-3-18F-fluorocyclobutane-1-carboxylic acid with PET/CT in prostate carcinoma. *J Nucl Med* 2007; **48**: 56-63.
22. Schadewaldt P, et al. Coupled enzymatic assay for estimation of branched-chain L-amino acid aminotransferase activity with 2-oxo acid substrates. *Anal Biochem* 1996; **238**: 65–71.
23. Sobel RE, et al. Cell lines used in prostate cancer research: a compendium of old and new lines. *J Urol* 2005; **173**: 342-59.
24. Dakubo GD, et al. Altered metabolism and mitochondrial genome in prostate cancer. *J Clin Pathol* 2006; **59**: 10-16.
25. Zacharias NM, Chan HR, Sallasuta N, Ross BD, Bhattacharya P. Real-time molecular imaging of tricarboxylic acid cycle metabolism in vivo by hyperpolarized 1-13C diethyl succinate. *J. Am. Chem. Soc.* 2012; **134**: 934-943.
26. Yen Y-F, Nagasawa K.; Nakada T. Promising application of dynamic nuclear polarization for in vivo 13C MR imaging. *Mag. Reson. Med. Sci.* 2011; **10**: 211-217.
27. Ager DJ, Prakash I. Pig liver esterase catalyzed hydrolyses of diesters. A new route to the syntheses of achiral half-esters. *Synth. Commun.* 1995; **25**: 739-742.
28. Merritt ME, Harrison C, Sherry AD, Malloy CR, Burgess SC. Flux through hepatic pyruvate carboxylase and phosphoenolpyruvate carboxykinase detected by hyperpolarized 13C magnetic resonance. *Proc. Natl. Acad. Sci. U.S.A.* 2011; **108**: 19084-19089.
29. Rudakova EV, Boltneva NP, Makhaeva GF. Comparative analysis of esterase activities of human, mouse, and rat blood. *Bull. Exp. Biol. Med.* 2011; **152**: 73-75.
30. Higuchi T, Miki T. Reversible formation of amides from free carboxylic acid and amine in aqueous solution. A case of neighboring group facilitation. *J. Am. Chem. Soc.* 1961; **83**: 3899-3901.
31. Chen H-T, Chang J-G, Musaev DG, Lin MC. Computational study on kinetics and mechanisms of unimolecular decomposition of succinic acid and its anhydride. *J. Phys. Chem. A* 2008; **112**: 6621-6629.

32. Dörwald FZ. *Side Reactions in Organic Synthesis*, Wiley-VCH: Weinheim, 2005 and reference therein.

11. Appendices

Reprints of Josan, et al, MRM, 2013. Billingsley, NMR Biomed, 2014, and Billinglsey, MRI, 2014.

Magnetic Resonance Imaging 32 (2014) 791–795

Contents lists available at ScienceDirect

Magnetic Resonance Imaging

journal homepage: www.mrijournal.com

Original contributions

The feasibility of assessing branched-chain amino acid metabolism in cellular models of prostate cancer with hyperpolarized [1-^{13}C]-ketoisocaproate

Kelvin L. Billingsley [a,*], Jae Mo Park [b], Sonal Josan [b,c], Ralph Hurd [d], Dirk Mayer [e], Eleanor Spielman-Sun [f], Dwight G. Nishimura [g], James D. Brooks [h], Daniel Spielman [b,g]

[a] Department of Chemistry & Biochemistry, San Francisco State University, San Francisco, CA 94132, USA
[b] Department of Radiology, Stanford University, Stanford, CA 94305, USA
[c] Neuroscience Program, SRI International, Menlo Park, CA 94025, USA
[d] Applied Sciences Laboratory, GE Healthcare, Menlo Park, CA 94025, USA
[e] Department of Diagnostic Radiology and Nuclear Medicine, University of Maryland–Baltimore, Baltimore, MD 21201, USA
[f] Department of Chemistry, Oberlin College, Oberlin, OH 44074, USA
[g] Department of Electrical Engineering, Stanford University, Stanford, CA 94305, USA
[h] Department of Urology, Stanford University, Stanford, CA 94305, USA

ARTICLE INFO

Article history:
Received 16 January 2014
Revised 28 March 2014
Accepted 15 April 2014

Keywords:
Hyperpolarized carbon-13
Dynamic nuclear polarization
Magnetic resonance spectroscopy/ spectroscopic imaging
Prostate cancer
Branched-chain aminotransferase

ABSTRACT

Recent advancements in the field of hyperpolarized ^{13}C magnetic resonance spectroscopy (MRS) have yielded powerful techniques capable of real-time analysis of metabolic pathways. These non-invasive methods have increasingly shown application in impacting disease diagnosis and have further been employed in mechanistic studies of disease onset and progression. Our goals were to investigate branched-chain aminotransferase (BCAT) activity in prostate cancer with a novel molecular probe, hyperpolarized [1-^{13}C]-2-ketoisocaproate ([1-^{13}C]-KIC), and explore the potential of branched-chain amino acid (BCAA) metabolism to serve as a biomarker. Using traditional spectrophotometric assays, BCAT enzymatic activities were determined in vitro for various sources of prostate cancer (human, transgenic adenocarcinoma of the mouse prostate (TRAMP) mouse and human cell lines). These preliminary studies indicated that low levels of BCAT activity were present in all models of prostate cancer but enzymatic levels are altered significantly in prostate cancer relative to healthy tissue. The MR spectroscopic studies were conducted with two cellular models (PC-3 and DU-145) that exhibited levels of BCAA metabolism comparable to the human disease state. Hyperpolarized [1-^{13}C]-KIC was administered to prostate cancer cell lines, and the conversion of [1-^{13}C]-KIC to the metabolic product, [1-^{13}C]-leucine ([1-^{13}C]-Leu), could be monitored via hyperpolarized ^{13}C MRS.

1. Introduction

Prostate cancer is the second most frequently diagnosed cancer in men worldwide [1]. It is currently diagnosed by blind biopsy, prompted by elevated serum prostate-specific antigen levels [2], but nearly 20% of these procedures result in false negatives [3]. There is also no reliable indicator for establishing the aggressiveness of prostate tumors [4]. These deficiencies have resulted in an increased number of painful biopsies, over-treatment of the disease and undesired side effects (e.g. impotence) for patients. The accurate non-invasive characterization of prostate cancer remains a critical unmet clinical challenge.

The development of imaging methods could find immediate application in prognostication and treatment planning in prostate cancer [5]. Current protocols for prostate magnetic resonance imaging (T_2-weighted MRI) provide anatomic details, but are limited by the failure to accurately assess tumor invasion and tumor aggressiveness [6]. Proton (^{1}H) MR spectroscopy, exploiting metabolic characteristics, has also been advocated as a potential method of diagnosing and monitoring prostate cancer [7]. However, ^{1}H-MR spectroscopy currently provides only moderately increased sensitivity and specificity beyond conventional T_2-weighted MRI, diffusion-weighted MRI, and dynamic contrast-enhanced MRI. Although molecular imaging techniques have also been advanced, the best molecular target identified to date, α-methyl CoA racemase, has shown minimal utility [8], and ^{18}F-FDG PET has had limited clinic applicability in the examination of prostate tumors due

* Corresponding author at: Department of Chemistry & Biochemistry, San Francisco State University, Thornton Hall 729, San Francisco, CA 94132, USA. Tel.:+1 415 405 0732; fax:+1 415 338 2384.
E-mail address: klbillin@sfsu.edu (K.L. Billingsley).

http://dx.doi.org/10.1016/j.mri.2014.04.015
0730-725X/

largely to poor uptake and rapid excretion of the tracer [9]. PET and PET/CT imaging techniques employing [^{11}C]- and [^{18}F]-labeled choline have also been used for the detection of prostate cancers and have shown particular benefit with the evaluation of disease recurrence [10].

The recent advent of hyperpolarized ^{13}C magnetic resonance spectroscopy (MRS) [11], which achieves dramatically enhanced signal-to-noise ratios using dynamic nuclear polarization (DNP), provides unprecedented opportunities for real-time imaging of in vivo metabolic pathways critical to the identification and evaluation of cancer [12]. To date, the leading in vivo hyperpolarized metabolic imaging candidate is [^{13}C]-labeled pyruvate ([^{13}C]-Pyr). Several important applications with this agent have been proposed including measurement of high glycolytic rates in tumors, and metabolic abnormalities in ischemic heart disease and inflammatory processes [13]. Studies of small and large animal models are currently ongoing, and [^{13}C]-Pyr is the first substrate for hyperpolarized MRS to enter clinical trials [14].

Novel substrates are also emerging for this powerful imaging technology [15]. As first reported by Karlsson et al. [16], [1-^{13}C]-2-ketoisocaproate ([1-^{13}C]-KIC) is a promising substrate for hyperpolarized ^{13}C MRS studies (Fig. 1) [17]. [1-^{13}C]-KIC is metabolized to [1-^{13}C]-leucine ([1-^{13}C]-Leu) by branched-chain aminotransferases (BCAT). In humans, BCAT has two major isoforms, BCAT1 (cytosol) and BCAT2 (mitochondria), and the enzyme also catalyzes the transamination of other branched-chain amino acids (BCAA) including isoleucine and valine [18]. BCAT, first identified as an overexpressed gene product in a mouse teratocarcinoma cell line [19], is a target of the proto-oncogene *c-myc* and a putative marker for metastasis [16,20]. Following the bolus injection of hyperpolarized [1-^{13}C]-KIC, the metabolic production of [1-^{13}C]-Leu has been recently shown to correlate with BCAT levels in murine lymphoma (EL4), a tumor with high BCAT activity [16].

Although unstudied using hyperpolarized ^{13}C MRS techniques, recent reports have demonstrated the critical role of BCAAs in the proliferation of tumorgenic prostate tissue [21]. In particular, a variety of cancerous tissues are characterized by altered BCAA availability and elevated rates of BCAA oxidation [22]. BCAA metabolism is primarily altered in malignant tissue in order to meet the demands of de novo protein synthesis [23]. BCAAs can alternatively be utilized for energy production through a catabolic pathway mediated initiated by BCAT. Several other lines of evidence support the potential importance of BCAT metabolism in prostate cancer. In a recent clinical PET study, anti-1-amino-3-^{18}F-fluorocyclobutane-1-carboxylic acid (anti-^{18}F-FACBC), a synthetic leucine analog, was demonstrated to be a promising radiotracer for imaging prostate cancer with significant uptake in both primary and metastatic disease [24]. Although hyperpolarized [1-^{13}C]-KIC has shown initial promise for investigating BCAA metabolism, this agent has yet to be thoroughly explored in other cancer models. In this report, BCAT activity is investigated in various models of prostate cancer and the ability of hyperpolarized [1-^{13}C]-KIC to probe BCAA metabolism is examined.

2. Methods

2.1. Imaging agent

The [1-^{13}C]-KIC free acid was prepared from the sodium salt, [1-^{13}C]-ketoisocaproic acid (Cambridge Isotopes, Andover, MA) [16] by the following procedure: [1-13C]-ketoisocaproic acid, sodium salt (250 mg, 1.63 mmol) was charged into a 10-mL glass vial and dissolved in water (3 mL). The solution was acidified to pH = 1 with 1 M hydrochloric acid (0.50 mL) and the aqueous layer was extracted with diethyl ether (3 × 3 mL). The combined organic layers were dried with sodium sulfate, filtered, and concentrated to afford [1-^{13}C]-KIC (214 mg, 96% yield) as colorless oil.

2.2. Polarization of [1-^{13}C]-KIC

The polarized samples consisted of 20 μL of a mixture of 8 M [1-^{13}C]-KIC and 11 mM Ox063 trityl radical. Dotarem (1 μL (1:50 dilution) Guerbet, France) was added just prior to polarization. The samples were polarized via DNP using a HyperSense system (Oxford Instruments Molecular Biotools, Oxford, UK), for 1–1.5 h each, to achieve liquid-state polarization at dissolution of 15%. The polarized sample was initially dissolved in a buffered solution (80 mM NaOH, 40 mM TRIS, 50 mM NaCl, 0.1 g/L EDTA-Na_2) followed by further dilution with non-basic buffered solution leading to a 4 mM solution of the hyperpolarized substrate with a pH of ~7.5.

2.3. Prostate cancer cell lines

Prostate cancer cell lines (PC-3 and DU-145) were purchased from American Type Culture Collection (Manassas, VA). LNCaP and LAPC-4 were donated by the Stanford Canary Center. Cell line was cultured with DMEM supplemented with 10% FBS and 1% penicillin/streptomycin and grown to >80% confluence prior to in vitro studies.

2.4. Spectrophotometric BCAT assays

Homogenates were prepared from both healthy and malignant patient prostate tissues, and BCAT activity levels were determined spectrophotometrically ($n = 4$ for both healthy and malignant tissues) [25]. Protein concentrations were determined via the Bradford assay. Tissues had been collected after patients signed informed consent under a Stanford University Institutional Review Board-approved protocol. A series of enzymatic assays ($n = 4$) were also performed with transgenic adenocarcinoma of the mouse prostate (TRAMP) mice (Charles River Laboratories, Wilmington, MA). For cellular experiments, BCAT activities in the human prostate

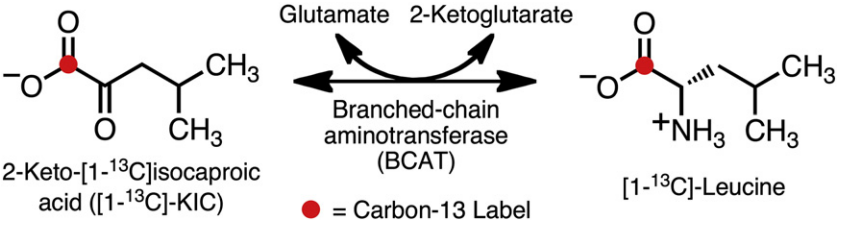

Fig. 1. Metabolism of [1-^{13}C]-KIC to [1-^{13}C]-Leu via BCAT.

cancer cell lines (PC-3, DU-145, LAPC-4 and LNCaP) were employed ($n \geq 3$). All BCAT activities are expressed as mean ± ste.

2.5. MR experiments

In vitro MRS studies ($n = 3$ for each cell line) were conducted on the human prostate cancer cell lines utilizing a clinical 3 T GE Signa MRI scanner (GE Healthcare, Waukesha, WI, USA). Immediately before dissolution, approximately 1×10^8 PC-3 or DU-145 cells were trypsinized and resuspended in 2 mL culture media. This was immediately followed by an injection of 2 mL of 4 mM hyperpolarized [1-^{13}C]-KIC solution. MR measurements were performed using a custom-built carbon-13 surface coil ($\varnothing_{inner} = 28$ mm), operating at 32.16 MHz, used for both radiofrequency (RF) excitation and signal reception. A dynamic free induction decay spectroscopy sequence (spectral width, 5000 Hz; spectral points, 2048) with non-selective RF pulse excitations (pulse width, 40 μs; nominal flip angle, 10°) was used to acquire spectra with 3 s of temporal resolution (total T_{acq} = 4:00 min).

The acquired data sets were apodized by a 10-Hz Gaussian filter and zero-filled by a factor of 4 in the spectral dimension. After a fast Fourier transform (MATLAB, Mathworks Inc., Natick, MA), the metabolite peaks were integrated in absorption mode after zero-order phase correction to quantify time-curves of the metabolites. For the display of spectra, both a zero- and a first-order phase correction were performed and the baseline was subtracted by fitting a spline to the signal-free regions of the smoothed spectrum. [1-^{13}C]-Leu-to-[1-^{13}C]-KIC ratios were calculated by summing the first 30 time-points (90 s) of each metabolite's time curve and taking ratios of the metabolite signal intensities.

3. Results

3.1. In vitro assessment of BCAT Activity in human prostate tissue

Healthy prostate tissue was found to display modest levels of BCAT activity (2.96 ± 0.10 U/gram of protein) (Fig. 2a). However, prostate cancer homogenates proved to have a significant decrease in enzyme activity as 1.68 ± 0.48 U/gram of protein was detected ($P = 0.0045$). Although BCAT activity is not at high levels in either state, malignant tissue displayed a unique metabolic profile relative to healthy prostate tissue.

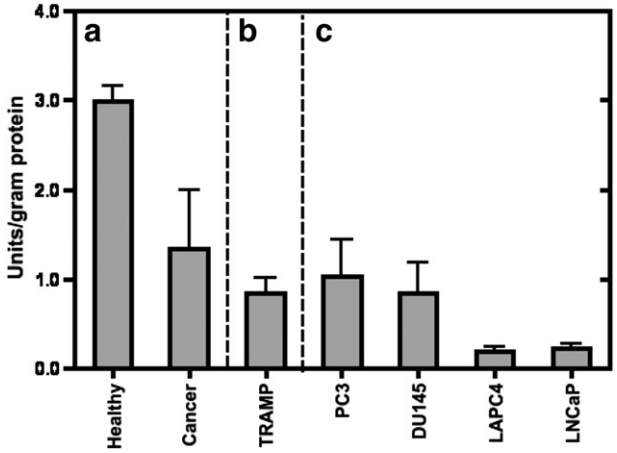

Fig. 2. BCAT activity detected from the various prostate sources: (a) human, (b) TRAMP mouse model, and (c) human prostate cancer cell lines. Human prostate cancer displayed significantly lower levels of BCAT activity than normal tissue. All BCAT activities are expressed as mean ± ste.

3.2. In vitro assessment of BCAT Activity in models of human prostate cancer

In ex vivo experiments, homogenates of TRAMP prostate tissues were found to possess an enzyme activity of 0.84 ± 0.17 U/gram of protein (Fig. 1b); therefore, TRAMP mice display a decreased level of BCAT activity relative to human disease ($P = 0.051$). A variety of human prostate cancer cell lines were also examined in order to determine whether they would serve as appropriate models for MR spectroscopic studies. BCAT assays were conducted with four cell lines: PC-3, DU-145, LNCaP and LAPC-4 (Fig. 1c) [26]. In the experiments among the human prostate cancer cell lines, the PC-3 cell line displayed the highest level of BCAT activity (1.05 ± 0.39 U/gram of protein) followed by the DU-145 cell line (0.97 ± 0.16 U/gram of protein) with no statistical difference between the two models ($P = 0.42$). Both cell lines were found to have increased enzyme activity in comparison to the TRAMP mouse model (PC-3: $P = 0.31$; DU-145: $P = 0.28$). Low levels of BCAT activity were detected in vitro from both the LNCaP and LAPC-4 cell lines (PC-3/LNCaP: $P = 0.043$; PC-3/LAPC-4: $P = 0.052$; DU-145/LNCaP: $P = 0.0001$; DU-145/LAPC-4: $P = 0.0001$). Importantly, the PC-3 and DU-145 cell lines displayed significantly lower BCAT activity than healthy human prostate tissue (PC-3/healthy prostate: $P = 0.0001$; DU-145/healthy prostate: $P = 0.0001$), but only moderate differences from malignant prostate tissue were observed (PC-3/malignant prostate: $P = 0.22$; DU-145/malignant prostate: $P = 0.13$).

3.3. Hyperpolarized ^{13}C MRS of human prostate cancer cell lines

Fig. 3 displays averaged (a) spectra and (b) time courses obtained after administration of hyperpolarized [1-^{13}C]-KIC to PC-3 cells in culture media (substrate concentration = 2 mM). In these experiments, [1-^{13}C]-KIC was observed at 172.6 ppm, and [1-^{13}C]-Leu was detected at 176.8 ppm. [1-^{13}C]-KIC•H_2O and [2-^{13}C]-KIC (natural abundance) were also present in the spectra but are not related to metabolism. The metabolic product, [1-^{13}C]-Leu, was immediately formed upon exposure of the prostate cancer cells to hyperpolarized [1-^{13}C]-KIC and was detected in all experiments. The maximum product signal was detected after 15–20 s. Higher concentrations (up to 5 mM) of [1-^{13}C]-KIC did not result in increased product formation, which may suggest saturation of the BCAT active site at 2 mM. BCAT has a $K_M = 0.14$ mM for KIC and substrate levels should not limit the transamination [25]. In addition, KIC has been demonstrated as an effective substrate for monocarboxylate transporters such as MCT1, which are readily expressed prostate cancer cell lines and prostate tissue [27–29]. Further, although leucine can serve as a co-substrate for the transaminase and potentially could increase isotopic flux, incubation (10 min) of cells with unlabeled leucine (1 mM) prior to [1-^{13}C]-KIC administration did not substantially affect [1-^{13}C]-Leu signal. Experiments were also performed with DU-145 cells and analogous metabolic products and time courses were found (Fig. 4). Ratios of [1-^{13}C]-Leu-to-[1-^{13}C]-KIC were obtained for PC-3 and DU-145 cell lines from hyperpolarized ^{13}C MRS analysis. The metabolic product was observed over the first 90 s of the experiment, and PC-3 cells displayed a conversion ratio of $1.73 \times 10^{-3} \pm 0.38 \times 10^{-3}$ a.u (mean ± ste, $n = 3$). The area under the curve for the metabolic product corresponding to [1-^{13}C]-Leu production was found to be $2.20 \times 10^{-3} \pm 0.47 \times 10^{-3}$ ratio (mean ± ste, $n = 3$) for the DU-145 cell line.

4. Discussion

Hyperpolarized ^{13}C MRS provides a unique opportunity to evaluate metabolism at the molecular level. Karlsson et al. [16] initially showed that [1-^{13}C]-Leu was successfully produced from the

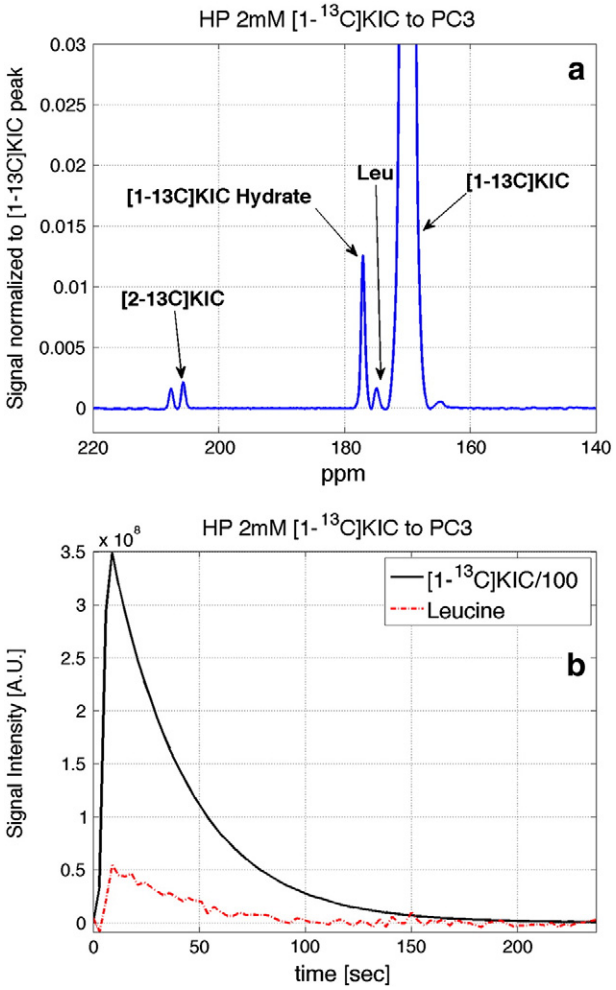

Fig. 3. (a) Representative time-averaged spectra obtained from PC-3 prostate cancer cell line after incubation with 2 mM [1-^{13}C]-KIC. The signal-to-noise ratio (SNR) for individual ^{13}C-labeled metabolites was 1.31×10^6 ([1-^{13}C]-KIC) and 2.07×10^3 ([1-^{13}C]-Leu), respectively. SNR was calculated by taking an integral over individual peaks divided by standard deviation of background noise. (b) Representative time course demonstrate rapid uptake of hyperpolarized substrate and production of metabolic product, [1-^{13}C]-Leu.

injection of hyperpolarized [1-^{13}C]-KIC in murine and rat models of cancer. In addition, it was demonstrated that the levels of [1-^{13}C]-Leu formation were proportional to the observed BCAT activities. Elevated pool sizes of glutamate and leucine were also detected in the cancerous tissue.

In this report, we investigated BCAT activity in several models of prostate cancer via both traditional spectrophotometric and hyperpolarized ^{13}C MRS methods. While the work of Karlsson et al. [16] demonstrated the initial observation of metabolite formation from hyperpolarized [1-^{13}C]-KIC, this study sought to determine whether [1-^{13}C]-KIC could serve as a practical method for characterizing malignant prostate tissues. Through initial examination of BCAT activity in vitro via conventional spectrophotometric methods, we demonstrated that, despite low levels of BCAT activity, alterations in BCAA metabolism are observed in various prostate cancer models. In particular, healthy human prostate tissue was found to have an elevated BCAT levels relative to malignant tissue. Normal prostate tissue relies upon fatty acid metabolism and glycolysis for energy production because the tricarboxylic acid (TCA) cycle is inhibited due to the high concentration of zinc. However, in prostate cancer, the TCA cycle is restored and can also contribute to meeting the energy requirements of the cell [30]; therefore, the observed changes in BCAT activity are in principle consistent with BCAAs being utilized for protein synthesis rather than for energy production. Importantly, although the observed activity was less in prostate cancer in comparison to healthy tissue, the significant difference between the two states could still provide a clinical opportunity for disease assessment and/or monitoring response to treatment. For example, hyperpolarized [1,4-$^{13}C_2$]-fumarate, which displays lower metabolic conversion rate to [1,4-$^{13}C_2$]-malate in tumors relative to normal tissue, has proven to be a valuable clinical tool for assessing cell necrosis and monitoring therapeutic response [31]. In a similar fashion, lower levels of BCAT activity in the disease state could potentially result in detectable decreases in [1-^{13}C]-Leu production from hyperpolarized [1-^{13}C]-KIC and thus provide a method for evaluating prostate tissue.

Animal and cellular models are vital tools for exploring the onset and progression of human disease. In addition, a sufficient model, which maintains comparable rates of BCAT activity as human prostate cancer, was necessary for spectroscopic evaluation with hyperpolarized [1-^{13}C]-KIC. However, there remain a limited number of reports concerning alterations in BCAA demand and metabolism in models of prostate cancer. Through the initial spectrophotometric examination of the TRAMP mouse and prostate

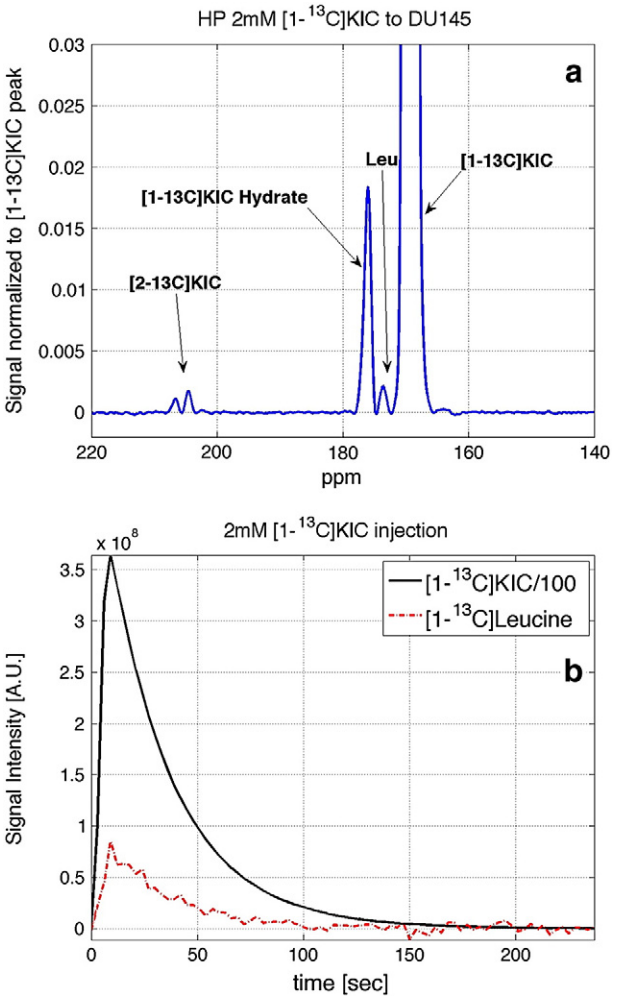

Fig. 4. (a) Representative time-averaged spectra obtained from DU-145 prostate cancer cell line after incubation with 2 mM [1-^{13}C]-KIC. The SNR for individual ^{13}C-labeled metabolites was 1.60×10^6 ([1-^{13}C]-KIC) and 2.66×10^3 ([1-^{13}C]-Leu), respectively. (b) Representative time course demonstrate rapid uptake of hyperpolarized substrate and production of metabolic product, [1-^{13}C]-Leu.

cancer cell lines, PC-3 and DU-145 cell lines were discovered to have relatively similar BCAT activity levels as detected in human disease. These models were then employed in the development of ^{13}C MRS techniques for analyzing BCAA metabolism with hyperpolarized [1-^{13}C]-KIC in prostate cancer. We demonstrated that hyperpolarized [1-^{13}C]-KIC could be employed in vitro for models of prostate cancer. In both the PC-3 and DU-145 cell lines, [1-^{13}C]-Leu production was observed after administration of the molecular probe. The [1-^{13}C]-Leu-to-[1-^{13}C]-KIC ratio also provided insight into the state of BCAA metabolism and, specifically, the propensity for BCAA oxidation, a pathway that can be utilized to drive energy production in proliferating cells. However, the low levels of BCAT activity in the examined prostate cancer cell lines may limit the future application of hyperpolarized [1-^{13}C]-KIC in the assessment of the disease.

5. Conclusions

Based upon our analysis, BCAA metabolism is altered in human prostate cancer relative to healthy tissue. However, only low levels of BCAT activity were found in all animal and cellular models examined. Despite these modest activities, we have demonstrated that [1-^{13}C]-Leu production can be determined with hyperpolarized ^{13}C MRS in vitro using [1-^{13}C]-KIC.

Acknowledgments

This work was supported by DOD grant PC100427, NIH grants AA018681, AA005965, AA013521-INIA, EB009070, and P41 EB015891, and GE Healthcare.

References

[1] Ferlay J, Shin HR, Bray F, Forman D, Mathers C, Parkin DM. GLOBOCAN 2008 v1.2, Cancer Incidence and Mortality Worldwide: IARC CancerBase No. 10. . Internet Lyon, France: International Agency for Research on Cancer; 2010.
[2] Singh H, Canto EI, Shariat SF, Kadmon D, Miles BJ, Wheeler TM, et al. Predictors of prostate cancer after initial negative systematic 12 core biopsy. J Urol 2004; 171(5):1850–18544.
[3] Jemal A, Siegel R, Ward E, Hao Y, Xu J, Murray T, et al. Cancer statistics. CA Cancer J Clin 2008;58(2):71–96.
[4] Makarov DV. Biomarkers for prostate cancer. Ann Rev Med 2009;60:139–51.
[5] Pound CR, Partin AW, Eisenberger MA, Chan DW, Pearson JD, Walsh PC. Natural history of progression after PSA elevation following radical prostatectomy. JAMA 1999;281(17):1591–7.
[6] Kirkham AP, Emberton M, Allen C. How good is MRI at detecting and characterising cancer within the prostate? Eur Urol 2006;50(6):1163–74.
[7] Kurhanewicz J, Vigneron DB. Advances in MR spectroscopy of the prostate. Magn Reson Imaging Clin N Am 2008;16(4):697–710.
[8] Jiang Z, Woda BA. Diagnostic utility of alpha-methylacyl CoA racemase (P504S) on prostate needle biopsy. Adv Anat Pathol 2004;11(6):316–21.
[9] Jadvar H. Molecular imaging of prostate cancer: PET radiotracers. AJR Am J Roentgenol 2012;199(2):278–91.
[10] Krause BJ, Souvatzoglou M, Treiber U. Imaging of prostate cancer with PET/CT and radioactively labeled choline derivatives. Urol Oncol 2013;31(4):427–35.
[11] Ardenkjaer-Larsen JH, Fridlund B, Gram A, Hansson G, Hansson L, Lerche MH, et al. Increase in signal-to-noise ratio of >10,000 times in liquid-state NMR. Proc Natl Acad Sci U S A 2003;100(18):10158–63.
[12] Day SE, Kettunen MI, Gallagher FA, Hu DE, Lerche M, Wolber J, et al. Detecting tumor response to treatment using hyperpolarized 13C magnetic resonance imaging and spectroscopy. Nat Med 2007;13(11):1382–7.
[13] Kurhanewicz J, Bok R, Nelson SJ, Vigneron DB. Current and potential applications of clinical 13C MR spectroscopy. J Nucl Med 2008;49(3):341–4.
[14] Nelson SJ, Kurhanewicz J, Vigneron DB, Larson PEZ, Harzstark AL, Ferrone M, et al. Metabolic imaging of patients with prostate cancer using hyperpolarized 1-C-13 pyruvate. Sci Transl Med 2013;5(198):198.
[15] Kurhanewicz J, Vigneron DB, Brindle K, Chekmenev EY, Comment A, Cunningham CH, et al. Analysis of cancer metabolism by imaging hyperpolarized nuclei: prospects for translation to clinical research. Neoplasia 2011;13(2): 81–97.
[16] Karlsson M, Jensen PR, in 't Zandt R, Gisselsson A, Hansson G, Duus JØ, et al. Imaging of branched chain amino acid metabolism in tumors with hyperpolarized (13)C ketoisocaproate. Int J Cancer 2010;127(3):729–36.
[17] Butt SA, Søgaard LV, Magnusson PO, Lauritzen MH, Laustsen C, Åkeson P, et al. Imaging cerebral 2-ketoisocaproate metabolism with hyperpolarized (13)C magnetic resonance spectroscopic imaging. J Cereb Blood Flow Metab 2012; 32(8):1508–14.
[18] Brosnan JT, Brosnan ME. Branched-chain amino acids: enzyme and substrate regulation. J Nutr 2006;136(1S):207S–11S.
[19] Niwa O, Kumazaki T, Tsukiyama T, Soma G, Miyajima N, Yokoro K. A cDNA clone overexpressed and amplified in a mouse teratocarcinoma line. Nucleic Acids Res 1990;18(22):6709.
[20] Ben-Yosef T, Yanuka O, Halle D, Benvenisty N. Involvement of Myc targets in c-myc and N-myc induced human tumors. Oncogene 1998;17(2):165–71.
[21] Wang Q, Bailey CG, Ng C, Tiffen J, Thoeng A, Minhas V, et al. Androgen receptor and nutrient signaling pathways coordinate the demand for increased amino acid transport during prostate cancer progression. Cancer Res 2011; 71(24):7525–36.
[22] Baracos VE, Mackenzie ML. Investigations of branched-chain amino acids and their metabolites in animal models of cancer. J Nutr 2006;136(1S):237S–42S.
[23] Blomstrand E, Eliasson J, Karlsson HKR, Köhnke R. Branched-chain amino acids: metabolism, physiological, function, and application. J Nutr 2006;136(1S): 269S–73S.
[24] Schuster DM, Votaw JR, Nieh PT, Yu W, Nye JA, Master V, et al. Initial experience with the radiotracer anti-1-amino-3-^{18}F-fluorocyclobutane-1-carboxylic acid with PET/CT in prostate carcinoma. J Nucl Med 2007;48(1):56–63.
[25] Schadewaldt P, Adelmeyer F. Coupled enzymatic assay for estimation of branched-chain L-amino acid aminotransferase activity with 2-oxo acid substrates. Anal Biochem 1996;238(1):65–71.
[26] Sobel RE, Sadar MD. Cell lines used in prostate cancer research: a compendium of old and new lines. J Urol 2005;173(2):342–59.
[27] Kilberg MS, Gwynn MB. Plasma membrane transport of 2-ketoisocaproate by rat hepatocytes in primary culture. J Biol Chem 1983;258(19):11524–7.
[28] Bröer S, Bröer A, Schneider HP, Stegen C, Halestrap AP, Deitmer JW. Characterization of the high-affinity monocarboxylate transporter MCT2 in *Xenopus laevis* oocytes. Biochem J 1999;341(Pt 3):529–35.
[29] Bröer S, Schneider HP, Bröer A, Rahman B, Hamprecht B, Deitmer JW. Characterization of the monocarboxylate transporter 1 expressed in *Xenopus laevis* oocytes by changes in cytosolic pH. Biochem J 1998;333(Pt 1):167–74.
[30] Dakubo GD, Parr RL, Costello LC, Franklin RB, Thayer RE. Altered metabolism and mitochondrial genome in prostate cancer. J Clin Pathol 2006;59(1):10–6.
[31] Gallagher FA, Kettunen MI, Hu DE, Jensen PR, Zandt RI, Karlsson M, et al. Production of hyperpolarized [1,4-$^{13}C_2$]malate from [1,4-$^{13}C_2$]fumarate is a marker of cell necrosis and treatment response in tumors. Proc Natl Acad Sci U S A 2009;106(47):19801–6.

Effects of Isoflurane Anesthesia on Hyperpolarized ^{13}C Metabolic Measurements in Rat Brain

Sonal Josan,[1,2]* Ralph Hurd,[3] Kelvin Billingsley,[2] Lasitha Senadheera,[4] Jae Mo Park,[2,5] Yi-Fen Yen,[2] Adolf Pfefferbaum,[1,6] Daniel Spielman,[2,5] and Dirk Mayer[1,2]

Purpose: Commonly used anesthetic agents such as isoflurane are known to be potent cerebral vasodilators, with reported dose-dependent increase in cerebral blood flow and cerebral blood volume. Despite the widespread use of isoflurane in hyperpolarized ^{13}C preclinical research studies, a quantitative assessment of its effect on metabolic measurements is limited. This work investigates the effect of isoflurane anesthesia dose on hyperpolarized ^{13}C MR metabolic measurements in rat brain for [1-^{13}C]pyruvate and 2-keto[1-^{13}C]isocaproate.

Methods: Dynamic 2D and 3D spiral chemical shift imaging was used to acquire metabolic images of rat brain as well as kidney and liver following bolus injections of hyperpolarized [1-^{13}C]pyruvate or 2-keto[1-^{13}C]isocaproate. The impact of a "low dose" vs. a "high dose" of isoflurane on cerebral metabolite levels and apparent conversion rates was examined.

Results: The cerebral substrate signal levels, and hence the metabolite-to-substrate ratios and apparent conversion rates, were found to depend markedly on isoflurane dose, while signal levels of metabolic products and their ratios, e.g. bicarbonate/lactate, were largely insensitive to isoflurane levels. No obvious dependence on isoflurane was observed in kidney or liver for pyruvate.

Conclusion: This study highlights the importance of careful attention to the effects of anesthesia on the metabolic measures for hyperpolarized ^{13}C metabolic imaging in brain. **Magn Reson Med 70:1117–1124, 2013.** ©**2012 Wiley Periodicals, Inc.**

Key words: hyperpolarized ^{13}C; isoflurane; anesthesia; brain; metabolite ratios; metabolic imaging

Hyperpolarized ^{13}C magnetic resonance spectroscopic imaging is a powerful tool for in vivo measurement of metabolism and has shown great promise in several applications including tumor diagnosis and treatment monitoring (1–9). Although transport across the blood brain barrier (BBB) within the short T_1 relaxation times of the hyperpolarized agents is a limiting factor for neurological applications, recent studies have demonstrated hyperpolarized ^{13}C brain imaging with a number of substrates. These include pyruvate (6–12), ethyl pyruvate (13), ketoisocaproate (14), acetate (15), dehydroascorbic acid (16), diethyl succinate (17) and dimethylethanol (18). The most commonly used agent, [1-^{13}C]pyruvate (Pyr) has been useful in the assessment of brain tumor metabolism by monitoring its conversion to lactate (Lac) and bicarbonate (Bic), allowing the differentiation of tumor from normal tissue in an animal model (6–9).

Despite the ubiquitous use of anesthetic agents in hyperpolarized ^{13}C preclinical research studies, a quantitative assessment of their effect on these metabolic measurements is limited (19). Isoflurane, which is the most widely used anesthetic agent, is known to be a potent cerebral vasodilator. A number of studies have reported a dose-dependent increase in cerebral blood flow (CBF) and cerebral blood volume (CBV) with isoflurane as well as heterogeneous changes in CBF distribution and glucose utilization in several species (20–26). These modulations could potentially impact the transport and uptake of the ^{13}C labeled substrate into brain tissue and its metabolic conversion.

This work aims to investigate the effect of isoflurane anesthesia dose on hyperpolarized ^{13}C MR metabolic measurements in rat brain for [1-^{13}C]pyruvate and 2-keto[1-^{13}C]isocaproate (KIC). Using dynamic chemical shift imaging (CSI), the impact of a "low dose" vs. a "high dose" of isoflurane on cerebral metabolite levels and apparent conversion rates was examined. As a complement to the brain study, experiments were also performed with pyruvate to examine the influence of isoflurane dose on metabolic measurements in kidney and liver.

METHODS

The samples to be polarized consisted of either 25 μL of a mixture of 14 M [1-^{13}C] pyruvic acid (Sigma-Aldrich, USA) and 15 mM Ox063 trityl radical, or 32 μL of a mixture of 8 M [1-^{13}C] ketoisocaproic acid (converted from corresponding sodium salt, Cambridge Isotope Laboratories, USA) and 11 mM Ox063 trityl radical. In both cases, 3 μL of a 1:50 dilution of dotarem (Guerbet, France) were added just prior to polarization.

The samples were polarized via dynamic nuclear polarization using a HyperSense system (Oxford Instruments Molecular Biotools, Oxford, UK), for 1–1.5 h each, to achieve liquid-state polarization at dissolution of

[1]SRI International, Neuroscience Program, Menlo Park, California, USA.
[2]Department of Radiology, Stanford University, Lucas MRI Center, Stanford, California, USA.
[3]GE Healthcare Applied Sciences Laboratory, Menlo Park, California, USA.
[4]Department of Radiation Oncology, Stanford University, Stanford, California, USA.
[5]Department of Electrical Engineering, Stanford University, Stanford, California, USA.
[6]Department of Psychiatry and Behavioral Sciences, Stanford University, Stanford, California, USA.

Grant sponsor: NIH; Grant numbers: AA018681, AA005965, AA013521-INIA, EB009070, P41 EB015891; Grant sponsor: DOD; Grant number: PC100427; Grant sponsor: GE Healthcare.

*Correspondence to: Sonal Josan, Ph.D., SRI International, BN 188, 333 Ravenswood Avenue, Menlo Park, CA 94025. E-mail: sjosan@stanford.edu

Received 5 September 2012; revised 25 September 2012; accepted 25 September 2012.
DOI 10.1002/mrm.24532
Published online 19 October 2012 in Wiley Online Library (wileyonlinelibrary.com).

~25% for pyruvate and 15% for KIC. The polarized samples were dissolved in a solution of 80 mM NaOH mixed with 40 mM TRIS buffer, 50 mM NaCl and 0.1 g/L EDTA-Na_2, leading to an 80 mM solution of the hyperpolarized substrate with a pH of about 7.5.

Healthy male Wistar rats (278 ± 59 g body weight, n = 13) were injected with 2.6–3.2 mL of the hyperpolarized solution (target dose = 1 mmol/kg body weight) through a tail vein catheter at a rate of ~0.25 mL/s. The time from dissolution to start of injection was ~18 s.

The rats were anesthetized initially with 2.5% isoflurane in oxygen (1.5 L/min) for tail vein catheterization. Respiration, rectal temperature, heart rate, and oxygen saturation were monitored throughout the experiments. The oxygen flow rate was kept constant at 1.5 L/min while the isoflurane level was adjusted to a "low" or "high" dose. The low dose was ~0.75–1.5% isoflurane in oxygen, targeting a respiration rate of about 80–85 breaths/min and the high dose was 2–3.25% targeting a respiration rate of about 50–55 breaths/min. Each animal received multiple (2–4) injections of the hyperpolarized substrate, ~1.5 h apart, alternating between low and high doses. Before each ^{13}C injection, isoflurane was slowly adjusted to the next target dose, and maintained at the target for at least 10 min and up to an hour before the injection. The first ^{13}C injection was performed at low isoflurane dose for approximately half of the rats and at high isoflurane dose for the others. All animal procedures were approved by the SRI Institutional Animal Care and Use Committee.

For the brain experiments, seven of the rats received four injections each of hyperpolarized Pyr (n = 3, rat ID P1-P3) or KIC (n = 4, rat ID K1-K4), two injections each at the low and high isoflurane doses. To assess variability among injections, three control rats (ID C1-C3) received three Pyr injections each while maintaining a constant isoflurane dose of 1.75–2.5% targeting a respiration rate of about 60 breaths/min throughout the experiment. For the body (kidney and liver) experiments, three rats (ID P4-P6) received two injections each of Pyr, alternately at low and high isoflurane dose.

All experiments were performed on a clinical 3T Signa MR scanner (GE Healthcare, Waukesha, WI), using a high-performance insert gradient coil operating at maximum amplitude of 500 mT/m with a slew rate of 1865 mT/m/ms (9) and custom-built dual-tuned ($^1H/^{13}C$) quadrature transmit-receive RF coils, operating at 127.9 and 32.2 MHz, respectively. The brain imaging experiments used a rat brain RF coil (diameter = 50 mm, length = 60 mm), while the body imaging studies used a bigger rat body RF coil (diameter = 80 mm, length = 90 mm). The transmit ^{13}C RF power was calibrated using a reference phantom, containing an 8 M solution of ^{13}C-urea, which was placed on top of the animal and removed before the first ^{13}C injection.

Single-shot fast spin-echo (FSE) ^1H MR images in the axial, sagittal and coronal planes with nominal inplane resolution of 0.47 mm and 2-mm slice thickness were acquired as anatomical references for prescribing the ^{13}C CSI experiments. Additional ^1H MR images matching the ^{13}C CSI prescriptions were also acquired for overlay of the ^{13}C metabolic maps. Dual-echo FSE images (0.25-mm in-plane resolution, 1-mm slice thickness, 58 slices, echo time TE1/TE2 = 11.3/56.7 ms, repetition time (TR) = 5000 ms, echo train length = 8, NEX = 2) were used for the brain 2D experiments, while 3D spoiled gradient–recalled echo (SPGR) images (0.625-mm in-plane resolution, 1.25-mm slice thickness, 96 slices, TE/TR = 2.1/8.9 ms, NEX = 2) were used for the body 3D experiments.

Brain 2D ^{13}C CSI

The single-shot 2D spiral CSI sequence described in Ref. 12 was used for dynamic metabolic imaging of the brain. Imaging parameters were: FOV = 43.5 mm, nominal resolution = 2.7 mm, 10-mm slice thickness, TR = 3 s, TE = 3 ms. Sixteen time points were acquired with a delay of 3 s from the start of the injection, using a variable flip angle scheme (27), $\theta_i = \tan^{-1}\left(1/\sqrt{16-i}\right)$ for the 16 excitations. The data for control rats was taken from the previously published study (12), with imaging starting at 9 s after start of injection, while all other parameters (including hardware, setup and imaging) were the same as described here. In one case (rat K1), a single time-point image was acquired at 25 s after KIC injection, instead of dynamic imaging, to achieve higher leucine (Leu) signal-to-noise ratio (SNR). This acquisition used a 90° excitation and all other parameters were the same as the dynamic brain imaging protocol.

Body 3D ^{13}C CSI

Dynamic 3D data were acquired from a volume covering both kidney and liver using the 3D spiral CSI sequence described in (28). Imaging parameters were: FOV = 80 × 80 × 60 mm^3, nominal resolution = 5 × 5 × 5 mm^3, 12 z-phase encoding steps, 4-cm slab excitation. The faster gradient insert coil allowed the total acquisition time per volume (T_{acq}) to be reduced to 1.6 s by using a single-shot spiral trajectory instead of the three spatial interleaves used in (28) for the same resolution. A constant flip angle of 5.625° was used for each excitation. Twenty-four time points were acquired, with a sampling interval of 2.5 s, starting with the Pyr injection.

The data were reconstructed similarly as the 2D and 3D spiral CSI cases described in Refs. 12 and 28. Metabolic maps were calculated by integrating the signal around each peak in absorption mode, using a width of ±18 Hz for the brain 2D data and ±24 Hz for the kidney/liver 3D data. The metabolic images were corrected for differences in the solid-state polarization level of each sample, and in the time delay from dissolution to start of injection assuming a T_1 of 60 s in solution. Regions of interest (ROIs) were drawn manually for each organ and for vasculature to calculate the time-resolved signal intensities for the metabolites. Apparent Pyr-to-Lac rate constants (K_{pl}) were estimated from the signal time-courses after RF correction (29). Metabolite ratios in the ROIs were calculated from the time-averaged metabolic maps.

Statistical significance was assessed using a paired Student's t-test to compare the low isoflurane data with the high isoflurane data. In cases where two

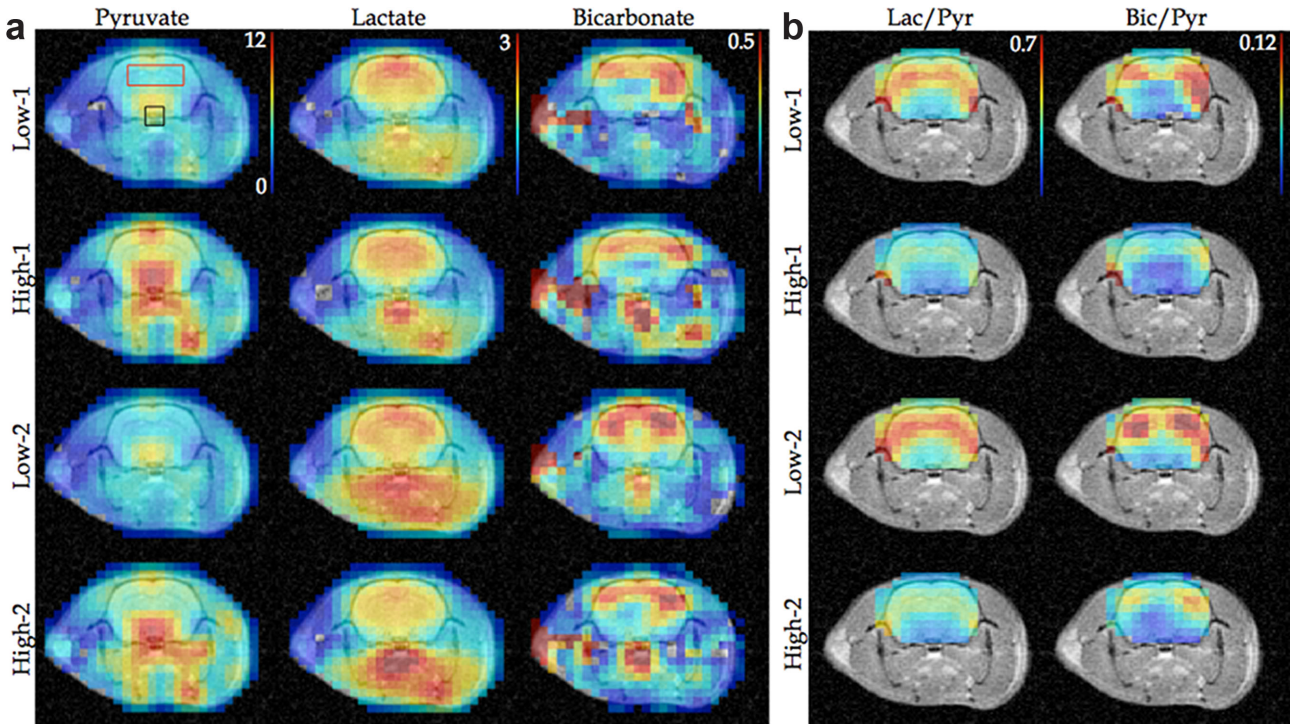

FIG. 1. Representative ^{13}C metabolic maps of a slice through the brain from four injections in one rat. Pyruvate was elevated at the high isoflurane level due to the vasodilation effect, while no change was observed in lactate and bicarbonate. Thus, the ratio maps showed lower values at high isoflurane. The spurious bicarbonate signal outside the brain region is likely from pyruvate signal contamination due to off-resonance as the B_0 homogeneity was optimized only over the brain.

measurements were taken at each isoflurane level, both measurements were included in the data. For the control rats, a paired *t*-test was done for the first and third injections.

RESULTS

Representative time-averaged ^{13}C metabolic maps superimposed onto ^{1}H MR images in Figure 1a show the metabolic products of [1-^{13}C]Lac and ^{13}C-bicarbonate (Bic) observed after hyperpolarized [1-^{13}C]Pyr injection. The conversion of Pyr to Lac takes place in the cytosol via the enzyme lactate dehydrogenase (LDH). Pyruvate is also converted to acetyl-coenzyme A (acetyl-CoA) in the mitochondria through pyruvate dehydrogenase (PDH), releasing the ^{13}C label as $^{13}CO_2$, which is in equilibrium with ^{13}C-Bic. [1-^{13}C]alanine (Ala), which is generated from pyruvate through alanine aminotransferase (ALT), was detected in the muscle tissues of the jaw and tongue but not in the brain, consistent with the low ALT activity in rat brain compared to LDH activity (12,30).

The ^{13}C maps in Figure 1a demonstrate greatly elevated Pyr in brain (red ROI) and vasculature (black ROI) at the high isoflurane level compared to the low isoflurane level, consistent with the vasodilation effect, whereas lactate and bicarbonate remain unchanged. This effect was observed over a repeated set of measurements in each animal. The Pyr and Lac images shown here are the average of all 16 time-points acquired, whereas the Bic images are the average of time-points 5–16 to increase SNR as the first four time-points had little Bic signal. While the metabolite signal intensities can have some variation due to fluctuations in polarization levels, the commonly used metrics of metabolite-to-substrate ratios and apparent rate constants are independent of polarization. The ratio maps in Figure 1b calculated from the images in Figure 1a reflect the large change in Pyr, with the Lac/Pyr and Bic/Pyr ratios being considerably lower at the high isoflurane level.

The Pyr and Lac time-courses from an ROI in the brain are plotted in Figure 2 along with Pyr time-courses from a vasculature ROI (ROIs shown in Fig. 1). The Bic time-courses are not shown due to insufficient SNR of the individual time-points. Similar to the metabolic maps, the time-courses show increased Pyr signal at the high isoflurane level, without any distinct changes in the shape of the dynamic time-curve. The brain Lac signal level was similar for all four injections, resulting in very different apparent K_{pl} estimated from the time-courses, with an average of $0.025 \pm 0.003\ s^{-1}$ (mean ± std, six measurements in three rats) at the low isoflurane vs. $0.016 \pm 0.002\ s^{-1}$ at the high level ($P = 0.0001$).

Figure 3 summarizes the time-averaged Pyr, Lac and Bic signal levels along with the corresponding Lac/Pyr, Bic/Lac and Bic/Lac ratios in the brain ROIs for six rats. For the rats P1–P3, the Pyr signal varied appreciably with isoflurane level (mean ± std: low = 5.99 ± 1.36, high = 10.28 ± 2.99, $P = 0.0031$), while the Lac and Bic signals did not change over multiple injections in one animal (Lac: low = 3.37 ± 0.82, high = 3.54 ± 1.15, $P = 0.5526$; Bic: low = 0.40 ± 0.11, high = 0.41 ± 0.08, $P = 0.7711$). Thus, the ratios of the metabolic products

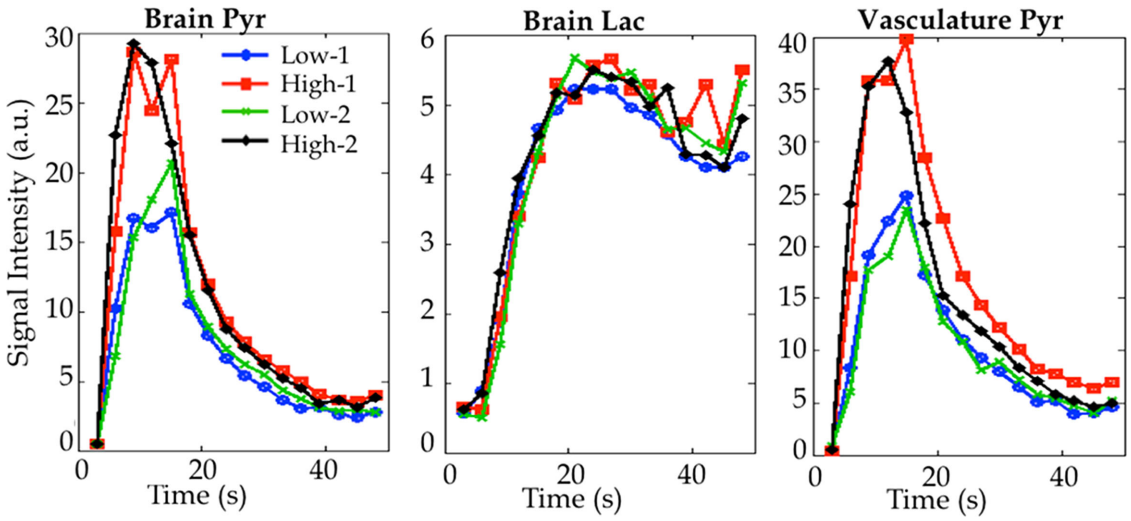

FIG. 2. Pyruvate time-courses from ROIs in the brain and in vasculature show the pronounced modulation of pyruvate by different isoflurane levels. Lactate signal levels over the time-course in the brain ROI did not change with isoflurane. [Color figure can be viewed in the online issue, which is available at wileyonlinelibrary.com.]

to the substrate, i.e. Lac/Pyr and Bic/Pyr, varied significantly with isoflurane dose. The average Lac/Pyr ratio decreased from 0.56 ± 0.04 at the low isoflurane to 0.34 ± 0.04 at the high level ($P < 0.0001$), with a percent change of 39.1 ± 1.8 from low to high isoflurane. The Bic/Pyr ratios show a similar trend as Lac/Pyr ratios, and the average Bic/Pyr ratio decreased from 0.07 ± 0.01 at the low isoflurane level to 0.04 ± 0.008 at high isoflurane ($P < 0.0001$), with a percent change of 41.1 ± 5.2 from low to high isoflurane. As the Bic and Lac signals were similar despite the large Pyr variation, the ratio of products, Bic/Lac, did not vary with isoflurane and was robust to the vasodilation effect on the substrate (low = 0.12 ± 0.04, high = 0.12 ± 0.03, $P = 0.9167$).

For the control rats (C1–C3) that had the isoflurane and respiration levels maintained constant throughout the experiment, the Pyr as well as the Lac and Bic signals did not differ between injections (Pyr:

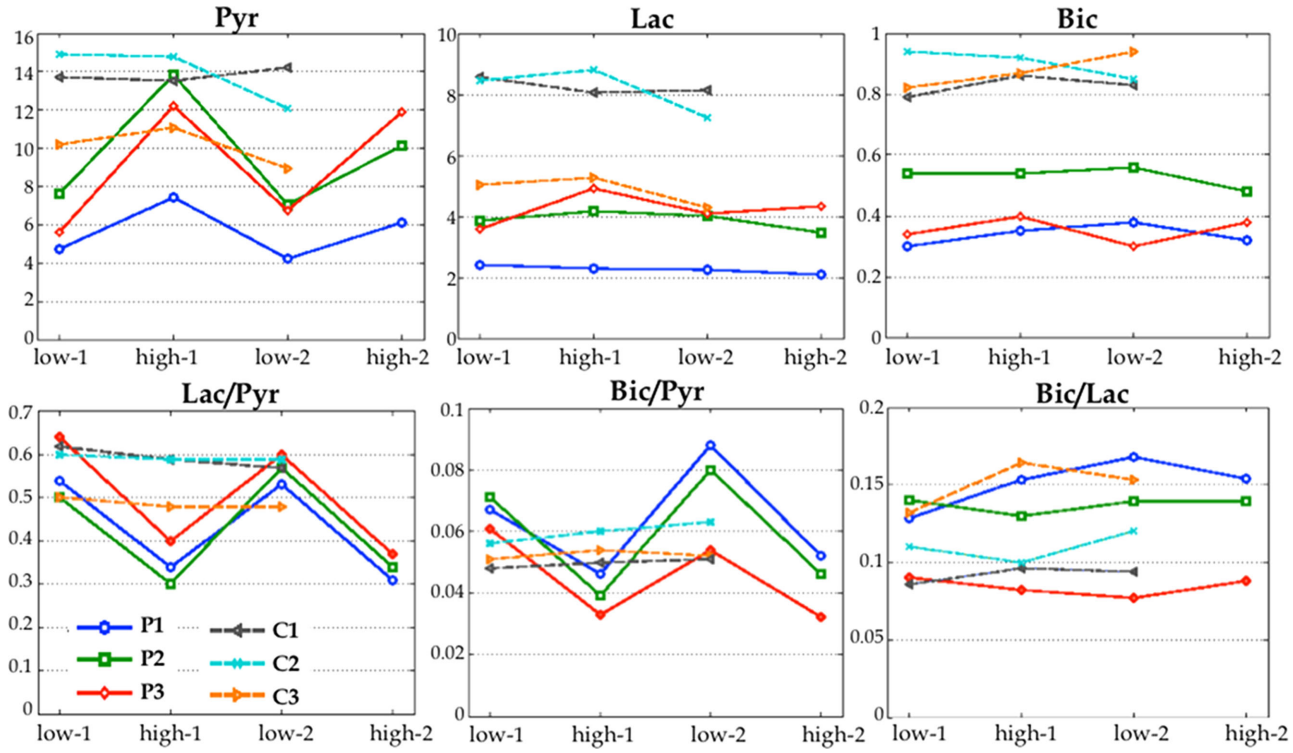

FIG. 3. Time-averaged signal intensities and corresponding metabolite ratios from a brain ROI for six rats. The strong variation of Pyr with isoflurane (rats P1–P3) leads to significant variation in the Lac/Pyr and Bic/Pyr ratios while the ratio of products, Bic/Lac, was relatively insensitive to the isoflurane changes. For the control rats (C1–C3) with constant isoflurane throughout, the metabolite signal intensities did not differ over multiple injections. [Color figure can be viewed in the online issue, which is available at wileyonlinelibrary.com.]

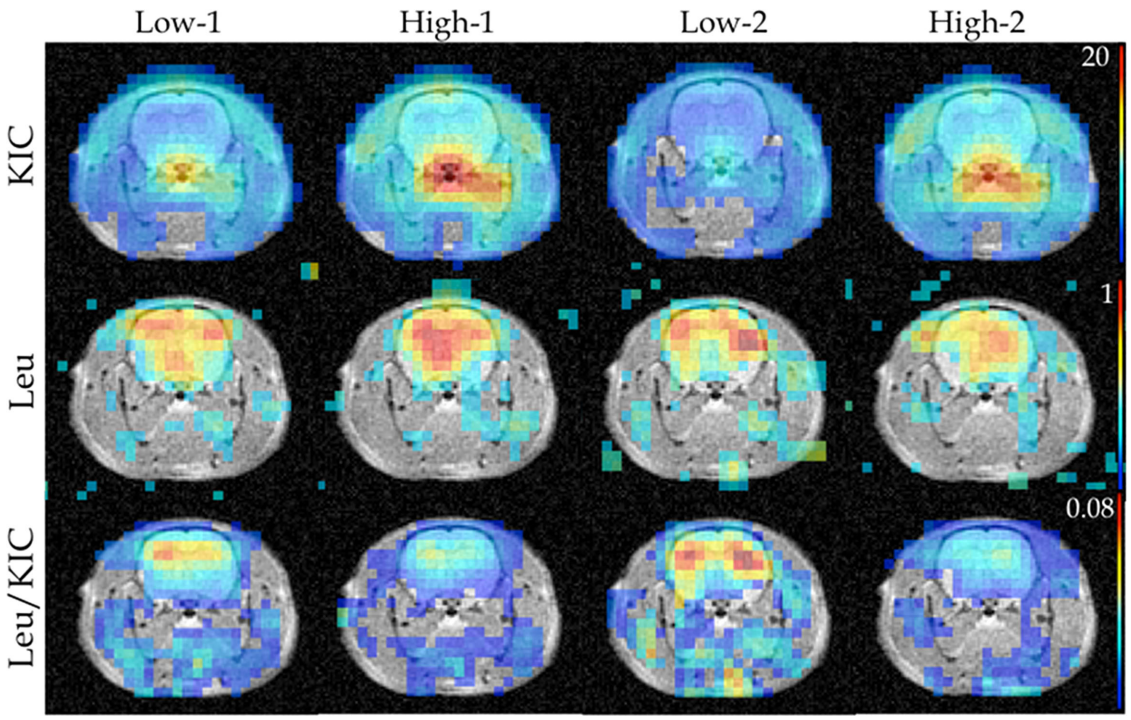

FIG. 4. Representative ^{13}C metabolic maps of KIC and Leu from a slice through the brain illustrates the changes in KIC signal with isoflurane dose while Leu signal is consistent for all four injections, resulting in a noticeable variation of the Leu/KIC ratios. [Color figure can be viewed in the online issue, which is available at wileyonlinelibrary.com.]

inj1 = 12.92 ± 2.46, inj3 = 11.74 ± 2.64, $P = 0.3457$; Lac: inj1 = 7.35 ± 2.00, inj3 = 6.54 ± 2.00, $P = 0.0736$; Bic: inj1 = 0.85 ± 0.08, inj3 = 0.87 ± 0.06, $P = 0.7397$). Therefore, the ratios were also similar (Lac/Pyr: inj1 = 0.57 ± 0.06, inj3 = 0.55 ± 0.06, $P = 0.1567$; Bic/Pyr: inj1 = 0.052 ± 0.004, inj3 = 0.055 ± 0.007, $P = 0.1732$; Bic/Lac: inj1 = 0.11 ± 0.02, inj3 = 0.12 ± 0.03, $P = 0.0846$). The isoflurane level for the control rats was closer to the high dose than the low dose. However, that data, which was taken from a previous study (12), started imaging at 9 s after Pyr injection for greater Lac and Bic SNR while this study used a 3 s delay to better capture the Pyr bolus. Hence, the metabolite signals and the ratios are higher for the control rats than the values for the high dose of the rats P1–P3.

Figure 4 depicts the images and ratio maps for hyperpolarized [1-^{13}C]KIC and its conversion to Leu in the brain. KIC is metabolized to Leu by the branched chain aminotransferase (BCAT) enzyme, with the concomitant conversion of glutamate to alpha-ketoglutarate. BCAT enzyme activity is upregulated in some tumors (31) and is also linked to glutamate-glutamine cycling between neurons and glia in the brain (32). The ^{13}C images here are from a single time-point acquisition at 25 s post KIC injection to achieve higher Leu SNR (rat K1). These images as well as the KIC time-courses (Fig. 5) from another rat demonstrate elevated KIC signal intensity at the high isoflurane level, indicating that the effect is not specific to Pyr. Leu time-courses are not shown in Figure 5 due to insufficient SNR. The KIC and Leu signals

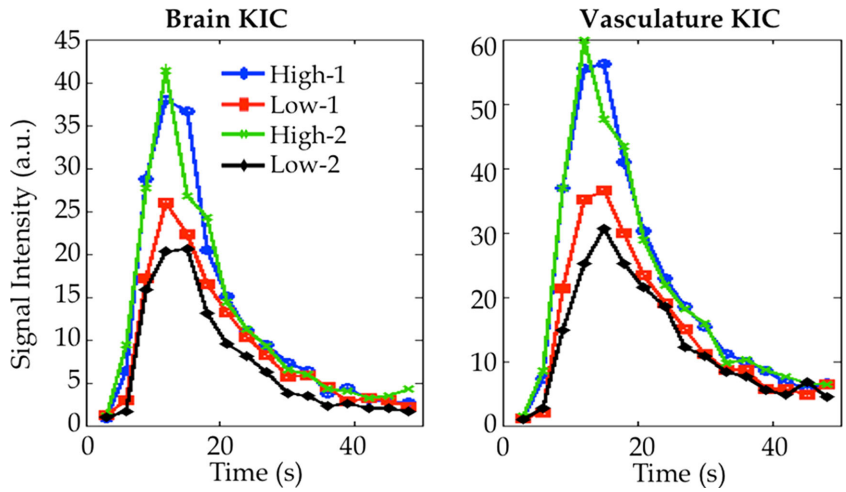

FIG. 5. KIC time-courses from the brain and vasculature ROIs show the modulation of KIC signal by different isoflurane levels. [Color figure can be viewed in the online issue, which is available at wileyonlinelibrary.com.]

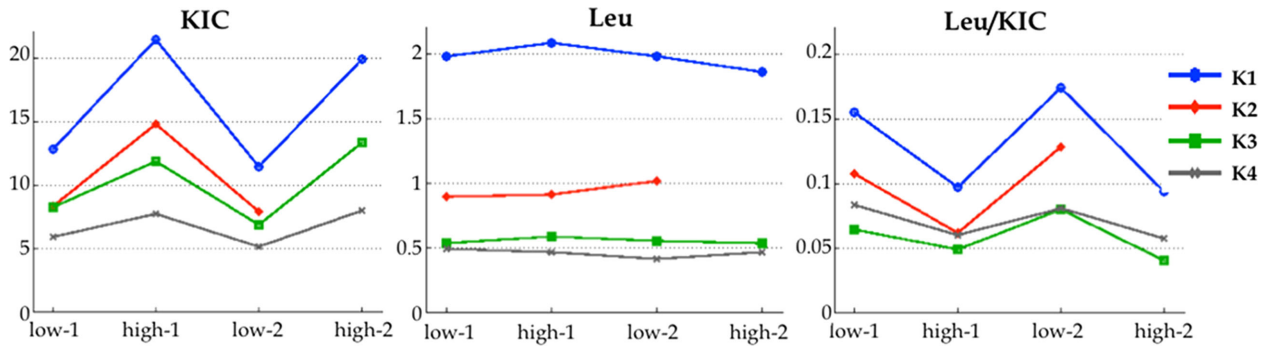

FIG. 6. Time-averaged signal intensities and corresponding metabolite ratios from a brain ROI for four rats. The strong difference in the KIC signal at the two isoflurane levels leads to significant variation in the Leu/KIC ratios. [Color figure can be viewed in the online issue, which is available at wileyonlinelibrary.com.]

averaged from a brain ROI and the corresponding Leu/KIC ratios are presented in Figure 6. The high Leu signal for rat K1 is due to the single time-point acquisition while the other data are from dynamic acquisitions averaged over the time-course. There was a strong modulation of the KIC signal by isoflurane (low = 8.31 ± 2.62, high = 13.86 ± 5.33, $P < 0.0001$), whereas the Leu signal was similar at both isoflurane levels (low = 0.98 ± 0.65, high = 0.98 ± 0.69, $P = 0.3842$). Consequently, the Leu/KIC ratios also vary considerably with different isoflurane levels (low = 0.11 ± 0.04, high = 0.06 ± 0.02, $P = 0.0032$), with a percent change of 36.7 ± 9.92 from low to high isoflurane. The statistical analysis above used a paired *t*-test by excluding the third injection on K2.

DISCUSSION

Hurd et. al. (11) showed that the hyperpolarized Pyr signal observed in the brain region arises largely from the CBV, as the conversion of Pyr to Lac in the brain is significantly faster than the transport of Pyr across the blood-brain barrier. Hence, any Pyr taken up by the brain tissue is converted quickly and observed as its metabolic products, whereas nearly all the Pyr observed is in the CBV. Therefore, the higher Pyr signal observed in the brain ROI with high isoflurane is consistent with the increase in CBV due to isoflurane.

The increased Pyr in CBV does not result in an increase in the metabolic products, as reflected by the similar Lac and Bic signals. Given the fast metabolic conversion of Pyr in brain, that would indicate that the transport of Pyr through the BBB is likely similar at the different isoflurane levels. Alternatively, it may be possible that there are changes in Pyr transport/uptake. However, that would imply a compensatory change in metabolic conversion for both Lac and Bic in order to maintain similar product signal levels at the different isoflurane levels as observed in this study. In either case, the strong modulation of the Lac/Pyr and Bic/Pyr ratios is present. The ratio of metabolic products, i.e., Bic/Lac did not vary with isoflurane level, and provides a metric that may be immune to the vasodilation effect on the substrate as well as to the differences in polarization levels.

The modulation of the substrate signal by isoflurane was observed for both Pyr and KIC. For both substrates, the transport across the BBB occurs via a saturable carrier-mediated transport as well as a nonsaturable diffusion transport. Pardridge (33) reported the kinetic parameters of BBB transport, with maximum velocity of transport V_{max} and nonsaturable transport constant K_d as 88 nmol/min/g and 0.034 mL/min/g respectively for Pyr (91 nmol/min/g and 0.019 mL/min/g respectively for Lac as comparison). The active transport is expected to saturate at the doses used here and the diffusive transport depends on substrate concentration. Conn et al. (34) reported a V_{max} of 71 nmol/min/g and K_d of 0.019 mL/min/g for KIC. The effect of isoflurane on other substrates may depend on their specific BBB transport and metabolic conversion rates.

While isoflurane acts as a cerebral vasodilator, enhancing CBF and CBV and hence the ^{13}C substrate signal, the response may be different for other anesthetic agents. For example, propofol, pentobarbital, and alpha-chloralose have been reported to show lower CBF than isoflurane, as well as lower CBV reported for propofol and pentobarbital (20–23). Halothane also shows a vasodilation effect similar to or greater than isoflurane, but with a different regional distribution of the changes in CBF compared to isoflurane (25).

In contrast to the striking variation observed in brain, there was no obvious dependence on isoflurane observed in kidney or liver. The time-averaged Pyr and Lac signal levels and the Lac/Pyr ratios from three rats in Figure 7 demonstrate no significant difference at the two isoflurane levels (Liver: $P = 0.2813$ for Pyr, $P = 0.2896$ for Lac; $P = 0.6017$ for Lac/Pyr ; Kidney: $P = 0.4398$ for Pyr, $P = 0.3029$ for Lac; $P = 0.1165$ for Lac/Pyr). The apparent K_{pl} estimated from the time-courses was 0.013 ± 0.001 s^{-1} at both isoflurane doses for kidney ($P = 0.7608$), and 0.028 ± 0.005 s^{-1} vs. 0.029 ± 0.004 s^{-1} for liver for low and high isoflurane doses respectively ($P = 0.4950$). Previous studies have reported no change in renal or total hepatic blood flow at low (~1%) isoflurane concentration, compared to controls anesthetized with alpha-chloralose, but ~15% decrease in blood flow in both regions at high (~2.4%) isoflurane concentration for rats (26). In comparison, a more than 2-fold increase in CBF has been reported in some brain structures at high isoflurane compared to low isoflurane (20,21). Without the BBB as a rate-limiting step in Pyr transport and uptake from blood

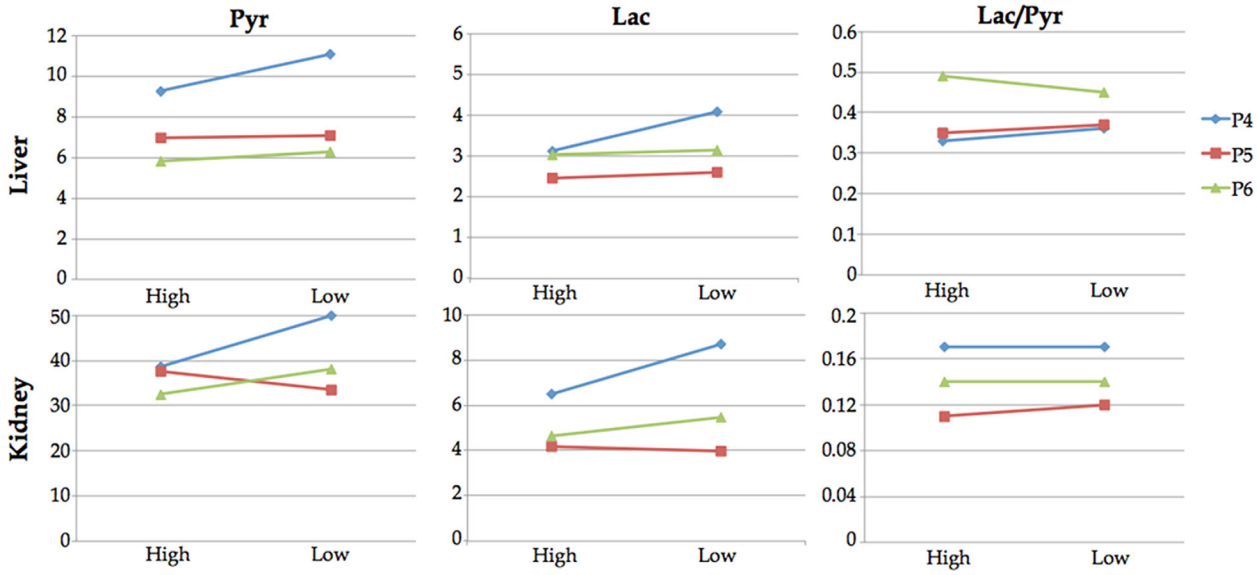

FIG. 7. Time-averaged signal intensities and metabolite ratios from ROIs in the kidney and liver for three rats. In contrast to the brain results, the metabolite signal intensities and corresponding ratios did not show a detectable dependence on the isoflurane level. [Color figure can be viewed in the online issue, which is available at wileyonlinelibrary.com.]

to tissue, the Pyr levels in blood and tissue may change similarly and could be expected to produce a corresponding change in Lac. However, if the Pyr-to-Lac conversion is saturated at the Pyr dose used here, a small decrease in Pyr levels may not lead to lower Lac signal.

A wide range of isoflurane levels was used in this study to quantify the effect on ^{13}C measurements. While an animal can normally be kept stable at a much tighter range of anesthesia during an experiment session, the large variation used here illustrates the need to consider the impact of isoflurane dose when comparing metabolite-to-substrate ratios and rate constants across multiple time-points or different studies for hyperpolarized metabolic imaging in brain. The long duration of anesthesia may also have an effect on the physiological state.

CONCLUSION

The cerebral substrate signal levels, and hence metabolite-to-substrate ratios and apparent rate constants acquired for metabolic imaging of hyperpolarized Pyr and KIC can depend markedly on anesthetic dose in rats anesthetized with isoflurane. In comparison, the signal levels of the metabolic products and their ratios were, within measurement accuracy, largely independent on isoflurane levels. This study highlights the importance of careful attention to the effects of anesthesia on the metabolic measures for hyperpolarized ^{13}C metabolic imaging.

REFERENCES

1. Kurhanewicz J, Vigneron DB, Brindle K, et al. Analysis of cancer metabolism by imaging hyperpolarized nuclei: prospects for translation to clinical research. Neoplasia 2011;13:81–97.
2. Brindle KM, Bohndiek SE, Gallagher FA, Kettunen MI. Tumor imaging using hyperpolarized 13C magnetic resonance spectroscopy. Magn Reson Med 2011;66:505–519.
3. Golman K, Zandt RI, Lerche M, Pehrson R, Ardenkjaer-Larsen JH. Metabolic imaging by hyperpolarized 13C magnetic resonance imaging for in vivo tumor diagnosis. Cancer Res 2006;66:10855–10860.
4. Day SE, Kettunen MI, Gallagher FA, Hu D-E, Lerche M, Wolber J, Golman K, Ardenkjaer-Larsen J-H, Brindle K. Detecting tumor response to treatment using hyperpolarized 13C magnetic resonance imaging and spectroscopy. Nat Med 2007;13:1382–1387.
5. Ross BD, Bhattacharya P, Wagner S, Tran T, Sailasuta N. Hyperpolarized MR imaging: neurologic applications of hyperpolarized metabolism. Am J Neuroradiol 2010;31:24–33.
6. Park I, Larson PEZ, Zierhut ML, Hu S, Bok R, Ozawa T, Kurhanewicz J, Vigneron DB, VandenBerg SR, James CD, Nelson SJ. Hyperpolarized 13C magnetic resonance metabolic imaging: application to brain tumors. Neuro-oncology 2010;12:133–144.
7. Day SE, Kettunen MI, Cherukuri MK, Mitchell JB, Lizak MJ, Morris D, Matsumoto S, Koretsky AP, Brindle M. Detecting response of rat C6 glioma tumors to radiotherapy using hyperpolarized [1-^{13}C]pyruvate and ^{13}C magnetic resonance spectroscopic imaging. Magn Reson Med 2011;65:557–563.
8. Park I, Bok R, Ozawa T, Phillips JJ, James CD, Vigneron DB, Ronen SM, Nelson SJ. Detection of early response to temozolomide treatment in brain tumors using hyperpolarized ^{13}C MR metabolic imaging. J Magn Reson Imaging 2011;33:1284–1290.
9. Park, JM, Josan S, Jang T, Merchant M, Yen, Y-F, Hurd RE, Recht L, Spielman DM, Mayer D. Metabolite kinetics in C6 rat glioma model using magnetic resonance spectroscopic imaging of hyperpolarized [1-^{13}C]pyruvate. Magn Reson Med 2012;68:1886–1893.
10. Marjańska M, Iltis I, Shestov AA, Deelchand DK, Nelson C, Uğurbil K, Henry P-G. In vivo ^{13}C spectroscopy in the rat brain using hyperpolarized [1-^{13}C]pyruvate and [2-^{13}C]pyruvate. J Magn Reson 2010; 206:210–218.
11. Hurd RE, Yen Y-F, Tropp J, Pfefferbaum A, Spielman D, Mayer D. Cerebral dynamics and metabolism of hyperpolarized [1-^{13}C]pyruvate using time-resolved MR spectroscopic imaging. J Cerebr Blood Flow Metabol 2010;30:1734–1741.
12. Mayer D, Yen Y, Takahashi A, Josan S, Tropp J, Rutt BK, Hurd RE, Spielman DM, Pfefferbaum A. Dynamic and high-resolution metabolic imaging of hyperpolarized [1-^{13}C]-pyruvate in the rat brain using a high-performance gradient insert. Magn Reson Med 2011;65:1228–1233.
13. Hurd RE, Yen Y-F, Mayer D, et al. Metabolic imaging in the anesthetized rat brain using hyperpolarized [1-^{13}C] pyruvate and [1-^{13}C] ethyl pyruvate. Magn Reson Med 2010;63:1137–1143.
14. Butt SA, Søgaard LV, Magnusson PO, Lauritzen MH, Laustsen C, Akeson P, Ardenkjaer-Larsen, JH. Imaging cerebral 2-ketoisocaproate metabolism with hyperpolarized ^{13}C magnetic resonance spectroscopic imaging. J Cerebr Blood Flow Metabol 2012;32:1508–1514.
15. Mishkovsky M, Comment A, Gruetter, R. In vivo detection of brain Krebs cycle intermediate by hyperpolarized MR. In Proceedings of the 19th Annual Meeting of ISMRM, Montreal, Canada, 2011. p. 660.

16. Keshari KR, Kurhanewicz J, Bok R, Larson PEZ, Vigneron DB, Wilson DM. Hyperpolarized ^{13}C dehydroascorbate as an endogenous redox sensor for in vivo metabolic imaging. Proc Natl Acad Sci 2011;108: 18606–18611.
17. Bhattacharya P, Zacharias NM, Sailasuta N, Chan HR, Perman WH, Epstein AL, Ross BD. Imaging TCA cycle metabolism in rat brain by hyperpolarization. In Proceedings of the 20th Annual Meeting of ISMRM, Melbourne, Australia, 2012. p. 4410.
18. Grant AK, Vinogradov E, Wang X, Lenkinski RE, Alsop DC. Perfusion imaging with a freely diffusible hyperpolarized contrast agent. Magn Reson Med 2011;66:746–755.
19. Marjanska M, Shestov A, Henry P-G. Brain metabolism under different anesthesia using hyperpolarized [1-^{13}C]-pyruvate. In Proceedings of the 20th Annual Meeting of ISMRM, Melbourne, Australia, 2012. p. 1692.
20. Todd MM, Weeks J. Comparative effects of propofol, pentobarbital, and isoflurane on cerebral blood flow and blood volume. J Neurosurg Anesthesiol 1996;8:296–303.
21. Maekawa T, Tommasino C, Shapiro HM, Keifer-Goodman J, Kohlenberger RW. Local cerebral blood flow and glucose utilization during isoflurane anesthesis in rat. Anesthesiology 1986;65: 144–151.
22. Hendrich KS, Kochanek PM, Melick JA, Schiding JK, Statler KD, Williams DS, Marion DW, Ho C. Cerebral perfusion during anesthesia with fentanyl, isoflurane, or pentobarbital in normal rats studied by arterial spin-labeled MRI. Magn Reson Med 2001;46:202–206.
23. Lenz C, Rebel A, van Ackern K, Kuschinsky W, Waschke KF. Local cerebral blood flow, glucose utilization and flow-metabolism coupling during sevoflurange vs isoflurane anesthesia in rats. Anesthesiology 1998;89:1480–1488.
24. Chi OZ, Anwar M, Sinha AK, Wei HM, Klein SL, Weiss HR. Effects of isoflurane on transport across the blood brain barrier. Anesthesiology 1992;76:426–431.
25. Hansen T, Warner D, Todd M, Vust L, Trawick D. Distribution of cerebral blood flow during halothane vs. isoflurane anesthesia in rats. Anesthesiology 1998;69:332–337.
26. Conzen PF, Vollmar B, Habazettl H, Frink EJ, Peter K, Messmer K. Systemic and regional hernodynamics of isoflurane and sevoflurane in rats. Anesth Analg 1992;74:79–88.
27. Zhao L, Mulker R, Tseng CH, Williamson D, Patz S, Kraft R, Walsworth RL, Jolesz FA, Albert MS. Gradient echo imaging considerations for hyperpolarized ^{129}Xe MR. J Magn Reson B 1996;113: 179–183.
28. Josan S, Spielman D, Yen Y-F, Hurd RE, Pfefferbaum A, Mayer D. Fast volumetric imaging of ethanol metabolism in the rat liver with hyperpolarized [1-^{13}C] pyruvate. NMR Biomed 2012:25:993–999.
29. Josan S, Hurd RE, Kerr AB, Yen Y-F, Larson PE, Pfefferbaum A, Spielman D, Mayer D. Effects of RF excitation scheme on signal-to-noise-ratio and apparent rate constant estimation in dynamic volumetric imaging of hyperpolarized [1-^{13}C]-pyruvate. In Proceedings of the 19th Annual Meeting of ISMRM, Montreal, Canada, 2011. p. 3528.
30. Erakovic V, Zupan G, Varljen J, Laginja J, Simonic A. Altered activities of rat brain metabolic enzymes in electroconvulsive shock-induced seizures. Epilepsia 2001;42:181–189.
31. Karlsson M, Jensen PR, Zandt, R, Gisselsson A, Hansson G, Duus J, Meier S, Lerche MH. Imaging of branched chain amino acid metabolism in tumors with hyperpolarized 13C ketoisocaproate. Int J Cancer 2010;127:729–736.
32. Hutson S. Structure and function of branched chain aminotransferases. Prog Nucleic Acid Res Mol Biol 2001;70:175–206.
33. Pardridge WM. Brain metabolism: a perspective from the blood-brain barrier. Physiol Rev 1983;63:1481–1535.
34. Conn AR, Fell DI, Steele RD. Characterization of a-keto acid transport across blood-brain barrier in rats. Am J Physiol 1983;245: E253–E260.

Research article

NMR IN BIOMEDICINE

Received: 8 August 2013, Revised: 10 December 2013, Accepted: 11 December 2013, Published online in Wiley Online Library: 13 January 2014

(wileyonlinelibrary.com) DOI: 10.1002/nbm.3071

Hyperpolarized [1,4-^{13}C]-diethylsuccinate: a potential DNP substrate for *in vivo* metabolic imaging

Kelvin L. Billingsley[a]*, Sonal Josan[b,c], Jae Mo Park[b], Sui Seng Tee[b], Eleanor Spielman-Sun[d], Ralph Hurd[e], Dirk Mayer[f] and Daniel Spielman[b,g]

The tricarboxylic acid (TCA) cycle performs an essential role in the regulation of energy and metabolism, and deficiencies in this pathway are commonly correlated with various diseases. However, the development of non-invasive techniques for the assessment of the cycle *in vivo* has remained challenging. In this work, the applicability of a novel imaging agent, [1,4-^{13}C]-diethylsuccinate, for hyperpolarized ^{13}C metabolic imaging of the TCA cycle was explored. *In vivo* spectroscopic studies were conducted in conjunction with *in vitro* analyses to determine the metabolic fate of the imaging agent. Contrary to previous reports (Zacharias NM *et al*. J. Am. Chem. Soc. 2012; 134: 934–943), [^{13}C]-labeled diethylsuccinate was primarily metabolized to succinate-derived products not originating from TCA cycle metabolism. These results illustrate potential issues of utilizing dialkyl ester analogs of TCA cycle intermediates as molecular probes for hyperpolarized ^{13}C metabolic imaging. Copyright © 2014 John Wiley & Sons, Ltd.
Additional supporting information may be found in the online version of this article at the publisher's web site.

Keywords: hyperpolarized carbon-13; dynamic nuclear polarization; magnetic resonance spectroscopy; tricarboxylic acid cycle

INTRODUCTION

Hyperpolarized ^{13}C MRS has shown considerable potential for disease diagnosis and treatment (1–10). This technique provides a complement to conventional metabolomic methods, adding real time dynamics at high spatial resolution. A key component of this emergent field is the development of novel molecular probes that can monitor these pathways distinctly faster. The tricarboxylic acid (TCA) cycle, in particular, has received significant attention as it plays a central role in cellular metabolism for the production of energy, and misregulation of the TCA cycle has increasingly been correlated with numerous diseases (11). For example, mutations in succinate dehydrogenase, fumarate hydratase, and isocitrate dehydrogenase are well documented in tumorigenesis (12), and TCA cycle enzymes have been utilized as key biomarkers in cancer diagnosis (13,14). Furthermore, prolonged alterations in TCA cycle metabolism can result in deleterious modifications to mitochondrial energy production, which has been causally implicated in the progression of various neurological disorders (15–17).

Several strategies have been proposed for monitoring the efficiency of the TCA cycle via hyperpolarized ^{13}C metabolic imaging. The most prominent method is the application of hyperpolarized [^{13}C]-pyruvate, which has typically been employed as an indirect marker of the pathway (Fig. 1(A)). [1-^{13}C]-pyruvate is converted to acetyl-CoA, which can enter the cycle, and [^{13}C]-bicarbonate, via pyruvate dehydrogenase (1,18–22). Although the detection of [^{13}C]-bicarbonate indicates flux into acetyl-CoA, this strategy does not provide any information pertaining to the TCA cycle and its intermediates. Alternatively, hyperpolarized [2-^{13}C]-pyruvate, which forms [1-^{13}C]-acetyl-CoA and subsequently integrates the label into TCA cycle intermediates, has been employed (23,24). However with the exception of citrate, only metabolites not on the TCA pathway (i.e. [5-^{13}C]-glutamate (23–25) and [1-^{13}C]-acetylcarnitine (26)) are regularly observed due in part to the relative rate of consumption of [2-^{13}C]-pyruvate by alternative pathways. Although [^{13}C]-pyruvate is metabolized by the TCA

* *Correspondence to: Kelvin L. Billingsley, San Francisco State University, Department of Chemistry and Biochemistry, San Francisco, CA, USA.*
E-mail: klbillin@sfsu.edu

a *K. L. Billingsley*
San Francisco State University, Department of Chemistry and Biochemistry, San Francisco, CA, USA

b *S. Josan, J. M. Park, S. S. Tee, D. Spielman*
Stanford University, Department of Radiology, Stanford, CA, USA

c *S. Josan*
SRI International, Neuroscience Program, Menlo Park, CA, USA

d *E. Spielman-Sun*
Oberlin College, Department of Chemistry, Oberlin, OH, USA

e *R. Hurd*
GE Healthcare, Applied Sciences Laboratory, Menlo Park, CA, USA

f *D. Mayer*
University of Maryland, Baltimore, Department of Diagnostic Radiology and Nuclear Medicine, Baltimore, MD, USA

g *D. Spielman*
Stanford University, Department of Electrical Engineering, Stanford, CA, USA

Abbreviations used: *TCA cycle, tricarboxylic acid cycle; DNP, dynamic nuclear polarization; PHIP, parahydrogen-induced polarization; DES, diethylsuccinate; MES, monoethylsuccinate.*

NMR IN BIOMEDICINE

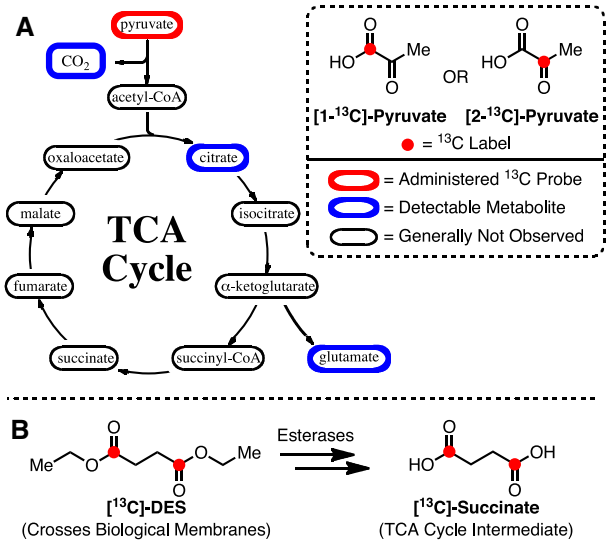

Figure 1. (A) Overview of compounds related to the TCA cycle that are generally detected when employing hyperpolarized [1-^{13}C]- or [2-^{13}C]-pyruvate. (B) Strategy for probing TCA cycle metabolism. DNP substrate, [^{13}C]-DES, enters the intracellular environment and is converted into a TCA cycle intermediate.

cycle, these probes have not been able to directly evaluate the catalytic activity of specific enzymes in the pathway.

Ongoing efforts are focused on the development of novel small molecule agents for monitoring TCA cycle metabolism that overcome the limitations associated with [^{13}C]-pyruvate. For example, [^{13}C]-labeled fumarate or succinate offers the advantage that they are primarily metabolized by the TCA cycle, whereas [^{13}C]-pyruvate can be diverted to several pathways (e.g. gluconeogenesis and fatty acid biosynthesis). Though both [^{13}C]-labeled fumarate (27,28) and succinate (29,30) derivatives have been successfully hyperpolarized, neither substrate is transported into the cytosol and mitochondria at a sufficient rate for evaluation within the 1–2 min T_1-limited time constraint of *in vivo* hyperpolarized ^{13}C experiments. Hence, the utility of these agents, particularly fumarate (27,28), has been limited to assessing cell necrosis, in which disruption of the cellular membranes allows TCA cycle enzymes to leak into the extracellular space.

A recent method was reported for the direct monitoring of TCA cycle metabolism via hyperpolarized ^{13}C MRS *in vivo*. This process relied upon the use of a new molecular probe, [1-^{13}C, 2,3-d_2]-diethylsuccinate, which was prepared via parahydrogen-induced polarization (PHIP) from the corresponding [1-^{13}C, 2,3-d_2]-diethylfumarate (31). Diethylsuccinate (DES), thought to be easily transported across biological membranes, can then be converted *in vivo* to succinate (via monoethylsuccinate (MES) as an intermediate) by endogenous esterases (Fig. 1(B)) (32–35). Upon entry into the mitochondria, succinate can then be metabolized by the TCA cycle and provide an analysis of the metabolic state in the intracellular environment. Importantly, this recent report utilizing PHIP hyperpolarized [1-^{13}C, 2,3-d_2]-diethylsuccinate was the first to suggest that various late-stage TCA cycle intermediates (e.g. fumarate and malate) could be monitored *in vivo*. Furthermore, aspartate, which plays a key role in the regulation of redox state in the mitochondria (36), was also detected. The PHIP method achieved 2.1% + 0.6% of hyperpolarized [1-^{13}C, 2,3-d_2]-diethylsuccinate, and spectra were obtained from the whole body of mice after either i.v. or i.p. injection of 20 mM substrate.

Dynamic nuclear polarization (DNP), which is widely employed for *in vivo* studies (37), also allows for substantial enhancement of nuclear polarization leading to improved detection limits for *in vivo* imaging and novel information concerning metabolic pathways. In this work, we explore the synthesis, development, and application of [1,4-^{13}C]-diethylsuccinate ([^{13}C]-DES) as a DNP substrate for hyperpolarized ^{13}C metabolic imaging of the TCA cycle. These studies, which are the first to examine DES as a DNP agent, resulted in a reexamination of the *in vivo* metabolic fate of [^{13}C]-labeled DES imaging agents.

EXPERIMENTAL DETAILS

General

All reagents were purchased from Aldrich unless otherwise noted and used without further purification.

Synthesis of [1,4-^{13}C]-diethylsuccinate

[^{13}C]-DES was prepared by the following procedure. To an oven-dried 100 mL round-bottom flask equipped with a magnetic stir bar, 425 mg (3.54 mmol) of [1,4-^{13}C]-succinic acid (99% 1,4-^{13}C, CLM-1084, Cambridge Isotopes, Andover, MA) was added. After the addition of anhydrous ethanol (35 mL), 1.8 mL (1.54 g, 14.2 mmol) of trimethylsilyl chloride was added dropwise via syringe over the course of two minutes. The reaction was allowed to stir at room temperature. After 5 h, the reaction was quenched with 10 mL of saturated sodium bicarbonate solution. Additional bicarbonate was removed via filtration, and ethanol was removed under vacuum. The desired product was extracted from the aqueous solution with 4 × 8 mL of dichloromethane. Organic layers were combined, dried over anhydrous sodium sulfate, and filtered; the solvent was removed by evaporation and 480 mg (77% yield) of pure product was isolated as a colorless oil. ^{1}H NMR ($CDCl_3$, 500 MHz) δ 4.15 (q, J = 7 Hz, 4H, –OCH_2–), 2.60 (s, 4H, –C(O)CH_2–), 1.12 (t, J = 7 Hz, 6H, –CH_3) ppm; ^{13}C NMR ($CDCl_3$, 125 MHz) δ 172.4 (–C(O)–), 60.8 (–OCH_2–), 29.1 (–C(O)CH_2–), 14.1 (–CH_3) ppm.

Synthesis of [1,4-^{13}C]-monoethylsuccinate

In order to reference [1,4-^{13}C]-monoethylsuccinate ([^{13}C]-MES), a sample containing [^{13}C]-succinate, [^{13}C]-MES and [^{13}C]-DES was prepared by the following procedure. To an oven-dried 100 mL round-bottom flask equipped with a magnetic stir bar, 100 mg (0.83 mmol) of [1,4-^{13}C]-succinic acid was added. After the addition of anhydrous ethanol (5 mL), 0.106 mL (90.5 mg, 0.83 mmol) of trimethylsilyl chloride was added dropwise via syringe over the course of 1 min. The reaction was allowed to stir at room temperature. After 30 min, the reaction was quenched with 2 mL of saturated sodium bicarbonate solution. Additional bicarbonate was removed via filtration, and ethanol was removed under vacuum. The desired product was extracted from the aqueous solution with 4 × 4 mL of dichloromethane. Organic layers were combined, dried over anhydrous sodium sulfate, and filtered; the solvent was removed by evaporation to yield a sample with 2:3:6 ratio of [^{13}C]-succinate:[^{13}C]-DES:[^{13}C]-MES as determined by ^{1}H-NMR (D_2O).

Dynamic nuclear polarization of [1,4-^{13}C]-diethylsuccinate

The samples to be polarized consisted of 40 μL of a mixture of [^{13}C]-DES (6 M, neat) and 20 mM α,γ-bisdiphenylene-β-phenylallyl (BDPA) radical. The samples were polarized via DNP using a HyperSense system (Oxford Instruments Molecular Biotools, Oxford, UK). The polarized samples were dissolved in a solution of 40 mM Tris buffer, 50 mM NaCl and 0.1 g/L EDTA-Na_2, leading to an 80 mM solution of the hyperpolarized substrate with a pH of approximately 7.5.

In vivo experiments

Healthy male Wistar rats (393 ± 48 g body weight, $n = 3$) were injected with 2.6–3.2 mL of the hyperpolarized solution (target dose = 1 mmol per kg body weight) through a tail vein catheter at a rate of approximately 0.25 mL/s. The time from dissolution to start of injection was approximately 20 s.

The rats were anesthetized initially with 2.5% isoflurane in oxygen (1.5 L/min) for tail vein catheterization. Respiration, rectal temperature, heart rate and oxygen saturation were monitored throughout the experiments, with temperature regulated using a warm water blanket placed underneath the animals. Each animal received two injections of the hyperpolarized substrate, approximately 1.5–2 h apart. All animal procedures were approved by the SRI Institutional Animal Care and Use Committee.

All experiments were performed on a clinical 3 T Signa MR scanner (GE Healthcare, Waukesha, WI), using a custom-built ^{13}C transmit/receive surface coil (diameter = 28 mm) placed over the heart with the rat supine. A quadrature volume rat ^{1}H coil (diameter = 70 mm) was used for anatomical localization and to confirm the position of the ^{13}C coil with respect to the heart. Single-shot fast spin-echo ^{1}H MR images in the axial, sagittal and coronal planes with nominal in-plane resolution of 0.47 mm and 2 mm slice thickness were acquired as anatomical references for prescribing the ^{13}C MRS experiments. A non-selective pulse-and-acquire sequence with an excitation flip angle of 6°, spectral width of 5 kHz and 2048 points was used to acquire ^{13}C spectra from the heart every 3 s over a 4 min period starting at the same time as the [^{13}C]-DES injection.

In vitro experiments

In vitro experiments were performed in order to facilitate the identification of the metabolites observed from [^{13}C]-DES *in vivo* experiments. These experiments include exposure of [^{13}C]-DES to the following.

(1) *Pig liver esterase*. [^{13}C]-DES (10 mM) was incubated at 37 °C with pig liver esterase (7.5 units/mL) in RPMI media supplemented with 10% fetal bovine serum and 5% penicillin–streptomycin. Pig liver esterase has been previously shown to selectively cleave a single ester of DES (38). After 5 min, the solution was then analyzed via ^{13}C-NMR on an 11.7 T instrument to determine the product distribution.

(2) *Rat blood*. Blood draws were performed from healthy male Wistar rats via tail vein catheter. The freshly drawn blood (1 mL) was immediately dosed with [^{13}C]-DES (100 mM) and the solution was incubated at 37 °C. At various time points

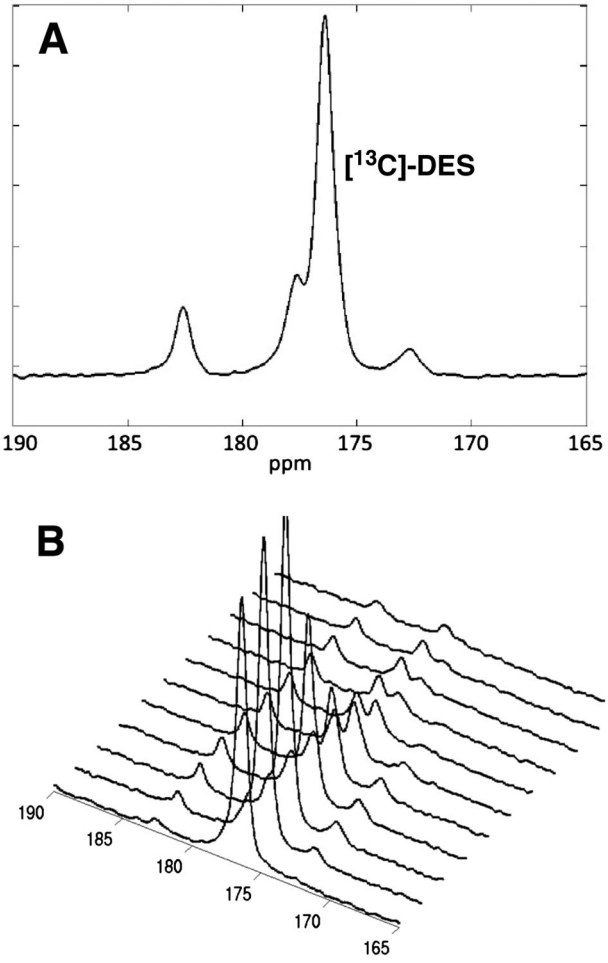

Figure 3. (A) Representative time-averaged spectrum from 6 to 45 s obtained from heart beginning at the administration of 80 mM [^{13}C]-DES. (B) Representative stackplot of spectra obtained from heart at 3 s intervals beginning at the administration of 80 mM [^{13}C]-DES.

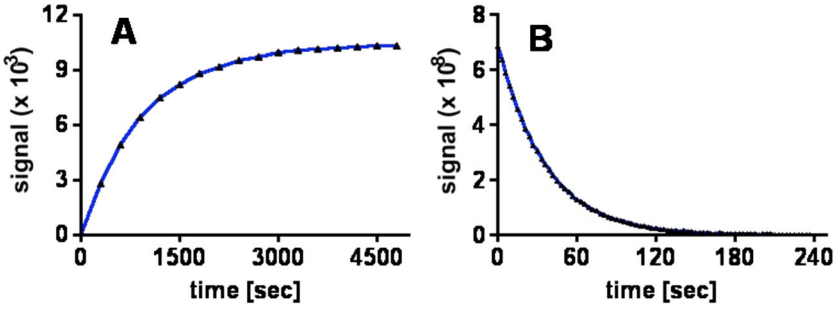

Figure 2. (A) Polarization buildup curve (3.35 T, 1.4 K) of [^{13}C]-DES doped with 20 mM BDPA taken at $P(+) = 94.116$ GHz. (B) Liquid-state T_1 decay (3 T, 298 K) of [^{13}C]-DES samples with 20 mM BDPA ($T_1 = 38$ s).

(1, 5, 20 and 60 min), a 0.25 mL aliquot of the solution was removed, and the sample was quenched with methanol (0.25 mL). Each sample was then analyzed via ^{13}C-NMR on an 11.7 T instrument to determine the metabolic fate of [^{13}C]-DES.

(3) *Homogenates of rat heart*. Rat hearts were obtained from male Wistar rats and samples were maintained at −80 °C. Samples were thawed, homogenized in buffer (210 mM mannitol, 70 mM sucrose, 5 mM MOPS and 1 mM EDTA in D_2O), and centrifuged at 3000 *g* to obtain desired homogenates. These homogenates were dosed with [^{13}C]-DES (10 mM) and incubated at 37 °C for 5 min. These samples were analyzed at various time points (5, 20, 60 and 300 min) via ^{13}C-NMR on an 11.7 T instrument to determine the product distribution.

RESULTS AND DISCUSSION

[^{13}C]-DES was successfully formulated for DNP through the addition of 20 mM BDPA to 6 M [^{13}C]-DES (neat). The solid-state polarization buildup time constant was 1517 ± 91 s ($n = 8$) with a liquid-state polarization level of 5.5% (Fig. 2). The T_1 (^{13}C-labeled carbonyls) was found to be 37.9 s in solution at 3 T. No observable toxicity (pulse or respiration) was detected upon i.v. administration of a Tris-buffered solution containing up to 80 mM [^{13}C]-DES. In addition, no detectable ester hydrolysis of [^{13}C]-DES to yield [^{13}C]-MES or [1,4-^{13}C]-succinate was observed when [^{13}C]-DES was exposed to the dissolution conditions (40 mM Tris buffer, 50 mM NaCl and 0.1 g/L EDTA-Na_2, pH = 7.5) for a period of up to 20 min. Furthermore, no hydrolysis was observed during the dissolution process, which requires superheating of the frozen sample (see supporting information).

Figure 3 displays a representative spectrum (A) and time-resolved stackplot (B) obtained from a rat heart after i.v. administration of hyperpolarized [^{13}C]-DES. In these experiments, a bolus injection of 80 mM [^{13}C]-DES was performed, and the substrate was observed at 176.4 ppm along with three other distinct signals at 182.5, 177.6 and 172.7 ppm. Lower substrate concentration (40 mM) did not significantly affect metabolites observed or the relative quantities detected. Importantly, our spectra closely resembled the previously observed product distribution found in the report by Zacharias *et al*. on PHIP-mediated hyperpolarization of [1-^{13}C, 2,3-d_2]-diethylsuccinate (31). The PHIP study of DES did, however, consistently detect a minor signal at 175.2 ppm, which is not observed in our experiments and was indicated to be fumarate. The previous work assigned the three major signals at 182.5, 177.6 and 172.7 ppm to succinate, malate and aspartate, respectively. Despite the overall similarity of the spectra, we found several inconsistencies with the previous report's assignments: (1) the chemical shifts found in the metabolite reference data did not agree with the assigned spectra (31), and (2) a single resonance was attributed to asymmetric compounds (i.e. malate and aspartate) that should display two resolvable signals due to scrambling of the ^{13}C label between the C1 and C4 positions (39). Given these issues, we sought to reexamine the fate of

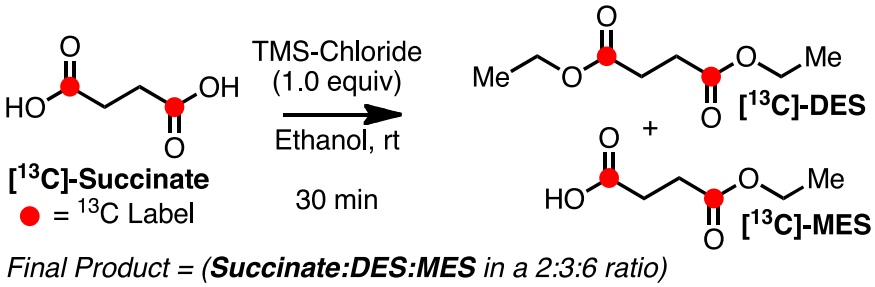

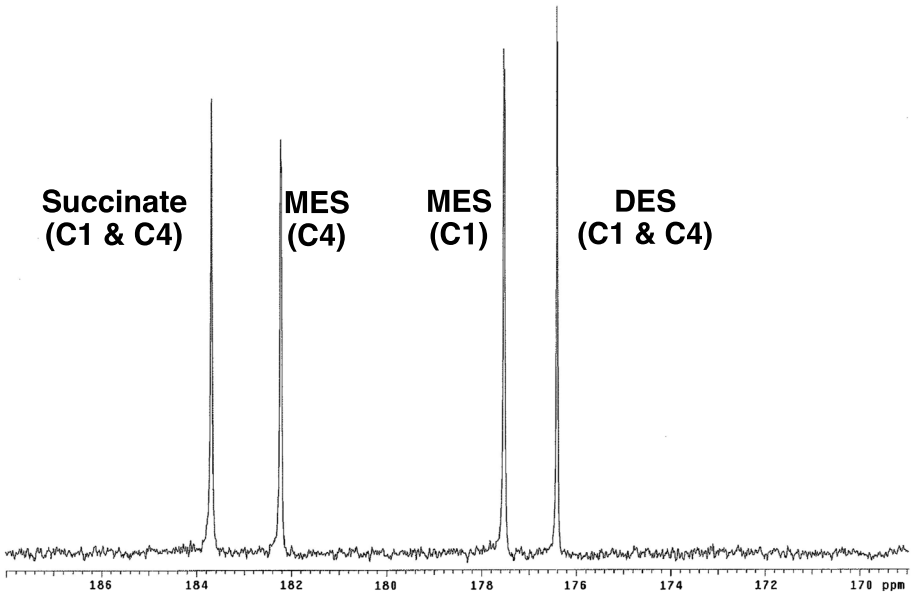

Figure 4. Synthesis of reference sample containing succinate, DES and MES. The ^{13}C-NMR spectrum displays the relative chemical shift of these compounds.

[^{13}C]-DES *in vivo* and conduct a thorough study to determine the metabolite distribution.

In order to evaluate whether the metabolites observed *in vivo* correspond to products of esterase cleavage (i.e. [^{13}C]-MES and/or [1,4-^{13}C]-succinate), a reference standard was prepared with a mixture of these products. A sample containing a 2:3:6 ratio of succinate:DES:MES was prepared through treating [1,4-^{13}C]-succinate with 1.0 equivalent of trimethylsilyl chloride in ethanol at room temperature (Fig. 4). The ratio of metabolites was determined through analysis of the ^{1}H-NMR of the sample. This standard was then used to reference the MES and succinate carbonyl shifts via ^{13}C-NMR on an 11.7 T NMR instrument. Both [1,4-^{13}C]-succinate (183.7 ppm) and [^{13}C]-DES (176.4 ppm) yield a single resonance, as they are symmetric molecules. It was discovered that the peaks at 182.5 and 177.6 ppm correspond to [^{13}C]-MES and do not originate from metabolism via the TCA cycle (Fig. 3(B)). Based upon the difference in chemical shifts, [1,4-^{13}C]-succinate should be resolvable *in vivo* from the signal corresponding to [4-^{13}C]-MES, so we conclude that [1,4-^{13}C]-succinate is not forming in detectable quantities during the time frame of the *in vivo* experiment.

DES was developed as an agent for hyperpolarized ^{13}C metabolic imaging because it was hypothesized to cross biological membranes more readily than the parent compound. However, given that esterases are known to be present in the blood (40), we sought to examine whether cleavage of [^{13}C]-DES to [^{13}C]-MES could occur extracellularly prior to entry into the cytosol or mitochondria. In order to initially confirm that [^{13}C]-DES was a substrate for esterases, the substrate was incubated with pig liver esterase. As anticipated, [^{13}C]-MES was cleanly formed and two signals (182.5 and 177.6 ppm) were observed. Next, [^{13}C]-DES was added to a freshly drawn rat blood sample, and [^{13}C]-MES was again rapidly formed in the first 5 min (Fig. 5). No signal corresponding to the unknown compound (172.7 ppm) was detected under these conditions.

In order to determine the identity of this unknown metabolite, we sought to generate, isolate and characterize the species via *in vitro* methods. [^{13}C]-DES was incubated with homogenates of rat heart tissue. In all trials, conversion to [^{13}C]-MES was observed. However, only trace levels of the unknown metabolite at 172.7 ppm were detected, and unfortunately the product could not be successfully characterized via this process. Furthermore, prostate cancer cells (PC-3) were dosed with [^{13}C]-DES (10 mM), but no metabolic product corresponding to the signal at 172.7 ppm was observed (see supporting information).

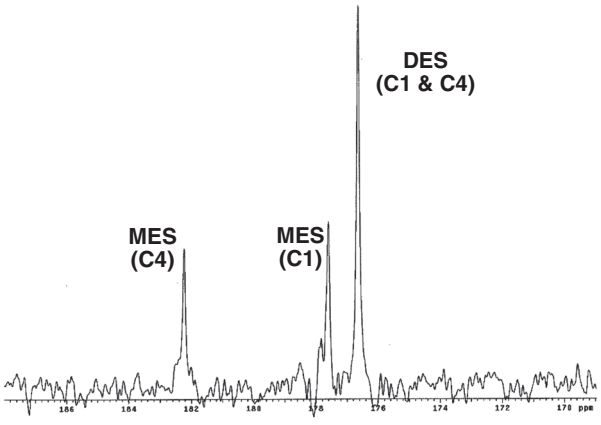

Figure 5. Exposure of [^{13}C]-DES to rat blood. Representative spectrum (20 min) shown to display the conversion to [^{13}C]-MES via endogenous esterases.

In order to assign the unknown signal, a series of succinate-derived compounds was referenced and compared with previously published TCA cycle metabolites (Table 1). As described above, the signal at 172.7 ppm did not coincide with any intermediate of the TCA cycle. The chemical shifts of aspartate and glutamate, which are products typically formed from TCA cycle intermediates, were also not consistent with the unknown metabolite. However, based upon this analysis, the unknown species in the *in vivo* spectra was tentatively assigned to [1,4-^{13}C]-succinic anhydride. This assignment was in agreement with the fact that only a single resonance is observed, which would be expected from a symmetrical molecule such as [1,4-^{13}C]-succinic anhydride. In addition, [1,4-^{13}C]-succinic anhydride maintains the carbon skeleton of [^{13}C]-DES without performing any C–C bond cleavage steps, which in the TCA cycle would be associated with the loss and subsequent observation of [^{13}C]-CO_2 at 125 ppm, which is in fast exchange with [^{13}C]-bicarbonate at 161 ppm. Neither resonance was observed in the *in vivo* experiment.

Succinate would be expected to have a relatively slow rate of dehydration under normal physiological conditions (41,42); therefore, it is unlikely that [1,4-^{13}C]-succinate converts to [1,4-^{13}C]-succinic anhydride. However, monoesters of succinate have been shown to be unstable due to the close proximity of the neighboring carboxyl group (43), which results in the formation of the corresponding anhydrides. Upon formation, [1,4-^{13}C]-succinic anhydride should slowly hydrolyze to furnish [1,4-^{13}C]-succinate, which may then be metabolized by the TCA cycle but is not observed at detectable levels in our experiments. Further, although studies with hyperpolarized [1,4-^{13}C]-succinate anhydride were attempted, immediate hydrolysis of the substrate to yield [1,4-^{13}C]-succinate was observed under standard dissolution conditions.

Table 1. Chemical shifts of TCA cycle intermediates, commonly observed metabolites and succinate-based compounds

compound	position	pH	^{13}C shift
succinate	C1	7.4	183.7[a]
citrate	C6	7.4	182.5[b]
monoethylsuccinat	C4	7.4	182.3[a]
glutamate	C5	7.4	181.8[c]
malate	C4	7.3	181.6[b]
isocitrate	C1,C5	7.0	181.4[b]
isocitrate	C6	7.0	180.7[b]
malate	C1	7.3	180.4[b]
citrate	C1,C5	7.4	179.7[b]
aspartate	C1	7.4	178.5[c]
monoethlsuccinate	C1	7.4	177.6[a]
diethylsuccinate	C1	7.4	176.4[a]
asparate	C1	7.4	175.3[a]
fumarate	C1	7.4	172.3[b]
glutamate	C1	7.4	175.1[c]
succinic anhydride	*C1*	7.4	172.8[a]

[a]Measurements conducted in 100 mM sodium bicarbonate buffer (ionic strength = 0.1) at pH = 7.4 and temperature = 23 °C.
[b]Ref. 32 (temperature = 23 °C).
[c]UT-Southwestern Advanced Imaging Research Center (AICR) metabolite database.

CONCLUSIONS

Although the diester analog, [^{13}C]-DES, of [^{13}C]-succinate is more adept at crossing cellular membranes, the substrate is not successfully metabolized by the TCA cycle. [^{13}C]-DES is initially metabolized to [^{13}C]-MES via endogenous esterases, which may occur in the blood rather than the intracellular environment. Further metabolism of the substrate leads to formation of [1,4-^{13}C]-succinic anhydride. Contrary to previous reports of PHIP hyperpolarized [^{13}C]-labeled DES, TCA cycle-derived metabolites (succinate, malate and aspartate) were not observed. However, the previous work was able to detect [^{13}C]-labeled fumarate *in vivo*. Ongoing research efforts are directed towards the development of novel agents that have the ability to monitor *in vivo* TCA cycle metabolism and, in turn, address the current limitations in this field.

Acknowledgements

The following grants and funding organizations are acknowledged: NIH grants AA018681, AA005965, AA013521-INIA, EB009070, P41 EB015891, DOD grant PC100427 and GE Healthcare.

REFERENCES

1. Golman K, Zandt RI, Lerche M, Pehrson R, Ardenkjaer-Larsen JH. Metabolic imaging by hyperpolarized ^{13}C magnetic resonance imaging for in vivo tumor diagnosis. Cancer Res. 2006; 66: 10855–10860.
2. Day SE, Kettunen MI, Gallagher FA, Hu D-E, Lerche M, Wolber J, Golman K, Ardenkjaer-Larsen JH, Brindle K. Detecting tumor response to treatment using hyperpolarized ^{13}C magnetic resonance imaging and spectroscopy. Nat. Med. 2007; 13: 1382–1387.
3. Ross BD, Bhattacharya P, Wagner S, Tran T, Sailasuta N. Hyperpolarized MR imaging: neurologic applications of hyperpolarized metabolism. Am. J. Neuroradiol. 2010; 31: 24–33.
4. Park I, Larson PEZ, Zierhut ML, Hu S, Bok R, Ozawa T, Kurhanewicz J, Vigneron DB, VandenBerg SR, James CD, Nelson SJ. Hyperpolarized 13C magnetic resonance metabolic imaging: application to brain tumors. Neuro Oncol. 2010; 12: 133–144.
5. Day SE, Kettunen MI, Cherukuri MK, Mitchell JB, Lizak MJ, Morris D, Matsumoto S, Koretsky AP, Brindle KM. Detecting response of rat C6 glioma tumors to radiotherapy using hyperpolarized [1-^{13}C]pyruvate and ^{13}C magnetic resonance spectroscopic imaging. Magn. Reson. Med. 2011; 65: 557–563.
6. Park I, Bok R, Ozawa T, Phillips JJ, James CD, Vigneron DB, Ronen SM, Nelson SJ. Detection of early response to temozolomide treatment in brain tumors using hyperpolarized ^{13}C MR metabolic imaging. J. Magn. Reson. Imaging 2011; 33: 1284–1290.
7. Kurhanewicz J, Vigneron DB, Brindle KM, Chekmenev EY, Comment A, Cunningham CH, DeBerardinis RJ, Green GG, Leach MO, Rajan SS, Rizi RR, Ross BR, Warren WS, Malloy CR. Analysis of cancer metabolism by imaging hyperpolarized nuclei: prospects for translation to clinical research. Neoplasia 2011; 13: 81–97.
8. Brindle KM, Bohndiek SE, Gallagher FA, Kettunen MI. Tumor imaging using hyperpolarized ^{13}C magnetic resonance spectroscopy. Magn. Reson. Med. 2011; 66: 505–519.
9. Park JM, Josan S, Jang T, Merchant M, Yen Y-F, Hurd RE, Recht L, Spielman DM, Mayer D. Metabolite kinetics in C6 rat glioma model using magnetic resonance spectroscopic imaging of hyperpolarized [1-^{13}C]pyruvate. Magn. Reson. Med. 2012; 68: 1886–1893.
10. Karlsson M, Jensen PR, Duus JØ, Meier S, Lerche MH. Development of dissolution DNP-MR substrates for metabolic research. Appl. Magn. Reson. 2012; 43: 223–236.
11. Briere JJ, Favier J, Gimenez-Roqueplo A-P, Rustin P. Tricarboxylic acid cycle dysfunction as a cause of human diseases and tumor formation. Am. J. Physiol. Cell Physiol. 2006; 291: C1114–C1120.
12. Cardaci S, Ciriolo MR. TCA cycle defects and cancer: when metabolism tunes redox state. Int. J. Cell Biol. 2012; 2012: 1–9.
13. Pollard PJ, Wortham NC, Tomlinson IP. The TCA cycle and tumorigenesis: the examples of fumarate hydratase and succinate dehydrogenase. Ann. Med. 2003; 35: 632–639.
14. Bayley J-P, Devilee P. Warburg tumours and the mechanisms of mitochondrial tumour suppressor genes. Barking up the right tree? Curr. Opin. Genet. Dev. 2010; 20: 324–329.
15. Beal MF. Energetics in the pathogenesis of neurodegenerative diseases. Trends Neurosci. 2000; 23: 298−304.
16. Henry PG, Lebon V, Vaufrey F, Brouillet E, Hantraye P, Bloch G. Decreased TCA cycle rate in the rat brain after acute 3-NP treatment measured by *in vivo* ^{1}H-^{13}C NMR spectroscopy. J. Neurochem. 2002; 82: 857−866.
17. Bubber P, Haroutunian V, Fisch G, Blass JP, Gibson GE. Mitochondrial abnormalities in Alzheimer brain: mechanistic implications. Ann. Neurol. 2005; 57: 695−703.
18. Golman K, Zandt R, Thaning M. Real-time metabolic imaging. Proc. Natl. Acad. Sci. U. S. A. 2006; 103: 11270−11275.
19. Arunachalam A, Whitt D, Fish K, Giaquinto R, Piel J, Watkins R, Hancu I. Accelerated spectroscopic imaging of hyperpolarized C-13 pyruvate using SENSE parallel imaging. NMR Biomed. 2009; 22: 867−873.
20. Wilson DM, Keshari KR, Larson PE, Chen AP, Hu S, Van Criekinge M, Bok R, Nelson SJ, Macdonald JM, Vigneron DB, Kurhanewicz J. Multi-channel metabolic imaging, with SENSE reconstruction, of hyperpolarized [1-13C] pyruvate in a live rat at 3.0 tesla on a clinical MR scanner. J. Magn. Reson. 2010; 205: 141−147.
21. Hurd RE, Yen Y-F, Mayer D, Chen A, Wilson D, Kohler S, Bok R, Vigneron D, Kurhanewicz J, Tropp J, Spielman D, Pfefferbaum A. Metabolic imaging in the anesthetized rat brain using hyperpolarized [1-^{13}C] pyruvate and [1-^{13}C] ethyl pyruvate. Magn. Reson. Med. 2010; 63: 1137−1143.
22. Park JM, Recht LD, Josan S, Merchant M, Jang T, Yen Y-F, Hurd RE, Spielman DM, Mayer D. Metabolic response of glioma to dichloroacetate measured in vivo by hyperpolarized 13C magnetic resonance spectroscopic imaging. Neuro Oncol. 2013; 15: 433–441.
23. Schroeder MA, Atherton HJ, Ball DR, Cole MA, Heather LC, Griffin JL, Clarke K, Radda GK, Tyler DJ. Real-time assessment of Krebs cycle metabolism using hyperpolarized ^{13}C magnetic resonance spectroscopy. FASEB J. 2009; 23: 2529–2538.
24. Park JM, Josan S, Grafendorfer T, Yen Y-F, Hurd RE, Spielman DM, Mayer D. Measuring mitochondrial metabolism in rat brain *in vivo* using MR Spectroscopy of hyperpolarized [2-^{13}C]pyruvate. NMR Biomed. 2013. DOI: 10.1002/nbm.2935
25. Marjanska M, Iltis I, Shestov AA, Deelchand DK, Nelson C, Ugurbil K, Henry P-G. In vivo 13C spectroscopy in the rat brain using hyperpolarized [1-13C]pyruvate and [2-13C]pyruvate. J. Magn. Reson. 2010; 206: 210–218.
26. Schroeder MA, Atherton HJ, Dodd MS, Lee P, Cochlin LE, Radda GK, Clarke K, Tyler DJ. The cycling of acetyl-coenzyme A through acetylcarnitine buffers cardiac substrate supply: a hyperpolarized ^{13}C magnetic resonance study. Circ. Cardiovasc. Imaging 2012; 5: 201–209.
27. Gallagher FA, Kettunen MI, Hu D-E, Jensen PR, Zandt R, Karlsson M, Gisselsson A, Nelson SK, Witney TH, Bohndiek SE, Hansson G, Peitersen T, Lerche MH, Brindle KM. Production of hyperpolarized [1,4-$^{13}C_2$]malate from [1,4-$^{13}C_2$]fumarate is a marker of cell necrosis and treatment response in tumors. Proc. Natl. Acad. Sci. U. S. A. 2009; 106: 19801–19806.
28. Clatworthy MR, Kettunen MI, Hu D-E, Matthews RJ, Witney TH, Kennedy BWC, Bohndiek SE, Gallagher FA, Jarvis LB, Smith KGC, Brindle KM. Magnetic resonance imaging with hyperpolarized [1,4-$^{13}C_2$]fumarate allows detection of early renal acute tubular necrosis. Proc. Natl. Acad. Sci. U. S. A. 2012; 109: 13374–13379.
29. Bhattacharya P, Chekmenev EY, Perman WH, Harris KC, Lin AP, Norton VA, Tan CT, Ross BD, Weitikamp DP. Towards hyperpolarized ^{13}C-succinate imaging of brain cancer. J. Magn. Reson. 2007; 186: 150–155.
30. Chekmenev EY, Hövener J, Norton VA, Harris K, Batchelder LS, Bhattacharya P, Ross BR, Weitekamp DP. PASADENA hyperpolarization of succinic acid for MRI and NMR spectroscopy. J. Am. Chem. Soc. 2008; 130: 4212–4213.
31. Zacharias NM, Chan HR, Sallasuta N, Ross BD, Bhattacharya P. Real-time molecular imaging of tricarboxylic acid cycle metabolism in vivo by hyperpolarized 1-^{13}C diethyl succinate. J. Am. Chem. Soc. 2012; 134: 934–943.
32. Ladriere L, Zhang TM, Malaisse WJ. Effects of succinic acid dimethyl ester infusion on metabolic, hormonal, and enzymatic variables in starved rats. J. Parenter. Enteral Nutr. 1996; 20: 251−256.

33. Malaisse WJ, Zhang TM, Verbruggen I, Willem R. Enzyme-to-enzyme channelling of Krebs cycle metabolic intermediates in Caco-2 cells exposed to [2-13C]propionate. Biochem. J. 1996; 317(3): 861−863.
34. Isaacs JS, Jung YJ, Mole DR, Lee S, Torres-Cabala C, Chung YL, Merino M, Trepel J, Zbar B, Toro J, Ratcliffe PJ, Linehan WM, Neckers L. HIF overexpression correlates with biallelic loss of fumarate hydratase in renal cancer: novel role of fumarate in regulation of HIF stability. Cancer Cell 2005; 8: 143−153.
35. Selak MA, Armour SM, MacKenzie ED, Boulahbel H, Watson DG, Mansfield KD, Pan Y, Simon MC, Thompson CB, Gottlieb E. Succinate links TCA cycle dysfunction to oncogenesis by inhibiting HIF-alpha prolyl hydroxylase. Cancer Cell 2005; 7: 77−85.
36. Mitchell M, Cashman KS, Gardner DK, Thompson JG, Lane M. Disruption of mitochondrial malate–aspartate shuttle activity in mouse blastocysts impairs viability and fetal growth. Biol. Reprod. 2009; 80: 295–301.
37. Yen Y-F, Nagasawa K, Nakada T. Promising application of dynamic nuclear polarization for in vivo 13C MR imaging. Mag. Reson. Med. Sci. 2011; 10: 211–217.
38. Ager DJ, Prakash I. Pig liver esterase catalyzed hydrolyses of diesters. A new route to the syntheses of achiral half-esters. Synth. Commun. 1995; 25: 739–742.
39. Merritt ME, Harrison C, Sherry AD, Malloy CR, Burgess SC. Flux through hepatic pyruvate carboxylase and phosphoenolpyruvate carboxykinase detected by hyperpolarized ^{13}C magnetic resonance. Proc. Natl. Acad. Sci. U. S. A. 2011; 108: 19084–19089.
40. Rudakova EV, Boltneva NP, Makhaeva GF. Comparative analysis of esterase activities of human, mouse, and rat blood. Bull. Exp. Biol. Med. 2011; 152: 73–75.
41. Higuchi T, Miki T. Reversible formation of amides from free carboxylic acid and amine in aqueous solution. A case of neighboring group facilitation. J. Am. Chem. Soc. 1961; 83: 3899–3901.
42. Chen H-T, Chang J-G, Musaev DG, Lin MC. Computational study on kinetics and mechanisms of unimolecular decomposition of succinic acid and its anhydride. J. Phys. Chem. A 2008; 112: 6621–6629.
43. Dörwald FZ. *Side Reactions in Organic Synthesis*. Wiley-VCH: Weinheim, 2005 and references therein.

SUPPORTING INFORMATION

Additional supporting information may be found in the online version of this article at the publisher's web site.